

Evaluation of $\log P$, $\text{p}K_a$, and $\log D$ predictions from the SAMPL7 blind challenge

Teresa Danielle Bergazin (ORCID: [0000-0002-0573-6178](https://orcid.org/0000-0002-0573-6178))^{1†}, Nicolas Tielker (ORCID: [0000-0003-0974-8739](https://orcid.org/0000-0003-0974-8739))⁶, Yingying Zhang (ORCID: [0000-0003-3769-079X](https://orcid.org/0000-0003-3769-079X))³, Junjun Mao (ORCID: <https://orcid.org/0000-0002-3106-3018>)⁴, M.R. Gunner (ORCID: [0000-0003-1120-5776](https://orcid.org/0000-0003-1120-5776))^{3,4}, Karol Francisco (ORCID: [0000-0001-9742-8801](https://orcid.org/0000-0001-9742-8801))⁵, Carlo Ballatore (ORCID: [0000-0002-2718-3850](https://orcid.org/0000-0002-2718-3850))⁵, Stefan M. Kast (ORCID: [0000-0001-7346-7064](https://orcid.org/0000-0001-7346-7064))⁶, David L. Mobley (ORCID: [0000-0002-1083-5533](https://orcid.org/0000-0002-1083-5533))^{1,2}

¹Department of Pharmaceutical Sciences, University of California, Irvine, Irvine, California 92697, United States;

²Department of Chemistry, University of California, Irvine, Irvine, California 92697, United States; ³Department of Physics, The Graduate Center, City University of New York, New York 10016; ⁴Department of Physics, City College of New York, New York 10031, United States; ⁵Physikalische Chemie III, Technische Universität Dortmund, Otto-Hahn-Str. 4a, 44227 Dortmund, Germany; ⁶Skaggs School of Pharmacy and Pharmaceutical Sciences, University of California, San Diego, La Jolla, CA 92093-0756

*For correspondence:

dmobley@uci.edu (David L. Mobley)

Abstract

0.1 Keywords

octanol-water partition coefficient · $\log P$ · blind prediction challenge · SAMPL · free energy calculations · solvation modeling · $\text{p}K_a$ · Macroscopic $\text{p}K_a$ · Microscopic $\text{p}K_a$ · Macroscopic protonation state · Microscopic protonation state · Relative free energy

0.2 Abbreviations

SAMPL Statistical Assessment of the Modeling of Proteins and Ligands

$\log P$ \log_{10} of the organic solvent-water partition coefficient (K_{ow}) of neutral species

$\log D$ \log_{10} of organic solvent-water distribution coefficient (D_{ow})

$\text{p}K_a$ $-\log_{10}$ of the acid dissociation equilibrium constant

SEM Standard error of the mean

RMSE Root mean squared error

MAE Mean absolute error

τ Kendall's rank correlation coefficient (Tau)

R^2 Coefficient of determination (R-Squared)

QM Quantum Mechanics

MM Molecular Mechanics

DL Database lookup

LFER Linear free energy relationship

QSPR Quantitative structure-property relationship

ML Machine learning

LEC Linear empirical correction

Abstract The Statistical Assessment of Modeling of Proteins and Ligands (SAMPL) challenges focuses the computational modeling community on areas in need of improvement for rational drug design. The SAMPL7 physical property challenge dealt with prediction of octanol-water partition coefficients and pK_a for 22 compounds. The dataset was composed of a series of N-acylsulfonamides and related bioisosteres 17 research groups participated in the log P challenge, submitting 33 blind submissions total. For the pK_a challenge, 7 different groups participated, submitting 9 blind submissions in total. Overall, the accuracy of octanol-water log P predictions in the SAMPL7 challenge was lower than octanol-water log P predictions in SAMPL6, likely due to a more diverse dataset. Compared to the SAMPL6 pK_a challenge, accuracy remains unchanged in SAMPL7. Interestingly, here, though macroscopic pK_a values were often predicted with reasonable accuracy, there was dramatically more disagreement among participants as to which microscopic transitions produced these values (with methods often disagreeing even as to the sign of the free energy change associated with certain transitions), indicating far more work needs to be done on pK_a prediction methods.

1 Introduction

Computational modeling aims to enable molecular design, property prediction, prediction of biomolecular interactions, and provide a detailed understanding of chemical and biological mechanisms. Methods for making these types of predictions can suffer from poor or unpredictable performance, thus hindering their predictive power. Without a large scale evaluation of methods, it can be difficult to know what method would yield the most accurate predictions for a system of interest. Large scale comparative evaluations of methods are rare and difficult to perform because no individual group has expertise in or access to all relevant methods. Thus, methodological studies typically focus on introducing new methods, without extensive comparisons to other methods.

The Statistical Assessment of Modeling of Proteins and Ligands (SAMPL) challenges tackle modeling areas in need of improvement, focusing the community on one accuracy-limiting problem at a time. In SAMPL challenges, participants predict a target property such as solvation free energy, given a target set of molecules. Then the corresponding experimental data remains inaccessible to the public until the challenge officially closes. By focusing on specific areas in need of improvement, SAMPL helps drive progress in computational modeling.

Here, we report on a SAMPL7 physical property challenge that focused on octanol-water partition coefficients (log P) and pK_a . The pK_a of a molecule, or the negative logarithm of the acid-base dissociation constant, is related to the equilibrium constant for the dissociation of a particular acid into its conjugate base and a free proton. The pK_a also corresponds to the pH at which the corresponding acid and its conjugate base each are populated equally in solution. Given that the pK_a corresponds to a transition between specific protonation states, a given molecule may have multiple pK_a values.

The pK_a is an important physical property to take into account in drug development. The pK_a value is used to indicate the strength of an acid. A lower pK_a value indicates a stronger acid, indicating the acid more fully dissociates in water. Molecules with multiple ionizable centers have multiple pK_a values, and knowledge of the pK_a of each of the ionizable moieties allows for the percentage of ionised/neutral species to be calculated at a given pH (if activity coefficients are known/assumed). pK_a plays a particularly important role in drug development because the ionization state of molecules at physiological pH can have important ramifications in terms of drug-target interactions (e.g., ionic interactions) and/or by influencing other key determinants of drug absorption, distribution, metabolism and excretion (ADME) [1], such as lipophilicity, solubility, membrane permeability and plasma protein binding [2].

Accurate pK_a predictions play a critical role in molecular design and discovery as well since pK_a comes up in so many contexts. For example, inaccurate protonation state predictions impair the accuracy of predicted distribution coefficients such as those from free energy calculations. Similarly, binding calculations can be affected by a change in protonation state [3]. If a ligand in a protein-ligand system has a different protonation state in the binding pocket compared to when the molecule is in the aqueous phase, then this needs to be taken into account in the thermodynamic cycle when computing protein-ligand binding affinities.

Multiprotic molecules, and those with multiple tautomeric states, have two types of pK_a , microscopic and macroscopic. The *microscopic* pK_a applies to a specific transition or equilibrium between microstates, i.e. for a transition between a specific tautomer at one formal charge and that at another formal charge (e.g. two states at different formal charges in Figure 2). It relates

86 to the acid dissociation constant associated with that specific transition. As a special case, a microscopic pK_a sometimes refers
87 to the pK_a of deprotonation of a single titratable group while all the other titratable and tautomerizable functional groups of
88 the same molecule are held fixed, but this might possibly not reflect the dominant deprotonation pathway of a given acidic
89 tautomer if the base state possesses energetically favored alternate tautomers. There is no pK_a between two tautomers with
90 the same formal charge because they have the same number of protons so their relative probability is independent of pH. The
91 pH-independent free energy difference between them determines their relative population [4].

92 At some level, the macroscopic pK_a can be thought of as describing the acid dissociation constant related to the loss of a
93 proton from a molecule regardless of which functional group the proton is dissociating from, but it may be more helpful to think
94 of it (in the case of polyprotic molecules) as a macroscopic observable describing the collective behavior of various tautomeric
95 states as the dominant formal charge of the molecule shifts. In cases where a molecule has only a single location for a titratable
96 proton, the microscopic pK_a becomes equal to the macroscopic pK_a .

97 In the current challenge, we explored how well methods could predict macroscopic pK_a 's through microscopic pK_a calcula-
98 tions.

99 The partition coefficient ($\log P$) and the distribution coefficient ($\log D$) are relevant to drug discovery, as they are used to
100 describe lipophilicity. Lipophilicity influences drug-target and off-target interactions through hydrophobic interactions, and rel-
101 atively high lipophilicity results in reduced aqueous solubility and increased likelihood of metabolic instability [5].

102 Prediction of partitioning and distribution has some relevance to drug distribution. Particularly, partitioning and distribution
103 experiments involve a biphasic system with separated aqueous and organic phases, such as water and octanol, so such experi-
104 ments have some of the features of the interface between blood or cytoplasm and the cell membrane [6, 7] and thus improved
105 predictive power for partitioning and distribution may pay off with an improved understanding of such *in vivo* events.

106 Methods to predict $\log P/\log D$ may also use (and test) some of the same techniques which can be applied to binding predic-
107 tions. Both types of calculations can use solvation free energies and partitioning between environments (though this could be
108 avoided by computing the transfer free energy). Such solute partitioning models are simple test systems for the transfer free en-
109 ergy of a molecule to a hydrophobic environment of a protein binding pocket, without having to account for additional specific
110 interactions which are present in biomolecular binding sites. Thus partitioning and distribution calculations allow separating
111 force-field accuracy from errors related to conformational sampling of proteins and protonation state predictions of proteins
112 and ligands.

113 The $\log P$ is usually defined as the equilibrium concentration ratio of the neutral state of a substance between two phases:

$$\log P = \log_{10} K_{ow} = \log_{10} \frac{[\text{unionized solute}]_{\text{octanol}}}{[\text{unionized solute}]_{\text{water}}} \quad (1)$$

114 Strictly speaking, this definition of the partition coefficient P as a thermodynamic equilibrium constant is independent of total so-
115 lute concentration in the infinite dilution limit only. This reference state is commonly assumed in physics-based prediction mod-
116 els. The $\log P$ prediction challenge explores how well current methods are able to model the transfer free energy of molecules
117 between different solvent environments without any complications coming from predicting protonation states.

118 1.1 Motivation for the $\log P$ and pK_a challenge

119 Previous SAMPL challenges have looked at the prediction of solvation free energies [8–12], guest-host [13–19] and protein-ligand
120 binding affinities [20–26], pK_a [27–33], distribution coefficients [34–37], and partition coefficients [38–41]. These challenges
121 have helped uncover sources of error, pinpoint the reasons various methods performed poorly or well and their strengths and
122 weaknesses, and facilitate dissemination of lessons learned after each challenge ends, ultimately leading to improved methods
123 and algorithms.

124 Several past challenges focused on solvation modeling in order to help address this accuracy-limiting component of protein-
125 ligand modeling. The SAMPL0 through SAMPL4 challenges included hydration free energy prediction, followed by cyclohexane-
126 water distribution coefficient prediction in SAMPL5, and octanol-water distribution coefficient prediction in SAMPL6. Large errors
127 were observed in the SAMPL5 cyclohexane-water $\log D$ prediction challenge due to tautomers and protonation states not being
128 taken into account [29, 42] or adequately handled. Many participants reported $\log P$ predictions in place of $\log D$ predictions,
129 in part because the different ionization states of the molecules were thought not to be particularly relevant in the challenge,
130 but this proved not to be the case. Methods that treated multiple protonation and tautomeric states and incorporated pK_a
131 corrections (which relies on accurate pK_a prediction) in their predictions performed better [42].

132 In order to pinpoint sources of error in $\log D$ predictions, separate $\log P$ and pK_a challenges were organized for SAMPL6 [27,
133 38, 43, 44]. Better prediction performance was seen in the SAMPL6 octanol-water $\log P$ challenge compared to the SAMPL5
134 cyclohexane-water $\log D$ challenge. Performance improved in SAMPL6 for several reasons. First, the latter challenge avoided the
135 pK_a prediction problem. Second, far more experimental training data was available (aiding empirical and implicit QM methods).
136 Finally, the more narrow chemical diversity in SAMPL6 were may have helped participants. For the present SAMPL7 physical
137 properties challenge, we focused on assessing the accuracy of $\log P$ and pK_a predictions, and then combined pK_a and $\log P$
138 predictions to obtain $\log D$ predictions.

139 1.2 Historical SAMPL pK_a performance

140 During the SAMPL6 challenge a broad range of conceptually different empirical and physics-based computational methods
141 were used to predict pK_a values, as discussed in the overview paper [43]. To provide some context for the results of the SAMPL7
142 challenge the main results are summarized here.

143 The empirical approaches used during SAMPL6 can be divided into three categories, Database Lookup (DL), Linear Free
144 Energy Relationship (LFER), and Quantitative Structure-Property/Machine Learning (QSPR/ML) approaches [12]. The physical
145 approaches can be divided into pure quantum-mechanical (QM) methods, QM with a linear empirical correction (QM+LEC) to
146 account for the free energy of the proton in solution or potential systematic errors caused by the chosen method, and QM in
147 combination with molecular mechanics (QM+MM). Generally speaking, the empirical methods require significantly less compu-
148 tational effort than their physics-based counterparts once they are parameterized.

149 The best-performing models included four empirical methods and one QM-based model. These five methods were able to
150 predict the acidity constants of the challenge compounds to within 1 pK_a unit. In fact, while most empirical models – except for
151 the DL and two of the five QSPR/ML approaches – were able to predict the acidity constants to within about 1.5 pK_a units, the
152 range of predictions was much wider for the QM-based models.

153 In SAMPL6, unlike SAMPL7, the number of submissions per group was not limited, so many groups submitted multiple
154 predictions to test the performance of different variations using the same basic methodology, encompassing, e.g. different
155 levels of theory, model parameters, or conformational ensembles.

156 Well-performing empirical models included both LFER methods, such as ACD/pKa Classic (submission ID *xmyhm*) and Epik
157 Scan (*nb007*), and QSPR/ML methods such as MoKa (*nb017*) and S+pKa (*gyuhx*), all performing with root mean square errors
158 (RMSE) between 0.73 and 0.95 pK_a units [45–48]. These well-established tools thus demonstrated their reliability and quality.

159 Among the physics-based models, the most straightforward approach involved calculation of the acidity constants without
160 any empirical corrections, including the experimental value for the free energy of solvation of the proton [49]. One group
161 applied different calculation schemes to the compounds of the SAMPL6 challenge that differed in the use of gas phase and/or
162 solution phase geometries as well as additional high-level single point gas phase calculations [30]. While the results achieved
163 by this method were quite promising, with an initial RMSE of 1.77 pK_a units (*ryzue*) that could be improved to 1.40 by including
164 a standard state correction and a different value for the free energy of the proton, the authors also showed the effectiveness
165 of a simple linear regression scheme to correct the raw acidity constants. In this case the RMSE of the best-performing model
166 decreased further from 1.40 to 0.73 pK_a units after regression.

167 This type of empirical correction was used by most QM-based approaches, including the best-performing method of the
168 SAMPL6 challenge [43], improving some systematic deficiencies of the QM level of theory and basis sets and accounting for the
169 proton's solvation free energy. The best-performing QM+LEC method, *xvzxd*, achieved an RMSE of 0.68 pK_a units during the
170 challenge using the COSMO-RS solvation model. This also made it the best-performing model overall, with two other methods
171 using the same solvation model only slightly worse (*yqkga* and *8xt50*, with RMSEs of 1.01 and 1.07 pK_a units, respectively [32, 43,
172 50]).

173 A QM+LEC method using a different solvation approach, EC-RISM, only achieved an RMSE of 1.70 pK_a units for the submitted
174 model (*nb001*), but a post-submission optimization of the conformer generation workflow and the electrostatic interactions
175 improved the RMSE to 1.13, which is more in line with the other well-performing QM+LEC methods [31]. The CPCM implicit
176 solvation model was used by one group [28, 43] and performed only slightly worse than COSMO-RS (RMSEs from the paper
177 do not agree with official numbers. Only officially submitted ones are discussed here). For these two models, differing only by
178 training either a single LEC for all compounds (*35bdm*) or two separate LECs for deprotonations of neutral compounds to anions
179 and deprotonations of cations to neutral compounds (*p0jba*), the RMSEs were 1.72 and 1.31 pK_a units, respectively. These results
180 show that accurate pK_a values can be predicted when using the QM+LEC approach with different solvation models.

181 A slightly different approach was used by one participant (*Owfzo*) where QM calculations of the free energy of deprotonation
 182 and thermodynamic integration, an MM method, were combined to calculate the difference of the solvation free energies be-
 183 tween the acid and its conjugate base [33]. This approach yielded an average level of performance, with an RMSE of 2.89 for the
 184 macroscopic acidity constants calculated from the submitted microscopic acidity constants, excluding two compounds (SM14
 185 and SM18) from the analysis as they exhibited multiple pK_a values too close to each other.

186 1.3 Approaches to predicting small molecule pK_a 's

187 Calculations of aqueous pK_a values have a long history in computational chemistry, with methods ranging from direct quantum-
 188 mechanical approaches for determining the free energy of protonated and deprotonated species in solution using explicit, im-
 189 plicit, or hybrid solvation models, to continuum electrostatics-based computations of relative pK_a shifts, and empirical or rule-
 190 based algorithms, as summarized in a number of review articles, e.g. Alongi et al. [51], and Liao et al. [52] and in the SAMPL6
 191 overview papers [27, 43].

192 Computational methods typically designate tautomeric states ("microstates") for acid and base forms of a compound sepa-
 193 rated by a unit charge upon (de-)protonation. Their free energies can be linked individually in a pair-wise manner ("microstate
 194 transitions") to yield so-called microstate pK_a values from which the macroscopic pK_a can be determined [53]. Alternatively, the
 195 tautomer free energies, combined across the underlying conformational states, contribute to the ratio of partition functions
 196 representing acid and base forms, allowing the direct calculation of macroscopic acidity constants [54]. A complication arises
 197 if, as is common practice with quantum-mechanical approaches, the difference of solution-state (standard) free energies for
 198 differently charged species, $G(A_{aq}^-)$ and $G(HA_{aq})$ for a general reaction



200 are scaled by a "slope" factor m and augmented by an intercept parameter b to account for the free energy of the proton,
 yielding a regression equation, given here for microstate j of the base and k of the acid form, respectively,

$$201 \quad pK_{a,jk} = b + \frac{m}{RT \ln 10} [G_j(A^-) - G_k(HA)] \quad (3)$$

202 where slope and intercept are typically adjusted with respect to databases of experimental pK_a values [54] and RT has the
 203 usual thermodynamic meaning. Here G denotes the Gibbs free energy, but a similar expression would hold for Helmholtz free
 energy depending on the choice of ensemble.

204 As derived in Tielker et al. [54], statistics over all connected microstates (in the "state transition" (ST) approach) and *a priori*
 205 partition function summation (in the "partition function" (PF) approach) are identical if and only if $m = 1$, though in practice the
 206 difference is usually negligible.

207 For the SAMPL7 pK_a challenge, participants were required to submit predictions in a novel format, reporting transition free
 208 energies between microstates as in the " ΔG^0 " formalism outlined in Gunner et al. [55] (and similar to the work of Selwa et
 209 al. [28]). Here, the pH-dependent free energy change between "states" k and j is defined by rewriting the well-known Henderson-
 210 Hasselbalch equation for, e.g., the general reaction (Eq. 3) in the form

$$211 \quad \Delta G_{jk}(\text{pH}) = \Delta m_{jk} C_{\text{units}} (\text{pH} - pK_{a,jk}) \quad (4)$$

212 with $C_{\text{units}} = RT \ln 10$ and, for a transition away from the reference state which involves loss of a proton, $\Delta m_{jk} = -1$, denoting
 213 the charge difference between the "reference state" k (second index, usually taken as a selected neutral microstate, in this case
 HA_{aq}) and the target state j .

214 For the thermodynamic standard state at $\text{pH} = 0$ we can write

$$215 \quad \Delta G_{jk}^0 = -\Delta m_{jk} C_{\text{units}} pK_{a,jk} \quad (5)$$

216 which shows that ΔG_{jk}^0 can be identified with a formal free energy of reaction. An advantage of this approach is that closed
 217 thermodynamic cycles by summing over ΔG_{jk}^0 with identical reference k would add to zero for consistent computational methods,
 which can serve as an added value for testing theoretical frameworks [55].

218 The macroscopic pK_a is obtained by computing the total fraction of all microstates with charge q and $j \in q$ via

$$x_{j \in q}(\text{pH}) = \frac{\exp[-\Delta G_{j \in q,k}(\text{pH})/RT]}{\sum_i \exp[-\Delta G_{ik}(\text{pH})/RT]} \quad (6)$$

219 and solving, usually numerically, for the pH at which

$$x_{j \in q(1)}(\text{pH}) = x_{j \in q(2)}(\text{pH}) \quad (7)$$

220 for adjacent net charges $q(1)$ and $q(2)$. At this pH, $\text{p}K_a = \text{pH}$ for these particular charge states, and this approach constitutes
221 a formal "titration".

222 Outlining the connection between the ΔG^0 and the ST and PF formalisms [54] is useful for practitioners who directly compute
223 microstate free energies (including corresponding tautomerization free energies for which no $\text{p}K_a$ is defined) or microstate
224 transition $\text{p}K_a$ values for single deprotonation reactions where a specific reaction direction is by definition implied. The general
225 algorithm is as follows, with subscript order $\text{p}K_{a,jk}$ implying the reaction $j \rightarrow k^- + \text{H}^+$ for any total charge on j and subscript order
226 ΔG_{jk}^0 meaning the reaction $k(+m\text{H}^+) \rightarrow j(+n\text{H}^+)$ with neutral k . For all states i not equal to the neutral reference microstate k we
227 have

- 228 a) If $q(i) = 0$, $\Delta G_{ik}^0 = m\Delta G^0(k \rightarrow i)$
229 b) If $q(i) - q(k) = +1$ (the reaction is $k + \text{H}^+ \rightarrow i^+$), then $\Delta G_{ik}^0 = -C_{\text{units}}\text{p}K_{a,ik}$
230 c) If $q(i) - q(k) = -1$ (the reaction is $k \rightarrow i^- + \text{H}^+$), then $\Delta G_{ik}^0 = +C_{\text{units}}\text{p}K_{a,ki}$
231 d) If $q(i) - q(k) = +2$ (the reaction is $k + 2\text{H}^+ \rightarrow i^{2+}$ via the individual reactions $k + \text{H}^+ \rightarrow j^+$ and $j^+ + \text{H}^+ \rightarrow i^{2+}$), then $\Delta G_{ik}^0 =$
232 $-C_{\text{units}}(\text{p}K_{a,jk} + \text{p}K_{a,ij})$
233 e) If $q(i) - q(k) = -2$ (the reaction is $k \rightarrow i^{2-} + 2\text{H}^+$ via the individual reactions $k \rightarrow j^- + \text{H}^+$ and $j^- \rightarrow i^{2-} + \text{H}^+$), then $\Delta G_{ik}^0 =$
234 $+C_{\text{units}}(\text{p}K_{a,kj} + \text{p}K_{a,ji})$

235 This scheme is readily generalized to changes of more than two unit charges. The scaling by the factor m in (a) guarantees
236 consistency over closed thermodynamic cycles in the common case of non-zero slope parameter for QM-based models.

237 To demonstrate how macroscopic $\text{p}K_a$ values computed this way relate to ST and PF results it is instructive to treat the simple
238 example of a two-tautomer acid in equilibrium with a single-tautomer base, i.e.



239 for which Eq. (3) yields [54]

$$K_a^{\text{ST}} = \left(\frac{1}{K_{a,1}} + \frac{1}{K_{a,2}} \right)^{-1} = 10^{-b} \frac{\exp[-mG(\text{A}^-)/RT]}{\exp[-mG(\text{HA}_1)/RT] + \exp[-mG(\text{HA}_2)/RT]} \quad (9)$$

240 Following the algorithm for ΔG_{jk}^0 above with HA_1 assumed as neutral reference and augmenting the pH dependence accord-
241 ing to Eq. (4) we have

$$\Delta G(\text{HA}_1) = 0 \quad (10)$$

$$\Delta G(\text{HA}_2) = m[G(\text{HA}_2) - G(\text{HA}_1)] \quad (11)$$

$$\Delta G(\text{A}^-) = -C_{\text{units}}(\text{pH} - \text{p}K_{a,1}) = m[G(\text{A}^-) - G(\text{HA}_1)] - C_{\text{units}}(\text{pH} - b) \quad (12)$$

242 From Eq. 5 and equating neutral and charged molar fractions it follows from $x(\text{HA}) = x(\text{A}^-)$

$$1 + \exp \left\{ -m \left[G(\text{HA}_2) - G(\text{HA}_1) \right] / RT \right\} = 10^{-b} \exp \left\{ +m \left[G(\text{HA}_1) - G(\text{A}^-) \right] / RT \right\} / K_a \quad (13)$$

243 which, upon rearrangement and comparison with (9), yields

$$K_a = K_a^{\text{ST}} \quad (14)$$

244 Generalization to more complex tautomeric mixtures and arbitrary reference states is possible, the latter by recognizing that
245 these would only imply cancelling additive constants. The ΔG^0 and ST formalisms are therefore equivalent, as is the PF approach
246 for $m = 1$.

1.4 Approaches to predicting $\log P$

Approaches for predicting octanol-water $\log P$ values include physical modeling methods, such as quantum mechanics (QM) and molecular mechanics (MM) approaches, and empirical knowledge-based prediction methods, such as contribution-type approaches. We give some brief background on these prediction methods.

QM approaches use a numerical solution of the Schrödinger equation to estimate solvation free energies and partitioning. These approaches are not practical for larger systems, so certain approximations need to be made so that they can be used for calculating transfer free energies. Methods typically represent the solvent using an implicit solvent model and make the assumption that the solute has a single or a small number of dominant conformations in the aqueous and non-aqueous phase. The accuracy of predictions can be influenced by the basis set, level of theory, and the tautomer used as input. Implicit solvent models are used to represent both octanol and water, and these models are often highly parameterized on experimental solvation free energy data. The abundance of training data contributes to the success of QM methods, much like empirical prediction methods. Solvent models such as SMD [56], the SM-n series of models [57], and COSMO-RS [37, 58–61] are frequently used by SAMPL participants.

MM approaches use a force field which gives the energy of a system as a function of the atomic positions and are usually used by SAMPL participants to compute solvation free energies and $\log P$ values. Force fields can be fixed charge and additive, or polarizable [62, 63], and typically include all atoms, though this need not always be the case. These approaches are usually applied by integrating the equations of motion to solve for the time evolution of the system. Force fields such as GAFF [64], GAFF2 [65], CGenFF [66], and OPLS-AA [67], and water models such as TIP3P [68], TIP4P [68], OPC3 [69] are frequently used in SAMPL challenges [70]. Free energy calculations can be combined with MM methods to give a partitioning estimate. These types of calculations often use alchemical free energy methods to estimate phase transfer via a non-physical thermodynamic cycle. Some examples of alchemical approaches include non-equilibrium switching [71, 72] and equilibrium alchemical free energy calculations [73] analyzed via thermodynamic integration [74] or BAR/MBAR estimation [75, 76]. Such simulations can also use techniques like Hamiltonian replica exchange molecular dynamics.

Some limitations of MM approaches include the accuracy of the force field and the limitation that motions can only be captured in simulations that are faster than simulation timescales. The state of the molecule that is used as input is also important—usually, a single tautomer/protonation state is selected and held fixed throughout the simulation, which can introduce errors if the wrong state was selected or if there are multiple relevant states.

Empirical prediction models are trained on experimental data and can be used to quickly characterize large virtual libraries. These include additive group methods, such as fragment- or atom-contribution approaches, and quantitative structure-property relationship (QSPR) methods. In atom contribution approaches, the $\log P$ is equal to the sum of contributions from the individual atom types multiplied by the number of occurrences of each in the molecule. These methods make the assumption that each atom contributes a certain amount to the solvation free energy and that these contributions are additive to the $\log P$. In fragment (or group) contribution approaches, the $\log P$ is equivalent to the sum of the contributions from the fragment groups (more than a single atom), and typically uses correction terms that consider intramolecular interactions. These approaches are generally calculated by adding together the sum of the fragment contributions times the number of occurrences and the sum of the correction contributions times the number of occurrences in the molecule. The other class of empirical $\log P$ prediction approaches relies on QSPR. In QSPR, molecular descriptors are calculated and then used to make $\log P$ predictions. Descriptors can vary in complexity—some rely on simple counts of heteroatoms and carbon, while others are derived from correlating the 3D shape, electrostatic, and hydrogen bonding characteristics with the $\log P$ of the molecule. To find the $\log P$, a regression model gets derived by fitting the descriptor contributions to experimental data. Machine learning approaches such as random forest models, deep neural network models, Gaussian processes, support vector machines, and ridge regression [77, 78] belong under this category.

Empirical methods tend to benefit from a large and diverse training set, especially when there's a large body of experimental data to train on, such as octanol-water data like in the present and previous $\log P$ challenge [79]. However, empirical methods can experience problems if a training set has an underrepresented functional group. Additionally, these techniques are geared towards partitioning predictions, and, unlike physical-based methods, are not able to be applied to protein-ligand binding.

2 Challenge design and evaluation

2.1 General challenge structure

The SAMPL7 physical property challenge focused on pK_a , partitioning, and permeability. As reported separately, KF and CB collected a set of measured water-octanol $\log P$, $\log D$, and pK_a values for 22 compounds, along with PAMPA permeability values [80]. Since this was our first time hosting a permeability challenge, and these calculations remain challenging for many methods, we did not have enough participants to form meaningful conclusions (one participant submitted two sets of predictions in total) so the challenge is not discussed in this paper, but we provide a link to the challenge's GitHub page (https://github.com/samplchallenges/SAMPL7/tree/master/physical_property/permeability).

The SAMPL7 challenge molecules had weights that ranged from 227 to 365 Da, and varied in flexibility (the number of non-terminal rotatable bonds ranged from 3-6). The dataset had experimental $\log P$ values in the range of 0.58–2.96, pK_a values in the range of 4.49–11.93, and $\log D$ values in the range of -0.87–2.96. Information on experimental data collection is presented elsewhere [80].

The physical properties challenge was announced on June 29th, 2020 and the molecules and experimental details were made available at this time. Additional input files, instructions, and submission templates were made available afterward and participant submissions were accepted until October 8th, 2020. Following the conclusion of the blind challenge, the experimental data was made public on October 9th, 2020, and results were discussed in a virtual workshop (on November 2-5, 2020) (SAMPL Community Zenodo page <https://zenodo.org/communities/sampl/?page=1&size=20>)

A machine-readable submission file format was specified for blind submissions. The submission files included fields for naming the method of the computational protocol, listing the average compute time across all of the molecules, detailing the computing and hardware used, listing the major software packages and the versions that were used, and a free text method section for providing the detailed documentation of each method, the values of key parameters with units, and to explain how statistical uncertainties were estimated. There was also a field where participants indicated whether or not they wanted their submission formally evaluated. In addition to their predictions, participants were asked to estimate the statistical error (expressed as a standard error of the mean (SEM)) associated with their predictions, and the uncertainty of their model. The SEM captures the statistical uncertainty of a method's predictions, and the model uncertainty corresponds to the method's expected prediction accuracy, which estimates how well a participant expects their predicted values will agree with experiment. Historically, model uncertainty estimates have received relatively little attention from participants, but we retain hope that participants may eventually predict useful model uncertainties since users benefit from knowing the accuracy of a predicted value.

Participants had the option of submitting predictions from multiple methods, and were asked to fill out separate template files for each different method. Each participant or organization could submit predictions from multiple methods, but could only have one ranked submission. Allowing multiple submissions gave participants the opportunity to submit prediction sets to compare multiple methods or to investigate the effect of varying parameters of a single method. All of the submissions were assigned a short descriptive method name based on the name they provided for their protocol in their submission file. This descriptive method name was used in the analysis and throughout this paper and is presented in Tables 1, 3, and 5.

2.2 $\log P$ challenge structure

The SAMPL7 $\log P$ challenge consisted of predicting the water-octanol partition coefficients of 22 molecules. Our goal was to evaluate how well current models can capture the transfer free energy of small molecules between different solvent environments through blind predictions. challenge participants were asked to predict the difference in free energy for the neutral form of each molecule between water and octanol. For the $\log P$ challenge, participants were required to report, for each molecule, the SAMPL7 molecule ID tag (the challenge provided neutral microstate), the microstate ID or IDs that were considered, and the predicted transfer free energy, transfer free energy SEM, and model uncertainty.

Participants were asked to categorize their methods as one of the five method categories— physical (QM), physical (MM), empirical, or mixed. Participants were asked to indicate their method based on the following definitions: Empirical models are prediction methods that are trained on experimental data, such as QSPR, machine learning models, artificial neural networks, etc. Physical models are prediction methods that rely on the physical principles of the system such as MM or QM based physical methods to predict molecular properties. Participants were asked to indicate whether their physical method was QM or MM based. Methods taking advantage of both kinds of approaches were asked to be reported as "Mixed". If a participant chose the "Mixed" category, they were asked to explain their decision in the method description section in their submission file.

We highlighted that octanol may be found in the aqueous phase, in case participants wanted to consider this in their predictions. The mole fraction of water in octanol was measured as 0.271 ± 0.003 at 25°C [7]

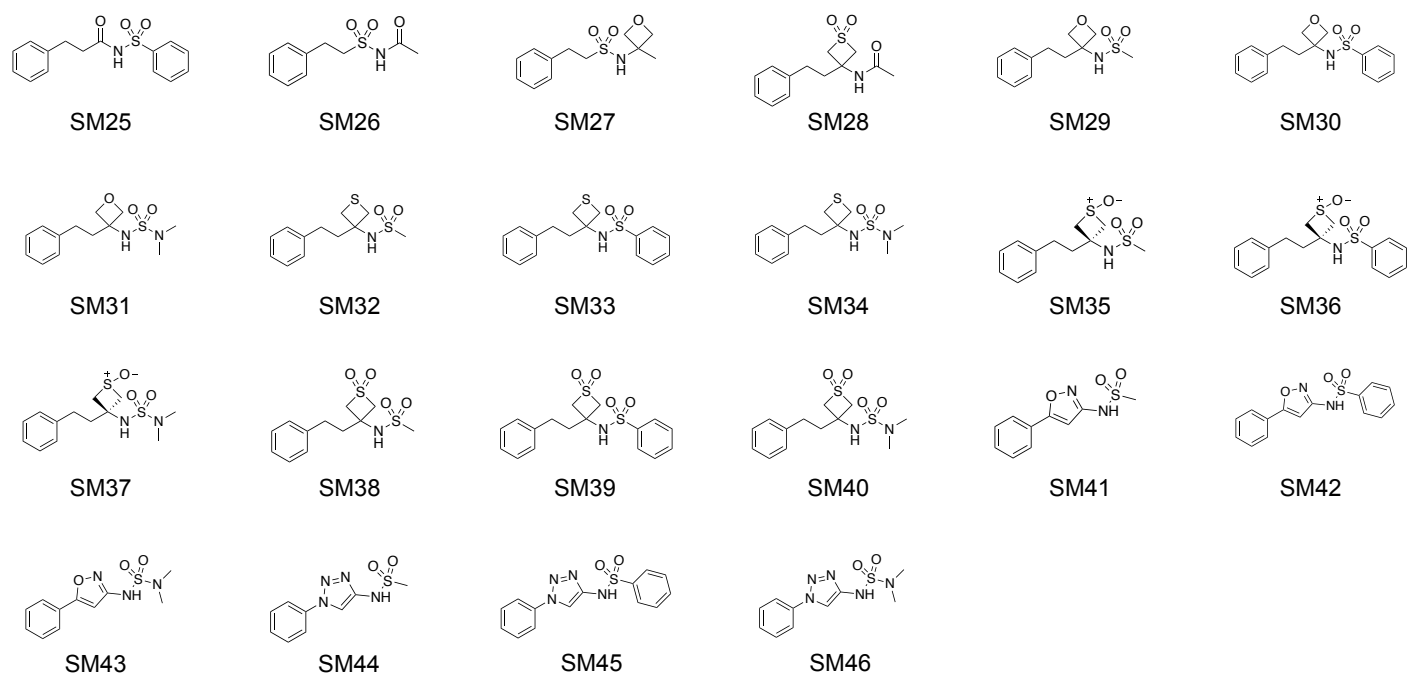


Figure 1. Structures of the 22 molecules used for the SAMPL7 physical property blind prediction challenge. Log of the partition coefficient between n-octanol and water was determined via potentiometric titrations using a Sirius T3 instrument. pK_a values were determined by potentiometric titrations using a Sirius T3 instrument. Log of the distribution coefficient between n-octanol and aqueous buffer at pH 7.4 were determined via potentiometric titrations using a Sirius T3 instrument, except for compounds SM27, SM28, SM30-SM34, SM36-SM39 which had log $D_{7.4}$ values determined via shake-flask assay. PAMPA assay data includes effective permeability, membrane retention, and log of the apparent permeability coefficient. Permeabilities for compounds SM33, SM35, and SM39 were not determined. Compounds SM35, SM36 and SM37 are single *cis* configuration isomers. All other compounds are not chiral.

2.3 pK_a challenge structure

The SAMPL7 pK_a challenge consisted of predicting relative free energies between microstates (microscopic pK_a 's) to determine the macroscopic pK_a of 22 molecules. Our goal for the SAMPL7 pK_a challenge was to assess how well current pK_a prediction methods perform for the 22 challenge molecules through blind predictions.

We chose to have participants report relative free energies of microstates for simplicity of analysis. Particularly, for each molecule, participants were asked to predict the relative free energy, including the proton free energy, between our selected neutral reference microstate and the rest of the enumerated microstates for that molecule at a reference pH of 0 (see Section 1.3 on approaches to calculating pK_a). This can also be thought of as a reaction free energy for the microstate transition where the reference state is the reactant and the other microstate the product (though a proton may also be a product, depending on the direction of the transition). As an example for one molecule, we asked for the reaction free energy (relative free energy) associated with each of the reactions as seen in Figure 2. This approach differs from that used in past pK_a challenges, which typically focused on macroscopic pK_a predictions. The shift, here, helps resolve several key problems:

1. A macroscopic pK_a can be reported for the wrong microstates, leading to predictions that are accidentally correct, but fundamentally wrong because the titration referred to a different states of the molecule.
2. Analysis of pK_a predictions requires pairing calculated macroscopic pK_a values with corresponding experimental macroscopic pK_a values [43] and such pairing can be very complex without information on which states are being predicted; while pairing is still required when specific transitions are predicted, it is aided by knowing *which* transitions are predicted (e.g. a -1 to 0 prediction from one participant can no longer accidentally be compared with a 0 to +1 transition from another participant)
3. Ultimately, populations and free energy differences between states drive the experimental measurements, so analysis ought to focus on state populations

In this work, all possible tautomers of each ionization (charge) state are defined as distinct protonation microstates. For the

365 pK_a challenge, participants were required to report, for each molecule and each microstate they considered, the microstate ID
366 of the reference state (selected by challenge organizers), the microstate ID of the microstate they were considering a transition
367 to, the formal charge for the target microstate, and the predicted free energy change associated with a transition to the target
368 microstate (Figure 2), the relative free energy SEM, and the relative free energy model uncertainty. In many cases, the transitions
369 to be considered were a particular physical reaction involving a change in a single protonation state or tautomer. However, in
370 some cases transitions involved a change of multiple protons (e.g. the F-A transition of Figure 2) and thus did not involve a
371 single protonation or deprotonation event. Additionally, all transitions were defined as *away* from the reference state (and thus
372 some involve gaining a proton, the opposite of a typical acid dissociation event), a point which caused confusion for a number
373 of participants.

374 All predictions were required to use free energy units, in kcal/mol, which was another point which caused confusion for
375 participants, as we received predictions in several different sets of units and had to handle unit conversion after the challenge
376 close.

377 Participants were asked to define and categorize their methods based on the following six method categories- experimental
378 database lookup (DL), linear free energy relationship (LFER) [12], quantitative structure-property relationship or machine learn-
379 ing (QSPR/ML) [12], quantum mechanics without empirical correction (QM) models, quantum mechanics with linear empirical
380 correction (QM+LEC), and combined quantum mechanics and molecular mechanics (QM+MM), or "Other". If the "Other" cate-
381 gory was chosen, participants were asked to explain their decision in the beginning of the method description section in their
382 submission file.

383 2.3.1 Microstate enumeration

384 The SAMPL7 pK_a challenge participants were asked to predict relative free energies between microstates to determine the pK_a
385 of molecules. We define distinct protonation microstates as all possible tautomers of each ionization (charge) state. Participants
386 could consider any of these microstates in their predictions, and had the option of submitting others. Participants were provided
387 a reference microstate for each compound, and asked to predict transition free energies to all microstates they viewed as
388 relevant, relative to this reference state.

389 Here, we provided some enumeration of potential microstates that participants might want to consider. To do so, we used
390 more than one toolkit to try and ensure all reasonable tautomers and protomers were included. Our microstates were gener-
391 ated using RDKit [81] and OpenEye QUACPAC [82] for protonation state/tautomer enumeration, and then cross checked with
392 ChemAxon Chemicalize [83] and Schrodinger Epik [46, 84] to ensure we had not missed states. We also allowed participants
393 to submit additional microstates they might view as important, and received one set of such submissions, which resulted in us
394 adding a microstate with a +1 formal charge to molecules SM31 (SM31_micro002) and SM34 (SM34_micro002). It is unclear why
395 this state was not identified by the tools we used to enumerate microstates.

396 We provided participants CSV (.csv) tables which included microstate IDs and their corresponding canonical isomeric SMILES
397 string, as well as individual MOL2 (.mol2) and SDF (.sdf) files for each individual microstate. These are available in the SAMPL7
398 GitHub repository.

399 2.4 Combining $\log P$ and pK_a predictions to estimate $\log D$

400 In the SAMPL7 challenge, $\log P$ and pK_a predictions were combined in order to estimate $\log D$. The relationship between partition
401 and distribution coefficients at a given pH can be computed via [85, 86]

$$\log D_{\text{pH}} = \log P - \log (1 + 10^{pK_a - \text{pH}}) \quad (15)$$

402 for bases (if no deprotonation site is present or if $pK_b < pK_a$) and

$$\log D_{\text{pH}} = \log P - \log (1 + 10^{\text{pH} - pK_a}) \quad (16)$$

403 for acidic compounds. The $\log D$ was calculated under the assumption that the ionic species cannot partition into the organic
404 phase [87], which may be important in some cases (e.g. in compounds with high lipophilicity or in cases where pH is so extreme
405 that partitioning of a charged species might become important).

406 2.5 Evaluation approach

407 We considered a variety of error metrics when analyzing predictions submitted to the SAMPL7 physical property set of challenges.
408 We report the following 6 error metrics: the root-mean-squared error (RMSE), mean absolute error (MAE), mean (signed) error

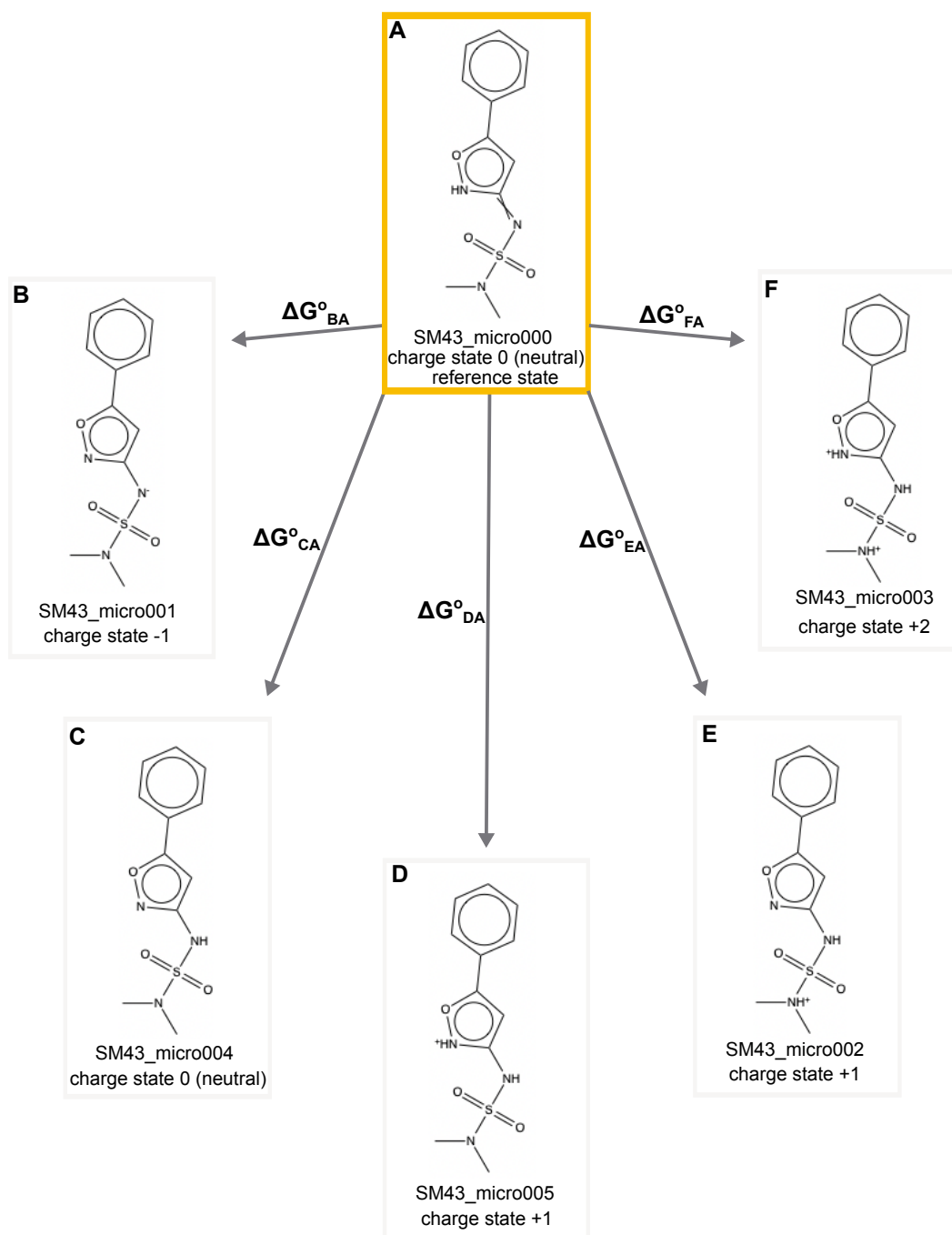


Figure 2. For each molecule in the SAMPL7 pK_a challenge we asked participants to predict the relative free energy between our selected neutral reference microstate and the rest of the enumerated microstates for that molecule. In this case, we asked for the relative state free energy including the proton free energy, which could also be called the reaction free energy for the microstate transition which has the reference state as the reactant and the alternate state as the product. Using SM43 as an example, participants were asked to predict the relative free energy between SM43_micro000 (our selected neutral microstate highlighted in yellow) and all of the other enumerated microstates (SM43_micro001–SM43_micro005) for a total of 5 relative state free energies (ΔG_{BA} , ΔG_{CA} , ΔG_{DA} , ΔG_{EA} , ΔG_{FA}). Some transitions involved a change in a single protonation state (e.g. the D-A transition of Figure 2) or tautomer (e.g. the C-A transition of Figure 2). A few cases involved a change of multiple protons (e.g. the F-A transition of Figure 2). All transitions were defined as *away* from the neutral reference state. Distinct microstates are defined as all tautomers of each charge state. For each relative free energy prediction reported, participants also submitted the formal charge after transitioning from the selected neutral state to the other state. For example, the reported charge state after transitioning from SM43_micro000 to SM43_micro001 would be -1, SM43_micro000 to SM43_micro004 would be 0 (these are tautomers of each other), SM43_micro000 to SM43_micro005 would be +1, and SM43_micro000 to SM43_micro003 would be +2.

409 (ME), coefficient of determination (R^2), linear regression slope (m), and Kendall's Tau rank correlation coefficient (τ). Additionally, 95% confidence intervals were computed for these values using a bootstrapping-over-molecules procedure (with 10,000 bootstrap samples), as in prior SAMPL challenges [12].

412 Accuracy based performance metrics, such as RMSE and MAE, are more appropriate than correlation-based statistics to evaluate methods because of the small dynamic range of experimental log P values (0.6-3.0). This is usually reflected in the confidence intervals on these metrics. Calculated error statistics of all methods can be found in Tables S1, S3, and S4. Summary statistics were calculated for each submission for method comparison. Details of the analysis and scripts are preserved on the SAMPL7 GitHub repository (described in the "Code and data availability" section).

417 For each challenge we included a reference and/or null method set of predictions in the analysis to provide perspective for performance evaluations of blind predictions. Null models or null predictions employ a model that is not expected to be useful and can provide a simple point of comparison for more sophisticated methods, as ideally, such methods should improve on predictions from a null model. Reference methods are not formally part of the challenge, but are provided as comparison methods. For the log P challenge we included a null prediction set which predicts a constant log P value of 2.66 for every compound, as described in a previous SAMPL paper [38]. For log D evaluation we included a set of null predictions that all of the molecules partition equally between the water and octanol phase.

424 For the log P and pK_a challenge and the log D evaluation, we provide reference calculations using ChemAxon's Chemicalize [83], a commercially available empirical toolkit, as a point of comparison. These include *REF#* in the method name in all of the figures so that they are easily recognized as non-blind reference calculations. The analysis is presented with and without the inclusion of reference and/or null calculations in the SAMPL7 GitHub repository. The figures and statistics tables pertaining to the log P and pK_a challenges and the log D evaluation in this manuscript include reference calculations.

429 For the log P and pK_a challenge, we list consistently well-performing methods that were ranked in the top consistently according to two error and two correlation metrics: RMSE, MAE, R^2 , and Kendall's Tau. These are shown in Table 2 and 4.

431 For each challenge, we also evaluated the relative difficulty of predicting the physical property of interest of each molecule in the set. We plotted the distributions of errors in prediction for each molecule considering all prediction methods. We also calculated the MAE for each molecule as an average of all methods, as well as for predictions from each method category.

434 2.5.1 Converting relative free energies between microstates to macroscopic pK_a

435 In the pK_a challenge, participants submitted predictions consisting of the free energy changes between a reference microstate and every other relevant microstate for each compound. Specifically, participants were asked to predict the relative free energy between a selected neutral reference microstate and the rest of the enumerated microstates for that molecule at a reference pH of 0. In order to compare participants' predictions to experimental pK_a values, these predicted relative free energies had to be converted to macroscopic pK_a values.

440 Here, we analyzed submissions using the titration method discussed above (Section 1.3). This approach computes the population of each charge state as a function of pH and finds the pH at which the population of one charge state crosses that of another (Figure 3); as noted above this approach is equivalent to the transition and free energy approaches detailed previously.

443 In our analysis Python code used in the present challenge we work from Equation 6 and Equation 7 to find the pH at which populations of the two charge states are equal. Here, we do this using `fsolve` from `scipy` in Python.

445 3 Results and Discussion

446 3.1 Overview of log P challenge results

447 A variety of methods were used in the log P challenge. There were 33 blind submissions collected from 17 groups (Tables of participants and their predictions can be found in the SAMPL7 GitHub Repository and in the Supporting Information.). In the SAMPL6 octanol-water log P challenge there were 91 blind submissions collected from 27 participating groups. In the SAMPL5 Cyclohexane-Water log D challenge, there were 76 submissions from 18 participating groups [88], so participation was lower than previous iterations. This modestly decreased participation (by one group) was likely in part because of COVID-19-related disruptions and because this challenge had to be conducted on a short timescale with relatively limited publicity because the experimental data was not generated specifically for SAMPL, and thus staging of the SAMPL7 challenge required delaying submission of an experimental study which was already complete.

455 Out of blind submissions of the SAMPL7 log P challenge, there were 10 in the physical (MM) category, 10 in the physical (QM) category, and 12 in the empirical category. An additional null and reference method were included in the empirical method

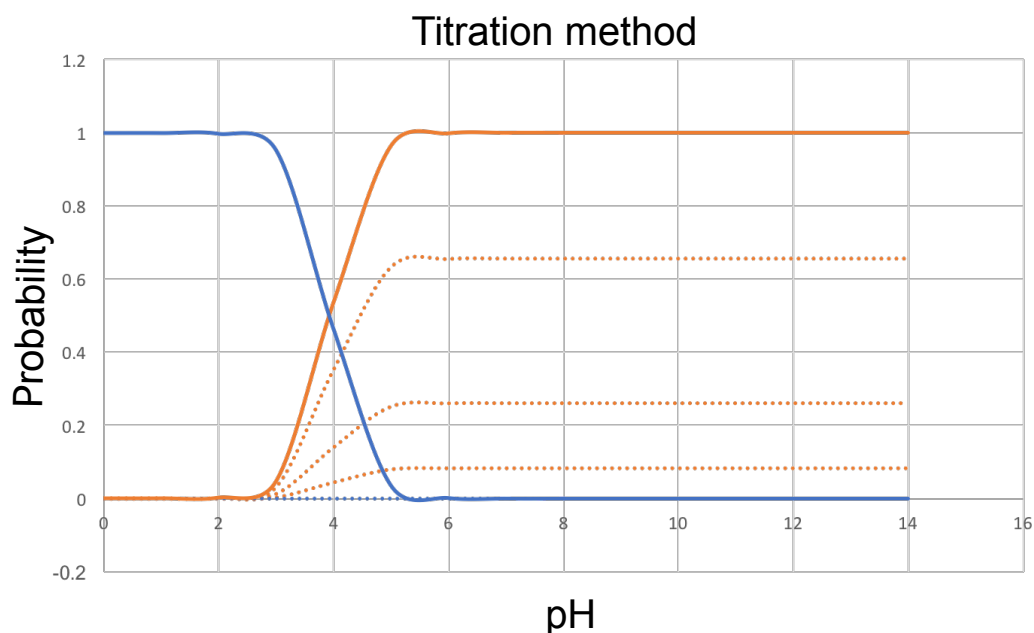


Figure 3. Using the microstate probability to convert microscopic pK_a predictions to macroscopic pK_a 's with the titration method pK_a 's. Blue and orange lines represent two states. Blue states have one more proton than the orange states, and thus a formal charge higher by +1. The blue state has one tautomer and the orange state has 3, denoted by the dashed lines. The solid lines are the ensemble averaged state probability for each group with a given charge. The crossing point between two ensemble lines is the macroscopic pK_a .

457 category.

458 The following sections evaluate the performance of $\log P$ prediction methods. Performance statistics of all the methods can
459 be found in Table S1. Methods are referred to by their method names, which are provided in Table 1.

460 3.1.1 Performance statistics to compare $\log P$ prediction methods

461 Some methods in the challenge achieved a good octanol-water $\log P$ prediction accuracy. Figure 4 shows the performance
462 comparison of methods based on accuracy with RMSE and MAE. The uncertainty in the correlation statistics was too high to
463 rank method performance based on correlation, but we provide an overall correlation assessment for all methods in the SI
464 in Figure S2. 16 submissions achieved a $RMSE \leq 1.0 \log P$ units, but no method achieved a $RMSE \leq 0.5 \log P$ units. Methods
465 that achieved a $RMSE \leq 1.0 \log P$ units were mainly empirical, but some were QM-based. Prediction methods include 15 blind
466 predictions and one reference method.

467 3.1.2 A shortlist of consistently well-performing methods in the $\log P$ challenge

468 Here, many performance differences are not statistically significant, but we identified five consistently well-performing ranked
469 methods that appear in the top 10 according to two accuracy based (RMSE and MAE) and two correlation based metrics (Kendall's
470 Tau and R^2), as shown in Table 2. The resulting 5 best-performing methods were made up of three empirical methods and two
471 QM-based physical methods.

472 Method *TFE MLR* [90] was an empirical method that used a multi-linear regression (MLR) made from experimental $\log P$ val-
473 ues from 60 sulfonamides obtained from PubChem [98] and DrugBank [99]. The dataset was mainly composed of sulfonamide
474 drugs and smaller molecules with other classical functional groups. The following descriptors were used to create the MLR: the
475 frequency of functional groups, hydrogen bond acceptors, hydrogen bond donors, molar refractivity, and topological polar sur-
476 face area. The functional group frequency was calculated with an in-house script from a modified function of Open Babel [100],
477 the rest was obtained from supplied Open Babel properties.

478 Method *Chemprop* was an empirical method which used the $\log P$ dataset of the OPERA models in their approach [91].
479 Molecules from the Opera set were compared with the challenge molecules and those with an ECFP_6 fingerprint (extended
480 connectivity fingerprint) tanimoto coefficient (TC) greater than 0.25 were flagged as test molecules for a total of 233 testing
481 molecules. The training set was created from the rest of the Opera data set by filtering out molecules with a ECFP_6 TC >0.4 to
482 test set molecules. Several models were built using a Directed-Message Passing Neural Network (D-MPNN) [101, 102] to predict

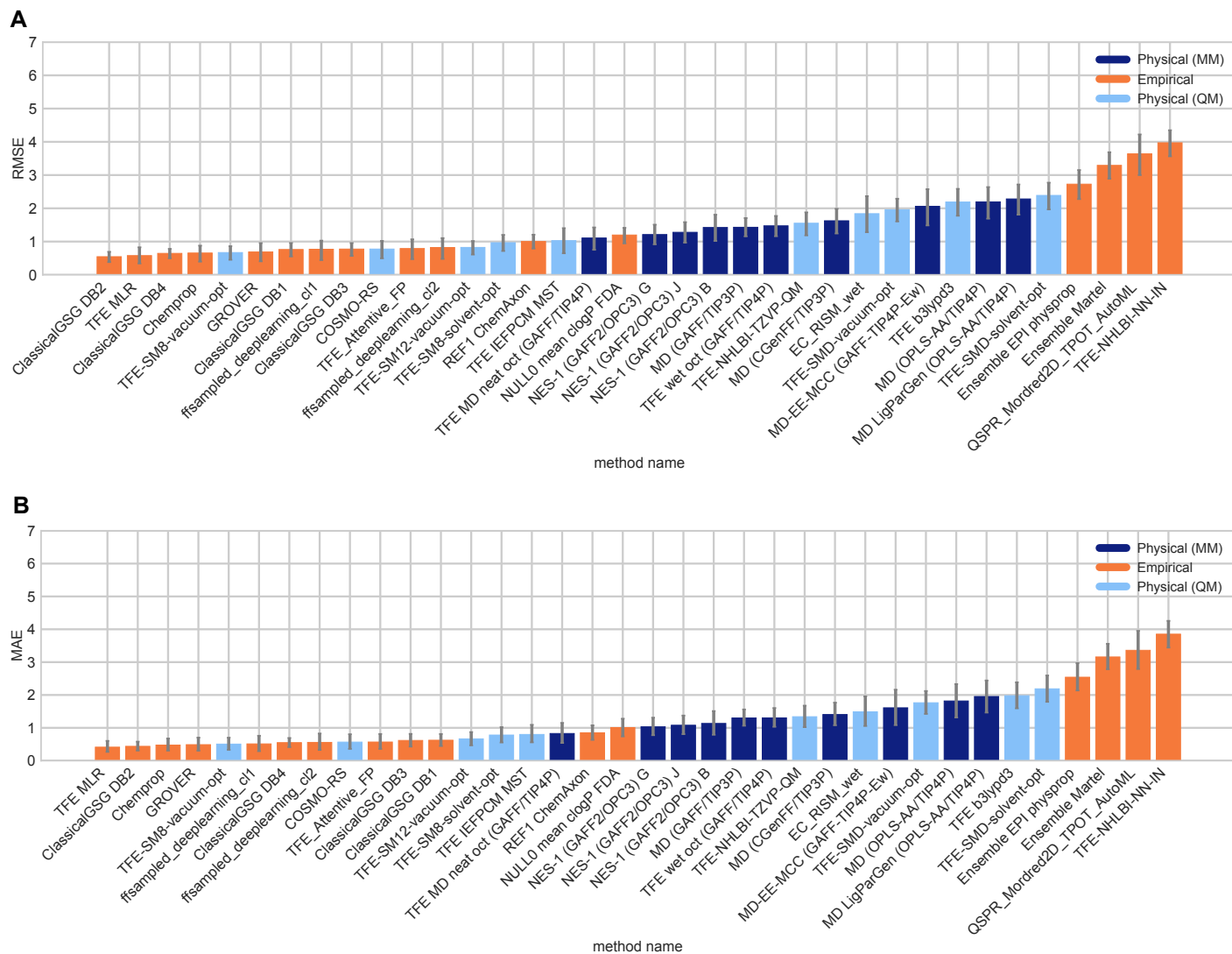


Figure 4. Overall accuracy assessment for all methods participating in the SAMPL7 log P challenge shows that many methods did not exhibit statistically significant differences in performance and there was no single clear winner; however, empirical methods tended to perform better in general. Both root-mean-square error (RMSE) and mean absolute error (MAE) are shown, with error bars denoting 95% confidence intervals obtained by bootstrapping over challenge molecules. Empirical methods outperform the majority of the other methods. Methods that achieved a RMSE ≤ 1.0 log P units were mainly empirical based, and some were QM-based physical methods. Submitted methods are listed in Table 1. The submission *REF1 ChemAxon* [83] was a reference method included after the blind challenge submission deadline, and *NULL0 mean cLogP FDA* is the null prediction method; all others refer to blind predictions.

Table 1. Method names, category, and submission type for all the log P calculation submissions. The “submission type” column indicates if submission was a blind submission (denoted by “Blind”) or a post-deadline reference or null calculation (denoted by “Reference”). The table is ordered from lowest to highest RMSE, although many consecutively listed methods are statistically indistinguishable. All calculated error statistics are available in Table S1.

Method Name	Category	Submission Type
<i>ClassicalGSG DB2</i> [89]	Empirical	Blind
<i>TFE MLR</i> [90]	Empirical	Blind
<i>ClassicalGSG DB4</i> [89]	Empirical	Blind
<i>Chemprop</i> [91]	Empirical	Blind
<i>TFE-SM8-vacuum-opt</i>	Physical (QM)	Blind
<i>GROVER</i>	Empirical	Blind
<i>ClassicalGSG DB1</i> [89]	Empirical	Blind
<i>ffsampled_deeplearning_cl1</i>	Empirical	Blind
<i>ClassicalGSG DB3</i> [89]	Empirical	Blind
<i>COSMO-RS</i> [92]	Physical (QM)	Blind
<i>TFE_Attentive_FP</i>	Empirical	Blind
<i>ffsampled_deeplearning_cl2</i>	Empirical	Blind
<i>TFE-SM12-vacuum-opt</i>	Physical (QM)	Blind
<i>TFE-SM8-solvent-opt</i>	Physical (QM)	Blind
<i>REF1 ChemAxon</i> [83]	Empirical	Reference
<i>TFE IEFPCM MST</i> [93]	Physical (QM)	Blind
<i>TFE MD neat oct (GAFF/TIP4P)</i>	Physical (MM)	Blind
<i>NULL0 mean clogP FDA</i> [79]	Empirical	Reference
<i>NES-1 (GAFF2/OPC3) G</i>	Physical (MM)	Blind
<i>NES-1 (GAFF2/OPC3) J</i>	Physical (MM)	Blind
<i>NES-1 (GAFF2/OPC3) B</i>	Physical (MM)	Blind
<i>MD (GAFF/TIP3P)</i> [94]	Physical (MM)	Blind
<i>TFE wet oct (GAFF/TIP4P)</i>	Physical (MM)	Blind
<i>MD (CGenFF/TIP3P)</i> [94]	Physical (MM)	Blind
<i>EC_RISM_wet</i> [95]	Physical (QM)	Blind
<i>TFE-SMD-vacuum-opt</i>	Physical (QM)	Blind
<i>MD-EE-MCC (GAFF-TIP4P-Ew)</i> [96]	Physical (MM)	Blind
<i>TFE b3lypd3</i> [97]	Physical (QM)	Blind
<i>MD (OPLS-AA/TIP4P)</i> [94]	Physical (MM)	Blind
<i>MD LigParGen (OPLS-AA/TIP4P)</i> [94]	Physical (MM)	Blind
<i>TFE-SMD-solvent-opt</i>	Physical (QM)	Blind
<i>TFE-NHLBI-TZVP-QM</i>	Physical (QM)	Blind
<i>Ensemble EPI physprop</i>	Empirical	Blind
<i>Ensemble Martel</i>	Empirical	Blind
<i>QSPR_Mordred2D_TPOT_AutoML</i>	Empirical	Blind
<i>TFE-NHLBI-NN-IN</i>	Empirical	Blind

483 the log P , which was then used to get the transfer free energy.

484 Submission *ClassicalGSG DB3* is an empirical method that employed neural networks (NNs) where the inputs are molecular
485 features generated using a method called Geometric Scattering for Graphs (GSG) [89]. In GSG, atomic features are transformed
486 into molecular features using the graph molecular structure. For atomic features, predictions used 4 physical quantities from
487 classical molecular dynamics forcefields: partial charge, Lennard-Jones well depth, Lennard-Jones radius and atomic type. A
488 training dataset was built from 7 datasets for a total of 44,595 unique molecules. Open Babel was used to convert RDKit gener-
489 ated canonical SMILES to MOL2 files, which were then used as input into CGenFF to determine partial charges and Lennard-Jones
490 parameters for all atoms in each molecule. The generation of CGenFF atomic attributes failed for some molecules, so the final
491 dataset had 41,409 molecules, and is referred to as the “full dataset”. A training set of 2,379 molecules was obtained by filtering
492 the full training set and keeping only those with sulfonyl functional groups. This was done using the `HasSubstructMatch` function
493 of the RDKit toolkit. The log P values were predicted by the model trained on this training set.

494 Method *COSMO-RS* was a QM-based physical prediction approach [92]. First, this approach used COSMOquick [103] to gener-
495 ate tautomers and discarded irrelevant states due to an internal energy threshold implemented in COSMOquick. The participants
496 conducted a conformational search of every microstate with COSMOconf [104] using up to 150 conformers. Second, for each
497 conformer they performed a geometry optimization using the BP86 functional with a TZVP basis set and the COSMO solvation
498 scheme, followed by a single point energy calculation using the BP86 functional with a def2-TZVPD basis set and the FINE COSMO

499 cavity. All density functional theory calculations were carried out with the TURBOMOLE 7.5 program package [105, 106]. Third,
500 a conformer selection was done by applying COSMOconf (using internally COSMOtherm) to reduce the number of conformers
501 and tautomers for the neutral molecule sets. The final set of the neutral state contained only those conformers and states that
502 are relevant in liquid solutions. Fourth, the COSMOtherm software (version 2020) [107] was used to calculate the free energy
503 difference for each molecule set (from the second step described here) and to calculate the relative weight of the microstates
504 in water. All free energy calculations were carried out using the BP-TZVPD-FINE 20 level of COSMO-RS in COSMOtherm. Within
505 the used COSMO-RS, an ensemble of conformers and microstates is automatically used and weighted according to the total free
506 energy in the respective liquid phase, i.e. different weights are used in water and octanol.

507 Submission *TFE-NHLBI-TZVP-QM* was a QM-based physical method that used the Def2-TZVP basis set for all calculations. Cal-
508 culations were performed in either Gaussian 09 or Gaussian 16. Structures were optimized with the B3LYP density functional
509 and were verified to be local minima via frequency calculations on an integration grid with harmonic frequencies. Details of
510 solvation handling were not included in the method description.

511 Figure 5 show predicted $\log P$ vs experimental $\log P$ value comparison plots of these 5 well-performing methods and also
512 a method that represents average performance in this challenge. Representative method *NES-1 (GAFF2/OPC3) G* was selected
513 because it has the median RMSE of all ranked methods analyzed in the challenge.

Table 2. Five consistently well-performing $\log P$ prediction methods based on consistent ranking within the top 10 according to various statistical metrics. Submissions were ranked according to RMSE, MAE, R^2 , and Kendall's Tau. Many top methods were found to be statistically indistinguishable when considering the uncertainties of their error metrics. Additionally, the sorting of methods was significantly influenced by the metric that was chosen. We determined which ranked $\log P$ prediction methods were consistently the best according to all four chosen statistical metrics by assessing the top 10 methods according to each metric. A set of five consistently well-performing methods were determined- three empirical methods and two QM-based physical methods. Performance statistics are provided as mean and 95% confidence intervals. Correlation plots of the best performing methods and one average method is shown in Figure 5. Additional statistics are available in Table S1.

Method Name	Category	RMSE	MAE	R^2	Kendall's Tau
<i>TFE MLR</i> [90]	Empirical	0.58 [0.34, 0.83]	0.41 [0.26, 0.60]	0.43 [0.06, 0.80]	0.56 [0.23, 0.83]
<i>Chemprop</i> [91]	Empirical	0.66 [0.39, 0.89]	0.48 [0.30, 0.69]	0.41 [0.11, 0.76]	0.54 [0.25, 0.82]
<i>ClassicalGSG DB3</i> [89]	Empirical	0.77 [0.57, 0.96]	0.62 [0.43, 0.82]	0.51 [0.18, 0.77]	0.48 [0.14, 0.75]
<i>COSMO-RS</i> [92]	Physical (QM)	0.78 [0.49, 1.01]	0.57 [0.36, 0.80]	0.49 [0.17, 0.80]	0.53 [0.25, 0.78]
<i>TFE-NHLBI-TZVP-QM</i>	Physical (QM)	1.55 [1.19, 1.87]	1.34 [1.02, 1.76]	0.52 [0.19, 0.78]	0.51 [0.19, 0.78]

514 3.1.3 Difficult chemical properties for $\log P$ predictions

515 To learn about chemical properties that are challenging for $\log P$ predictions, we analyzed the prediction errors of the molecules
516 (Figure 6). We chose to use MAE for this analysis because it is less affected by outliers compared to RMSE and is therefore
517 more appropriate for following global trends. Although methods varied in performance, as indicated by large and overlapping
518 confidence intervals, the MAE calculated for each molecule as an average across all methods indicates that some of the molecules
519 were better predicted than others (Figure 6A). For reference, compound classes and structures of the molecules are available in
520 Figure S3. Molecules such as SM26, SM27, and SM28 were well predicted on average. Molecules such as SM42, SM43, and SM36
521 were not well predicted on average.

522 Certain groups of molecules seem to be more challenging for $\log P$ predictions. Two of the most poorly predicted molecules,
523 SM42 and SM43, are isoxazoles. Isoxazoles are oxygen and nitrogen-containing heteroaromatics. When we consider the cal-
524 culated MAE of each molecule separated out by method category, we find that predictions for 2 out of the 3 molecules (SM41
525 and SM43) belonging to the isoxazole compound class are less accurate with MM-based physical methods than with QM-based
526 physical and empirical method categories (Figure 6B).

527 Figure 6C shows error distribution for each challenge molecule over all prediction methods. Molecules such as SM33, SM36,
528 SM41, SM42, and SM43 are shifted to the right, indicating that methods likely had a tendency to overestimate how much these
529 molecules favored the octanol phase.

530 Figure 6D shows the error distribution for each molecule calculated for 5 methods from submissions that were determined to
531 be consistently well-performing (method names: *TFE MLR* [90], *Chemprop* [91], *COSMO-RS* [92], *ClassicalGSG DB3* [89], *TFE-NHLBI-*

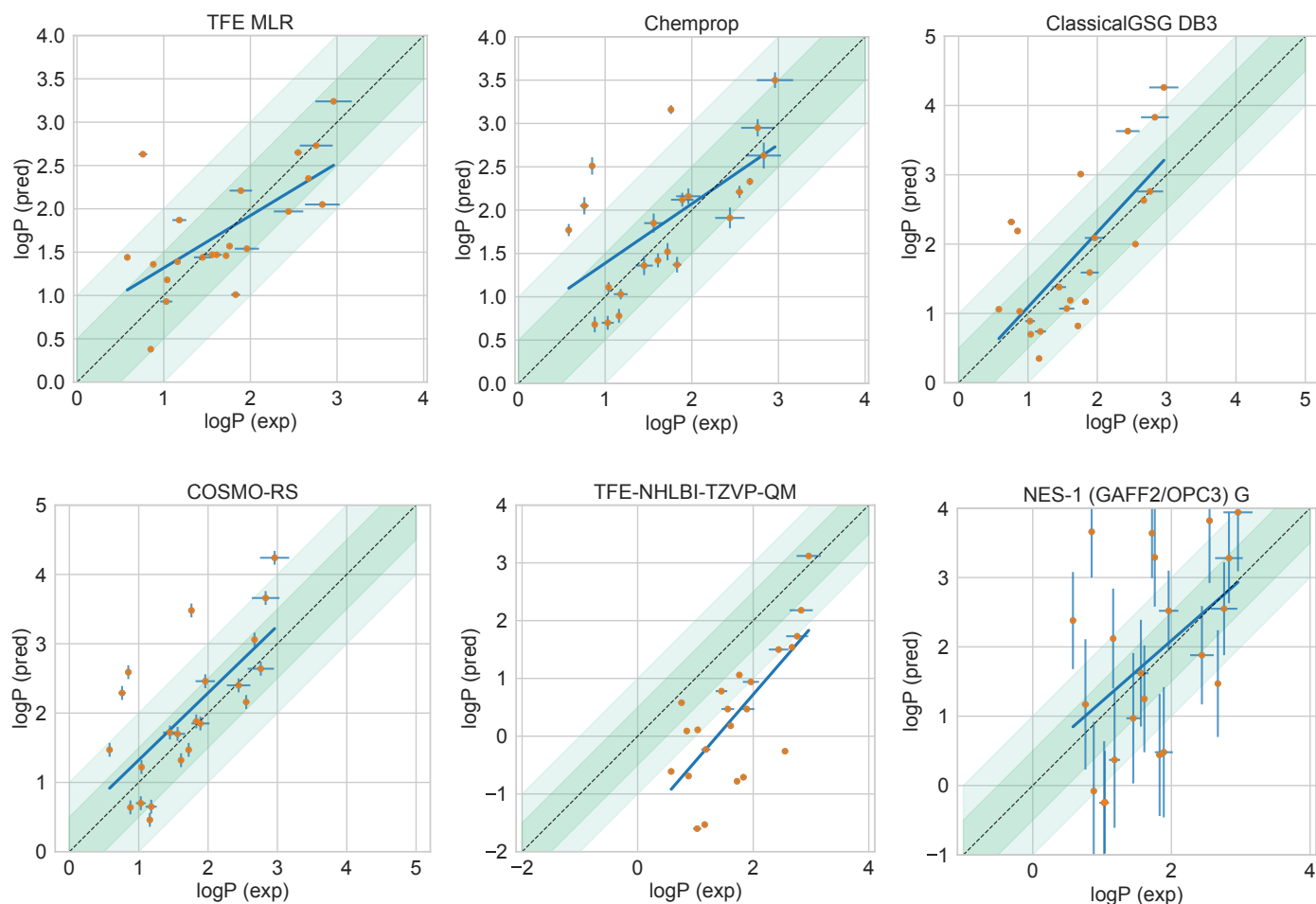


Figure 5. Predicted vs. experimental value correlation plots of 5 best performing methods and one representative average method in the SAMPL7 log P challenge. Dark and light green shaded areas indicate 0.5 and 1.0 units of error. Error bars indicate standard error of the mean of predicted and experimental values. In some cases, log P SEM values are too small to be seen under the data points. The best-performing methods were made up of three empirical methods (*ClassicalGSG DB3* [89], *TFE MLR* [90], *Chemprop* [91]) and two QM-based physical methods (*COSMO-RS* [92], *TFE-NHLBI-TZVP-QM*). Details of the methods can be found in Section 3.1.2 and performance statistics are available in 2. Method *NES-1 (GAFF2/OPC3) G* was selected as the representative average method, which has a median RMSE.

Table 3. Method names, category, and submission type for all the pK_a submissions. The “submission type” column indicates if submission was a blind submission (denoted by “Blind”) or a post-deadline reference calculation (denoted by “Reference”). The table is ordered from lowest to highest RMSE, although many consecutively listed methods are statistically indistinguishable. All calculated error statistics are available in Table S3.

Method Name	Category	Submission Type
<i>REF00_Chemaxon_Chemicalize</i> [83]	QSPR/ML	Reference
<i>EC_RISM</i> [95]	QM	Blind
<i>IEFPCM/MST</i> [93]	QM	Blind
<i>DFT_M05-2X_SMD</i> [97]	QM	Blind
<i>TZVP-QM</i>	QM	Blind
<i>Standard Gaussian Process</i>	QSPR/ML	Blind
<i>DFT_M06-2X_SMD_implicit</i>	QM	Blind
<i>DFT_M06-2X_SMD_implicit_SAS</i>	QM	Blind
<i>DFT_M06-2X_SMD_explicit_water</i>	QM	Blind
<i>Gaussian_corrected</i>	QM+LEC	Blind

532 *TZVP-QM*). Although there is a spread in error for many of the molecules, the better performing methods overestimate the log P
 533 of some of the molecules (as indicated by a shift to the right), such as isoxazoles (SM41–SM43) and most notably for SM36.
 534 The better performing methods also slightly underestimate the log P for molecules belonging to the 1,2,3-triazole compound
 535 class– molecules SM44–SM6 are slightly shifted to the left meaning participants tended to predict the molecules would favor the
 536 aqueous phase.

537 3.2 Overview of pK_a challenge results

538 In the SAMPL7 pK_a challenge there were 9 blind submissions from 7 different groups. Blind submissions included 7 QM-based
 539 physical methods, 1 QM+LEC method, and 1 QSPR/ML method. An additional reference prediction method was included in the
 540 QSPR/ML method category.

541 3.2.1 pK_a performance statistics for method comparison

542 Some methods in the SAMPL7 challenge achieved a good prediction accuracy for pK_a 's. Figure 7 shows the performance compari-
 543 son of methods based on accuracy with RMSE and MAE. Two submissions achieved a RMSE < 1.0 pK_a units, no methods achieved
 544 a RMSE \leq 0.5 pK_a units. One of the methods that achieved a RMSE < 1.0 pK_a units was a QM-based physical prediction method
 545 (*EC_RISM* [95]), and the other was a QSPR/ML method that was submitted as a reference method (*REF00_Chemaxon_Chemicalize* [83]).

546 Correlation-based statistics methods provide a rough comparison of methods. Figure 8 shows R^2 and Kendall's Tau values
 547 calculated for each method, sorted from high to low performance. It is not possible to truly rank these methods based on
 548 correlation due to the high uncertainty of each correlation statistic. Over half of the methods have R^2 and Kendall's Tau values
 549 equal to or greater than 0.5 and can be considered as the better half, however individual performance is largely indistinguishable
 550 from one another. For R^2 , two methods (*EC_RISM*, *REF00_Chemaxon_Chemicalize*), seem to have a greater ranking ability than the
 551 other methods.

552 There were six methods with an $R^2 \geq 0.5$ — four of the methods were QM methods, one was a QM+LEC method, and one was
 553 a QSPR/ML method. Seven methods had a Kendall's Tau ≥ 0.50 . Of these, five were QM methods, one was a QM+LEC method,
 554 and one was a QSPR/ML method.

555 3.2.2 A shortlist of consistently well-performing methods in the pK_a challenge

556 We determined a group of consistently well-performing methods in the pK_a challenge. When looking at individual error metrics,
 557 many submissions are not different from one another in a way that is statistically significant. Ranking among methods changes
 558 based on the chosen statistical metric and does not necessarily lead to strong conclusions due to confidence intervals that often
 559 overlap with one another. Here, we determined consistently well-performing methods according to two accuracy (RMSE and
 560 MAE) and two correlation metrics (Kendall's Tau and R^2). For ranked submissions, we identified two consistently well-performing

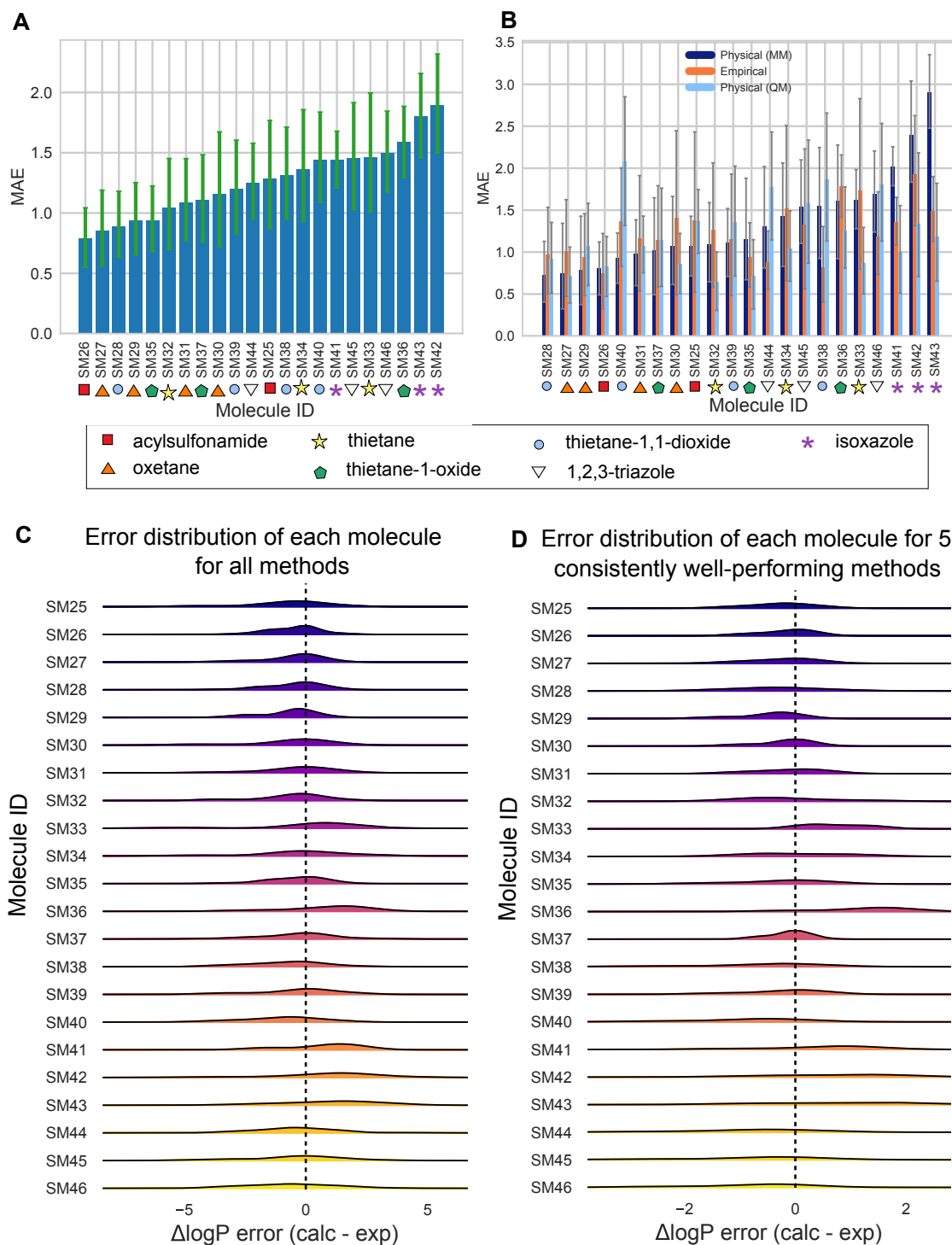


Figure 6. Molecule-wise prediction accuracy in the log P challenge point to isoxazoles as poorly predicted, especially by MM-based physical methods. Molecules are labeled with their compound class as a reference. **(A)** The MAE calculated for each molecule as an average of all methods. **(B)** The MAE of each molecule separated by method category. **(C)** log P prediction error distribution for each molecule across all prediction methods. **(D)** log P prediction error distribution for each molecule calculated for only 5 methods from blind ranked submissions that were determined to be consistently well-performing (*TFE MLR* [90], *Chemprop* [91], *COSMO-RS* [92], *ClassicalGSG DB3* [89], *TFE-NHLBI-TZVP-QM*).

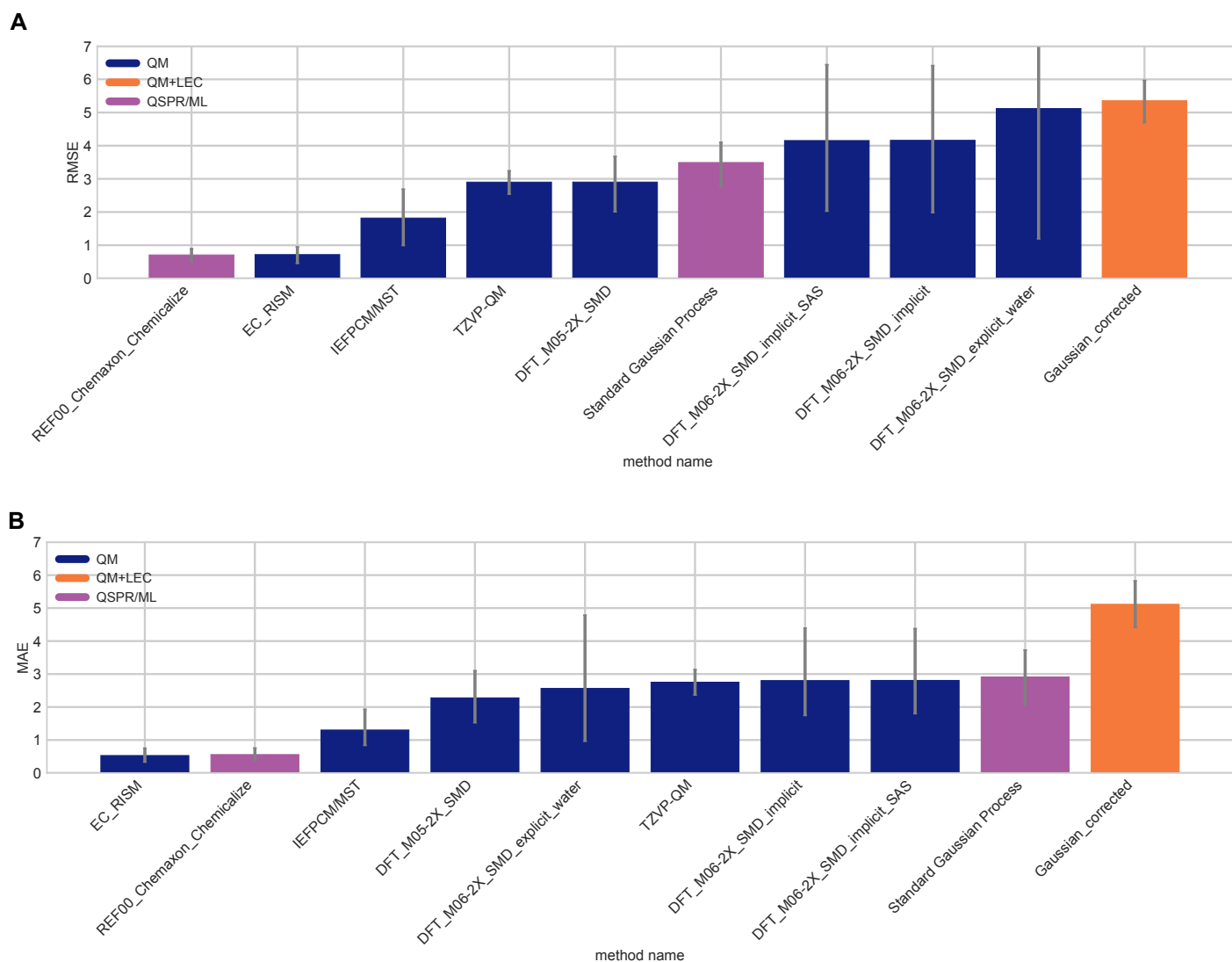


Figure 7. Overall accuracy assessment for all methods participating in the SAMPL7 pK_a challenge shows that two methods, one a Physical (QM) method and one a QSPR/ML, performed better than other methods. Both root-mean-square error (RMSE) and mean absolute error (MAE) are shown, with error bars denoting 95% confidence intervals obtained by bootstrapping over challenge molecules. *REF00_Chemaxon_Chemicalize* [83] is a reference method that was included after the blind challenge submission deadline, and all other method names refer to blind predictions. Methods are listed out in Table 3 and statistics calculated for all methods are available in Table S3.

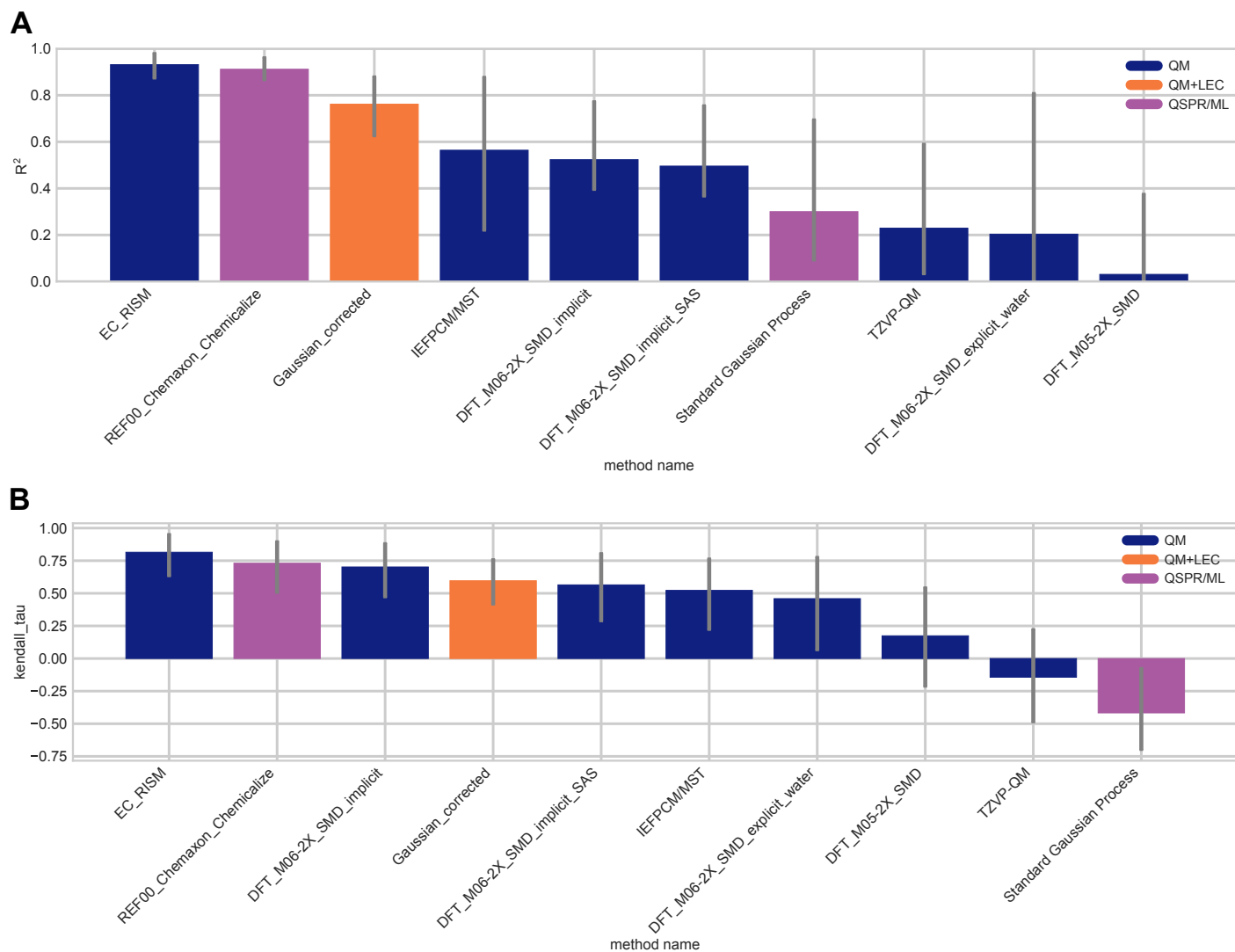


Figure 8. Overall correlation assessment for all methods participating in the SAMPL7 pK_a challenge shows that one Physical (QM) method and one QSPR/ML reference method exhibited modestly better performance than others. Pearson's R^2 and Kendall's Rank Correlation Coefficient Tau (τ) are shown, with error bars denoting 95% confidence intervals obtained by bootstrapping over challenge molecules. Submission methods are listed out in Table 3. *REF00_Chemaxon_Chemicalize* [83] is a reference method that was included after the blind challenge submission deadline, and all other method names refer to blind predictions. Most methods have a statistically indistinguishable performance on ranking, however, for R^2 , two methods (*EC_RISM* [95], *REF_Chemaxon_Chemicalize*), tend to have a greater ranking ability than the other methods. Evaluation statistics calculated for all methods are available in Table S3 of the Supplementary Information.

561 methods that were ranked in the top three according to these statistical metrics. The list of consistently well-performing methods
562 are presented in Table 4. The resulting two best-performing methods were both QM-based physical methods.

563 Submission *EC_RISM* was a QM-based physical method [95]. In this approach, multiple geometries were generated for each
564 microstate using the EmbedMultipleConfs function of RDKit. These structures were pre-optimized with Amber 12 using GAFF 1.7
565 parameters and AM1-BCC charges with an ALPB model to represent the dielectric environment of water. Conformations with an
566 energy of more than 20 kcal/mol than the minimum structure of that microstate were discarded and the remaining structures
567 clustered with a structural RMSD of 0.5 Angstrom. The cluster representatives were then optimized using Gaussian 16revC01
568 with IEF-PCM using default settings for water at the B3LYP/6-311+G(d,p) level of theory. Additional stereoisomers were treated
569 as if they were additional conformational states of the same microstate so that for each microstate only up to 5 conformations
570 with the lowest PCM energies for each solvent were treated with EC-RISM/MP2/6-311+G(d,p) using the PSE2 closure [54] and the
571 resulting EC-RISM energies were corrected. To calculate the relative free energies with respect to each neutral reference state,
572 4 different formulas were used, depending on the difference in the protonation state. Macrostate pK_a values were calculated
573 using the partition function approach of equation 5 found elsewhere [54].

574 Submission *IEFPCM/MST* was a QM-based physical method [93]. This approach used the Frog 2.14 software [108, 109] to
575 explore microstate conformations. The molecular geometries of the compounds were fully optimized at the B3LYP/6-31G(d) level
576 of theory, taking into account the solvation effect of water on the geometrical parameters of the solutes, using the IEFPCM version
577 of the MST model. The resulting minima were verified by vibrational frequency analysis, which gave positive frequencies in all
578 cases. The relative energies of the whole set of conformational species were refined from single-point computations performed
579 at the MP2/aug-cc-pVDZ levels of theory. In addition, the gas phase estimate of the free energy difference for all microstates
580 was derived by combining the MP2 energies with zero point energy corrections. Finally, solvation effects were added by using
581 the B3LYP/6-31G(d) version of the IEFPCM/MST model, which is a quantum mechanical self-consistent continuum solvation
582 method. The pK_a was determined using both the experimental hydration free energy of the proton (-270.28 kcal/mol) and a
583 Boltzmann's weighting scheme to the relative stabilities of the conformational species determined for the microstates involved
584 in the equilibrium constant for the dissociation reaction following the thermodynamic cycle reported in previous studies [110].

585 Figure 9 show predicted pK_a vs experimental pK_a value comparison plots of the two well-performing methods and also
586 a method that represents average performance. Representative average method *DFT_M05-2X_SMD* [97] was selected as the
587 method with the median RMSE of all ranked methods analyzed in the challenge.

Table 4. Two consistently well-performing pK_a prediction methods based on consistent ranking within the top three according to various statistical metrics. Ranked submissions were ranked/ordered according to RMSE, MAE, R^2 , and Kendall's Tau. Many methods were found to be statistically indistinguishable when considering the uncertainties of their error metrics. Additionally, the sorting of methods was significantly influenced by the metric that was chosen. We determined which methods are repeatedly among the top two according to all four chosen statistical metrics by assessing the top three methods according to each metric. Two QM-based methods consistently performed better than others. Performance statistics are provided as mean and 95% confidence intervals. All statistics for all methods are in Table S3.

Method Name	Category	RMSE	MAE	R^2	Kendall's Tau
<i>EC_RISM</i> [95]	QM	0.72 [0.45, 0.95]	0.53 [0.33, 0.75]	0.93 [0.87, 0.98]	0.81 [0.63, 0.96]
<i>IEFPCM/MST</i> [93]	QM	1.82 [1.00, 2.69]	1.30 [0.84, 1.92]	0.56 [0.22, 0.87]	0.52 [0.22, 0.76]

588 3.2.3 Difficult chemical properties for pK_a predictions

589 To learn about chemical properties that pose challenges for pK_a predictions, we analyzed the prediction errors of the molecules
590 (Figure 10). For reference, compound classes and structures of the molecules are available in Figure S3. We chose to use MAE
591 for molecular analysis because it is less affected by outliers compared to RMSE and is, therefore, more appropriate for follow-
592 ing global trends. When we consider the calculated MAE of each molecule separated out by method category the prediction
593 accuracy of each molecule varies based on method category (Figure 10B). The MAE calculated for each molecule as an average
594 of all methods shows that SM25 was the most poorly predicted molecule. The QM+LEC method category appears to be less
595 accurate for the majority of the molecules compared to the other method categories. Compared to the other two method cat-

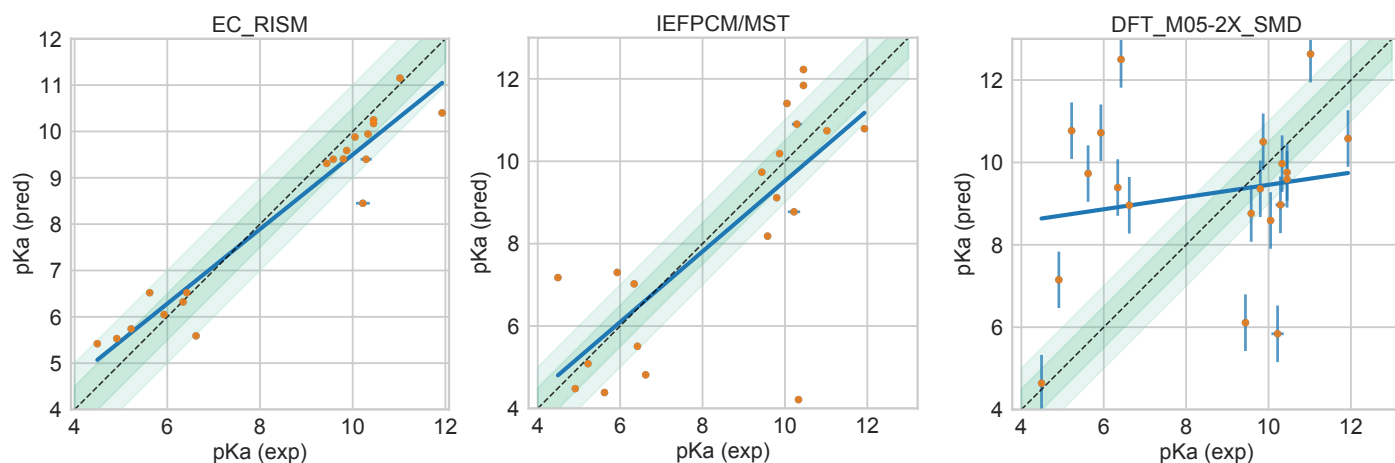


Figure 9. Predicted vs. experimental value correlation plots of 2 best performing methods and one representative average method in the SAMPL7 pK_a challenge. Dark and light green shaded areas indicate 0.5 and 1.0 units of error. Error bars indicate standard error of the mean of predicted and experimental values. Some SEM values are too small to be seen under the data points. Method *DFT_M05-2X_SMD* [97] was selected as the method with the median RMSE of all ranked methods analyzed in the challenge. Performance statistics of these methods is available in Table 4

egories, QSPR/ML methods performed better for molecules SM41-SM43, which are isoxazoles (oxygen and nitrogen containing heteroaromatics), and molecule SM44-SM46, which are 1,2,3-triazoles (nitrogen containing heteroaromatics). Physical QM methods performed poorly for molecules SM25 and SM26 (acylsulfonamide compound class). Figure 10C shows error distribution for each challenge molecule over all the prediction methods. Molecule SM25 has the most spread in pK_a prediction error.

3.2.4 Microscopic pK_a performance

SAMPL7 challenge pK_a participants were asked to report the relative free energy between microstates, using a provided neutral microstate as reference. Microstates are defined as the enumerated protomers and tautomers of a molecule. Details of how microstates were found can be found in Section 2.3.1. Some molecules had 2 microstates, while others had as many as 6 (Table S7).

Figure 12 shows the predicted free energy change between the reference state and each microstate, on average, for all transitions across all predictions. Molecules are labeled with their compound class as a reference. Predictions disagree widely for some transitions, like those from the reference state to SM26_micro002, SM28_micro001, SM43_micro003, SM46_micro003, while predictions for other transitions such as that from the reference microstate to SM26_micro004 are in agreement (as shown by small error bars in Figure 12A, 14).

Figure 14 shows examples of some microstate transitions where participants' predicted transition free energies disagree. We also examined how the microstate transition free energies (relative to the reference state) are distributed across predictions (Figure 12B). We find that some transitions are much more consistently predicted than others, but in some cases there is broad disagreement even about the sign of the free energy change associated with the particular transition – so methods disagree as to which protonation state or tautomer is preferred at the reference pH.

To further analyze which transitions were difficult, we focused on how consistently methods agreed as to the sign of the free energy change for each transition. Particularly, we calculated the Shannon Entropy (H) for the transition *sign* for each transition, shown in Figure 13. For each microstate, we calculated H via:

$$H = - \sum_i P_i \ln(P_i) \quad (17)$$

where P_i is the probability of a particular outcome i ; here, we use i to indicate a positive sign or a negative sign for the predicted free energy change. So P_{positive} is the fraction of positive sign predictions, P_{negative} is the fraction of negative sign predictions, and P_{neutral} is the fraction of neutral sign predictions (which were somewhat frequent as a few participants predicted a free energy change of exactly 0 for some transitions). For example, for SM25_micro001, given the predictions we received, the

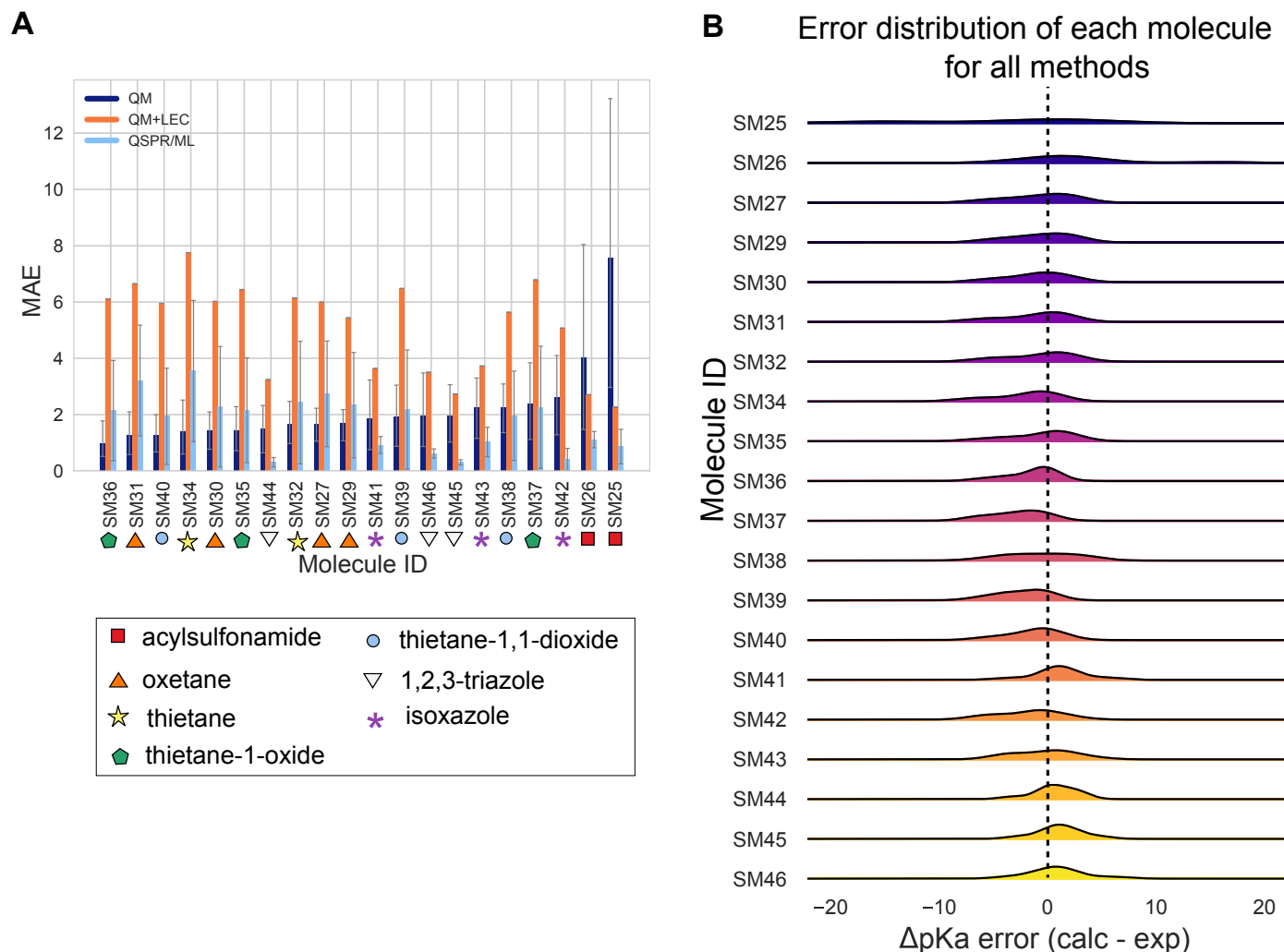


Figure 10. Molecule-wise prediction error distribution plots show the prediction accuracy for individual molecules across all prediction methods for the pK_a challenge. Molecules are labeled with their compound class as a reference. Molecule SM25 stood out as particularly poorly predicted. **(A)** The MAE of each molecule separated by method category suggests the most challenging molecules were different for each method category. It is difficult to draw statistically significant conclusions where there are large overlapping confidence intervals. The QM+LEC method category appears to be less accurate for the majority of the molecules compared to the other method categories. QSPR/ML methods performed better for isoxazoles (SM41-SM43) and 1,2,3-triazoles (SM44-SM46) compared to the other two method categories. Physical QM-based methods performed poorly for acylsulfonamides (SM26 and SM25). **(B)** Error distribution for each molecule over all prediction methods. SM25 has the most spread in pK_a prediction error.

Table 5. Method names, category, and submission type for all the log *D* estimations. Method names are based off the submitted pK_a and log *P* method names, with the log *P* method name listed first followed by “+” and then the pK_a method name. The “submission type” column indicates if submission was a blind submission (denoted by “Blind”) or a post-deadline reference calculation (denoted by “Reference”). All calculated error statistics are available in Table S4.

Method Name	Category	Submission Type
<i>REFO ChemAxon</i>	Empirical	Reference
<i>TFE IEFPCM MST + IEFPCM/MST</i>	Physical (QM)	Standard
<i>NULL0</i>	Empirical	Reference
<i>EC_RISM_wet + EC_RISM</i>	Physical (QM)	Standard
<i>TFE-NHLBI-TZVP-QM + TZVP-QM</i>	Physical (QM)	Standard
<i>TFE b3lypd3 + DFT_M05-2X_SMD</i>	Physical (QM)	Standard
<i>MD (CGenFF/TIP3P) + Gaussian_corrected</i>	Physical (MM) + QM+LEC	Standard
<i>TFE-SMD-solvent-opt + DFT_M06-2X_SMD_explicit_water</i>	Physical (QM)	Standard

P_{positive} is 0.5, the P_{negative} is 0.4 and the P_{neutral} is 0 (no neutral sign predictions). The Shannon entropy *H* is then $-(0.5 \ln(0.5) + 0.4 \ln(0.4) + 0)$, which is roughly 0.7 and indicates predictions had difficulty agreeing on the sign.

While the Shannon entropy may not be a perfect tool for analyzing this issue, we find it helpful here. For a particular transition, a value of 0 indicates all predictions agreed as to the sign of the free energy change (whether positive, negative, or neutral), while values greater than 0 reflect an increasing level of disagreement in the sign of the prediction. 32 of the microstates had a *H* value of 0, 21 had a values that ranged from 0.5-0.7, and 3 microstates had values greater than 0.9 (the highest level of disagreement). The 3 microstates with the most disagreement belong to the thietane-1-oxide compound class (one from SM35, one from SM36 and one from SM37).

Transitions that pose difficulty for participants involve a protonated nitrogen and keto-enol neutral state tautomerism. Chemical transformations involving a protonated nitrogen in terminal nitrogen groups, 1,2,3-triazoles, and isoxazoles were all found to occur in molecules that have high levels of disagreement in sign prediction. Depictions of some of these types of transitions are presented in Figure 11. Predictions for these transitions were substantially divided on the predicted sign – roughly half of the methods predict a positive sign, while the other half predict a negative sign. This means methods could not agree on the preferred state at the reference pH. The number of positive, negative, and neutral sign predictions per microstate is available in Table S5

In several cases, the SAMPL input files provided a reference microstate with unspecified stereochemistry, then a separate but otherwise equivalent microstate with specified stereochemistry (SM35_micro002, SM36_micro002, SM37_micro003). Experiments were done on the compound with specified stereochemistry, so participants were instructed to assume that the reference microstate (which had unspecified stereochemistry) had the same free energy as the microstate with specified stereochemistry. However, many participants didn’t use the microstate with specified stereochemistry as the reference state, and most ended up predicting a nonzero relative free energy between the reference state and the microstate with specified stereochemistry, despite instructions.

3.3 Overview of log *D* challenge results

In the SAMPL7 physical property prediction challenge, log *P* and pK_a predictions were combined in order to estimate log *D*, as described in Section 2.4.

There were 6 log *D* estimates and 2 reference methods. Methods are listed in Table 5 and statistics for all log *D* prediction methods are available in Table S4. There were 5 methods that belonged to the physical (QM) category, and 1 in the Physical (MM) + QM+LEC category (this category used a MM-based physical method in the log *P* challenge, and a QM+LEC method in the pK_a challenge). The null and reference method were included in the empirical method category.

3.3.1 log *D* performance statistics for method comparison

Figure 15 compares the accuracy of methods based on RMSE and MAE. No method achieved a $RMSE \leq 1.0$ log *D* units, and the overall RMSE ranged from 1.1 to 4.5 log *D* units. Four methods had a RMSE between 1 and 2, and three methods had an RMSE between 2 and 3. Accuracy is better than the previous log *D* challenge. In the SAMPL5 log *D* challenge, out of 63 submissions, no

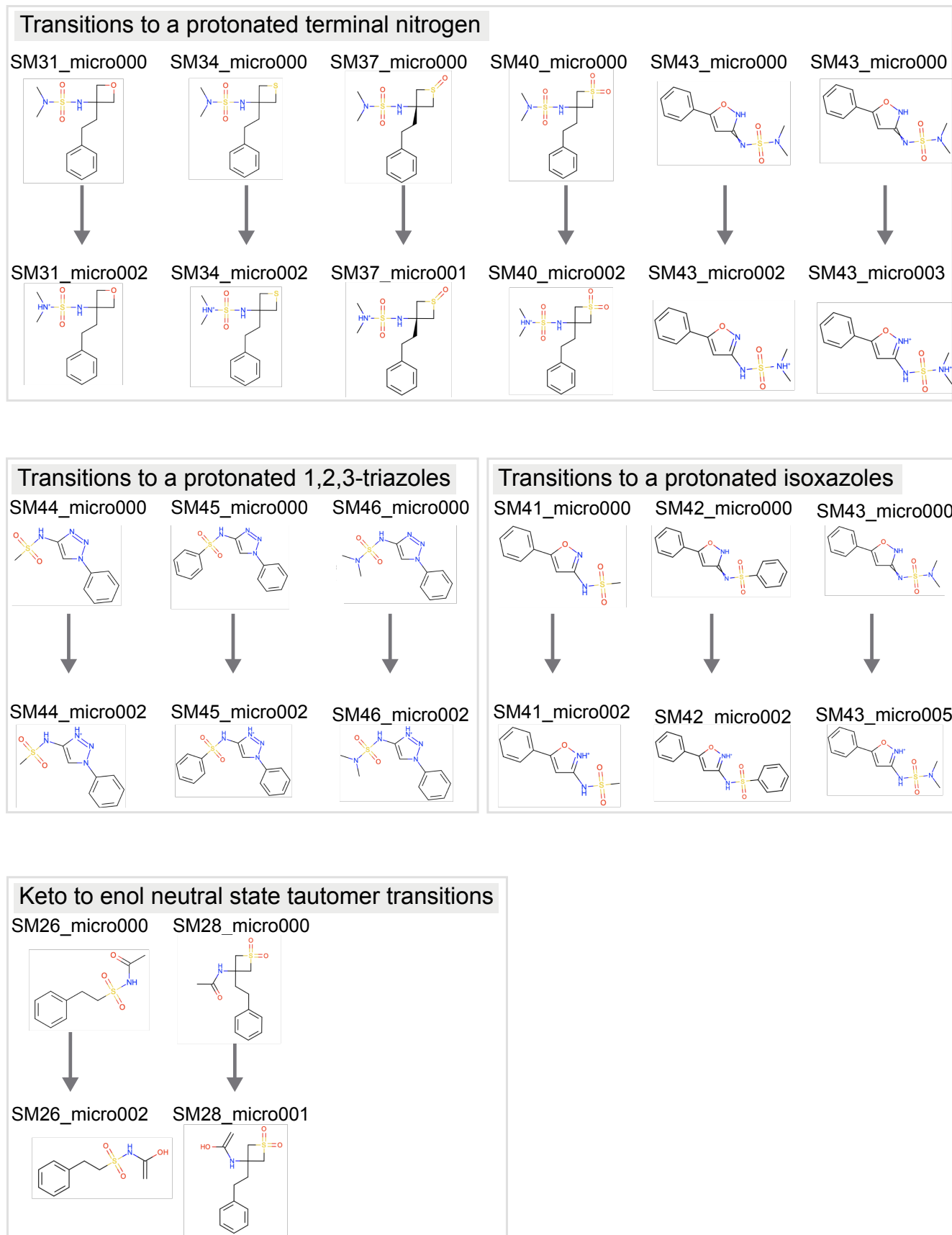


Figure 11. Chemical transformations that lead to common sign disagreements among participants typically involve a protonated nitrogen in terminal nitrogen groups, 1,2,3-triazoles, and isoxazoles. Shown are some chemical transformations that repeatedly show up as having large disagreement on the sign of the relative free energy prediction, as seen in Figure 13.

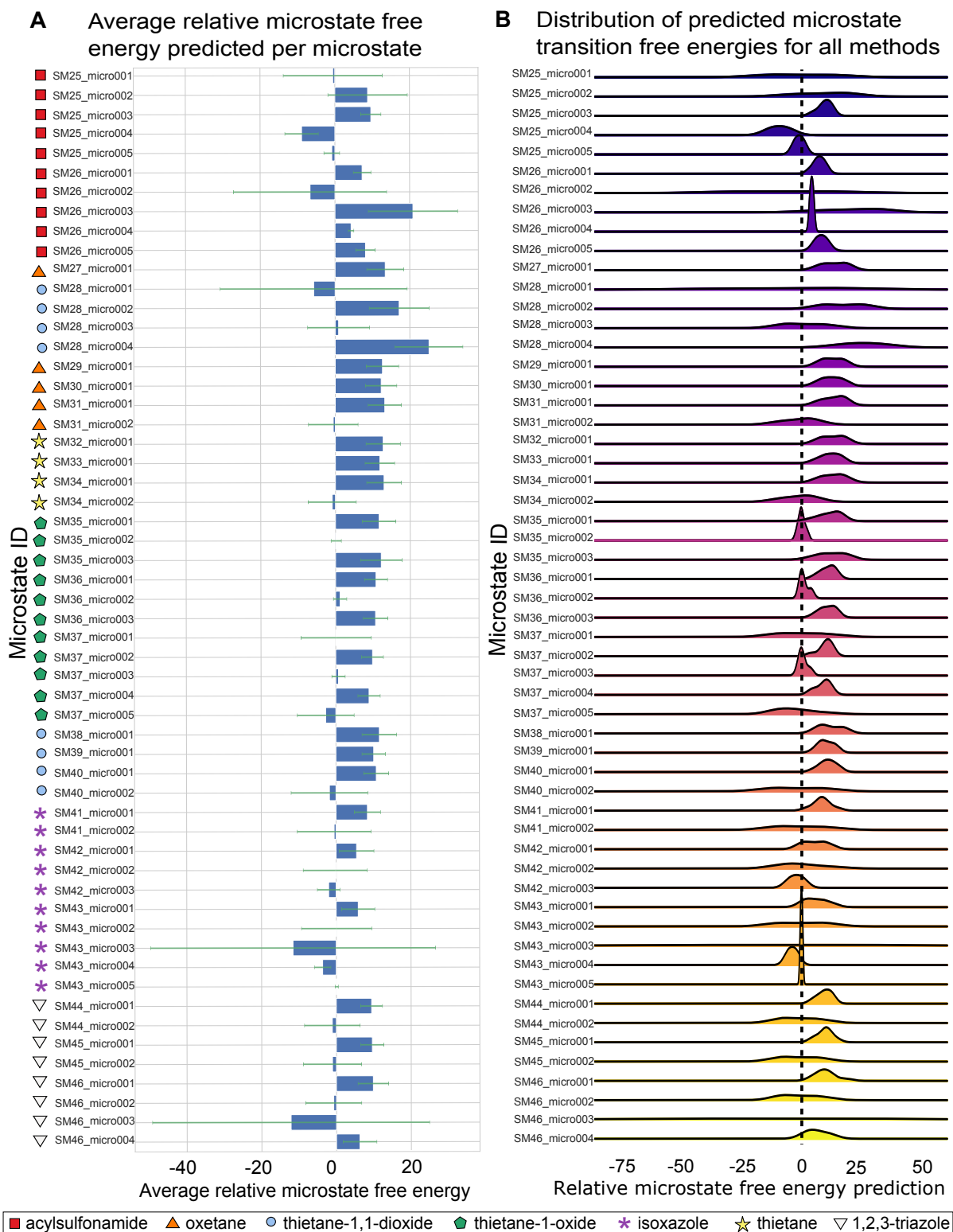


Figure 12. The average relative microstate free energy predicted per microstate and the distribution across predictions in the SAMPL7 pK_a challenge show how varied predictions were. Molecules are labeled with their compound class as a reference. **(A)** The average relative microstate free energy predicted per microstate. Error bars are the standard deviation of the relative microstate free energy predictions. A lower standard deviation indicates that predictions for a microstate generally agree, while a larger standard deviation means that predictions disagree. Predictions made for microstates such as SM25_micro001, SM26_micro002, SM28_micro001, SM43_micro003, SM46_micro003 widely disagree, while predictions for microstates such as SM26_micro004 are in agreement. **(B)** Distribution for each relative microstate free energy prediction over all prediction methods shows how prediction agreement among methods varied depending on the microstate.

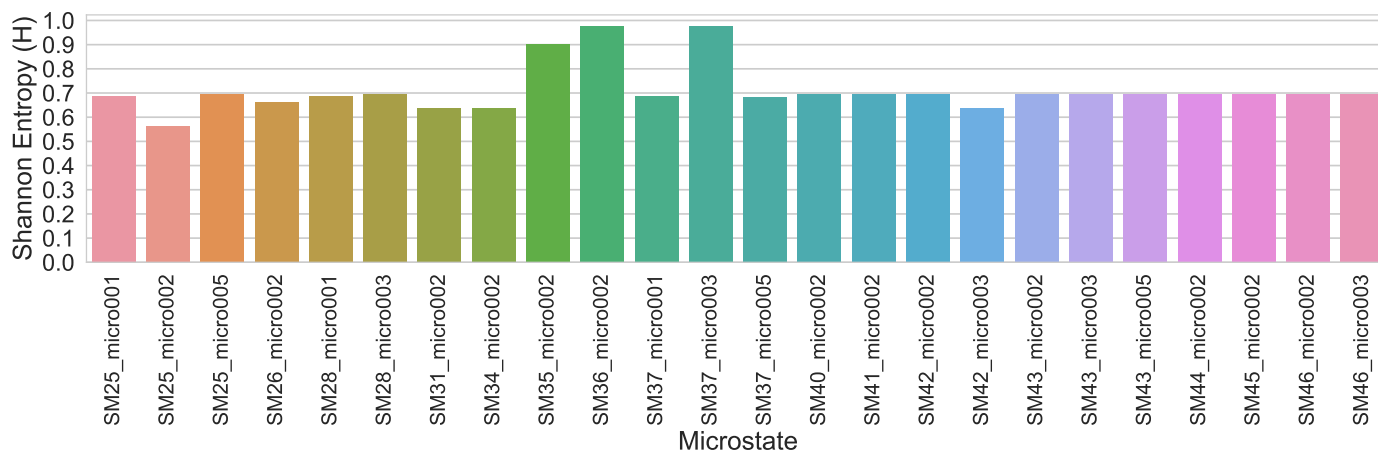


Figure 13. The Shannon entropy (H) per microstate transition shows that participants disagree on many of the signs of the relative free energy predictions. Microstates with entropy values greater than 0 reflect increasing disagreement in the predicted sign. Microstates with an entropy of 0 are not shown here, but indicate that methods made predictions which had the same sign for the free energy change associated with a particular transition. About 44% of all microstates predictions disagreed with one another based on the sign, and the rest agreed. Roughly 5% of microstates strongly disagreed on the sign of predictions— meaning that predicted relative free energies were fairly evenly split between positive, neutral, and negative values. This indicates that these transitions were particularly challenging.

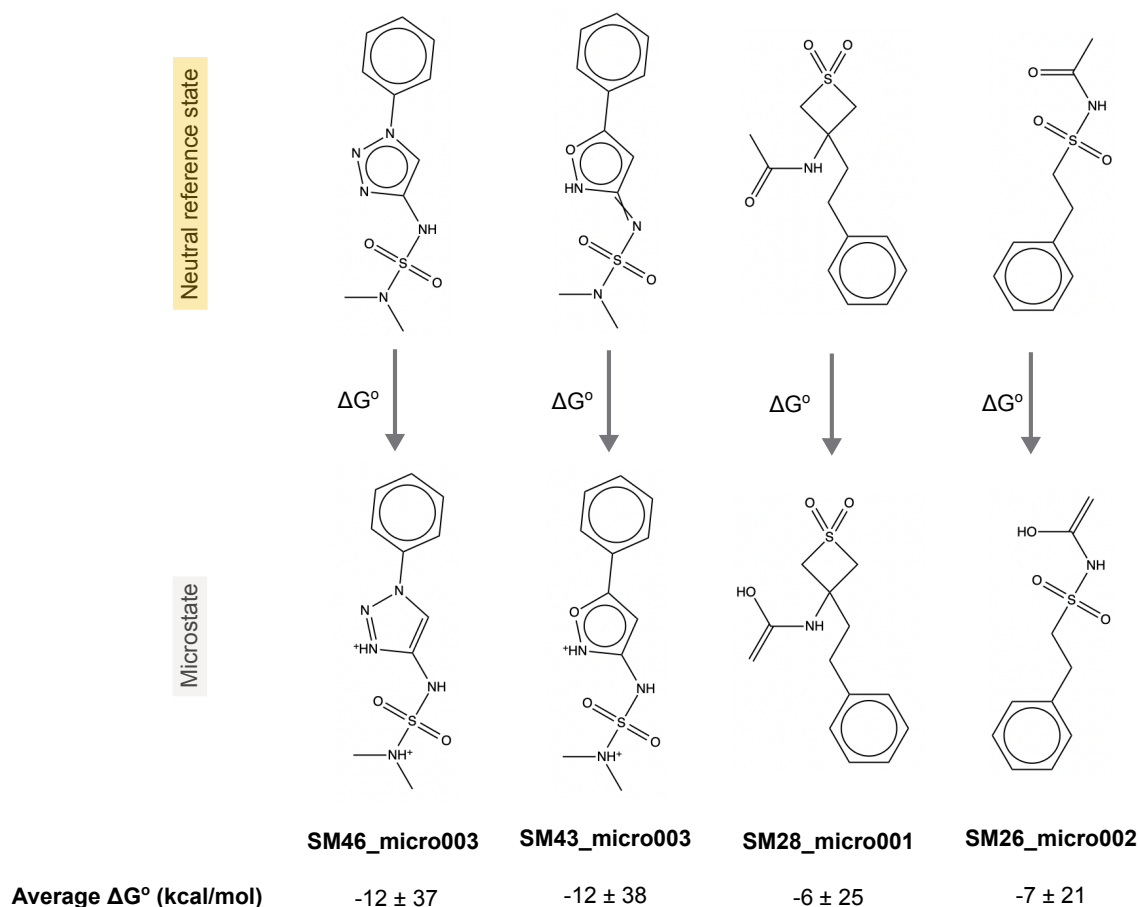


Figure 14. Structures of microstates where relative microstate free energy predictions disagree. Shown are some of the microstate transitions where participants predictions largely disagree with one another, based on Figure 12. The average relative free energy prediction (ΔG) along with the standard deviation are listed under each transition.

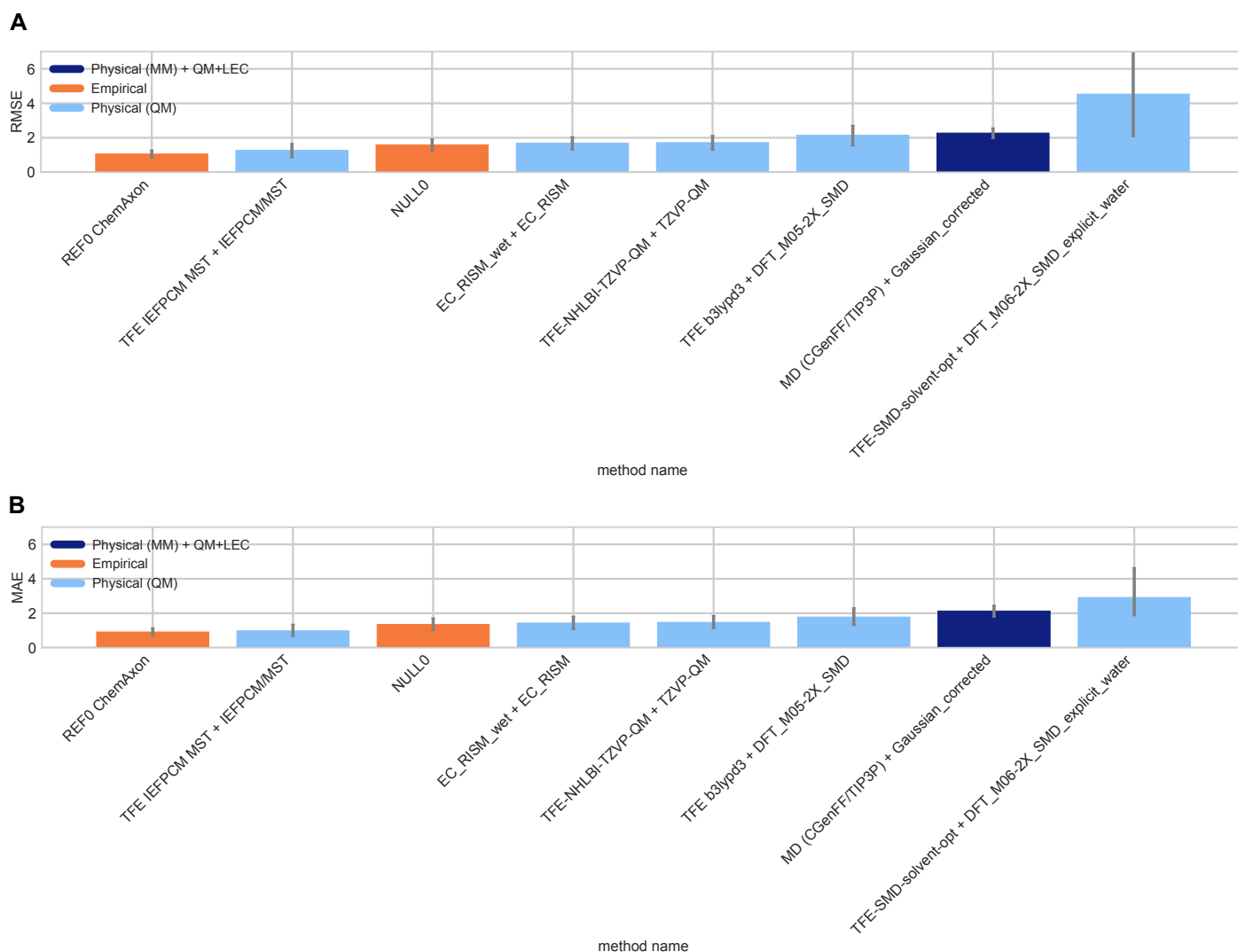


Figure 15. Overall accuracy assessment for $\log D$ estimation. Both root-mean-square error (RMSE) and mean absolute error (MAE) are shown, with error bars denoting 95% confidence intervals obtained by bootstrapping over challenge molecules. *REF00_ChemAxon* [83] is a reference method and *NULL0* is a null method that was included after the blind challenge submission deadline, and all other method names refer to blind predictions. Methods are listed out in Table 5 and statistics calculated for all methods are available in Table S4.

655 submissions had a RMSE below 2 $\log D$ units. Here, eight methods were submitted and half of them achieved a RMSE below 2
 656 $\log D$ units. Overall, $\log D$ prediction accuracy has improved since SAMPL5.

657 When the best $\log P$ and pK_a prediction methods are combined we find that the resulting composite approach outperforms
 658 most of the other ranked methods, achieving a RMSE of 0.6 (see Figure17, method name *TFE MLR + EC_RISM*).

659 When the experimental $\log P$ and pK_a are combined to yield a $\log D$ (as in Section 2.4), the resulting $\log D$ values do not
 660 perfectly match with the reported experimental $\log D$ values, an inconsistency we are currently investigating.

661 3.3.2 A consistently well performing method in $\log D$ estimation

662 For ranked submissions, we identified a single consistently well-performing method that was ranked in the top three according
 663 to RMSE, MAE, Kendall's Tau, and R^2 (all statistics are available in Table S4). The best-performing method was *TFE IEFPCM MST +*
 664 *IEFPCM/MST*, which used a QM-based physical method for pK_a and $\log P$ predictions [93]. The *IEFPCM/MST* model has previously
 665 been used to predict the $\log D$ of over 35 ionizable drugs, where it achieved a RMSE of 1.6 [111], all little worse than a RMSE of
 666 1.3 in SAMPL7. The pK_a prediction protocol used in the challenge is described in Section 3.2.2, where it was ranked among the
 667 consistently well performing pK_a methods.

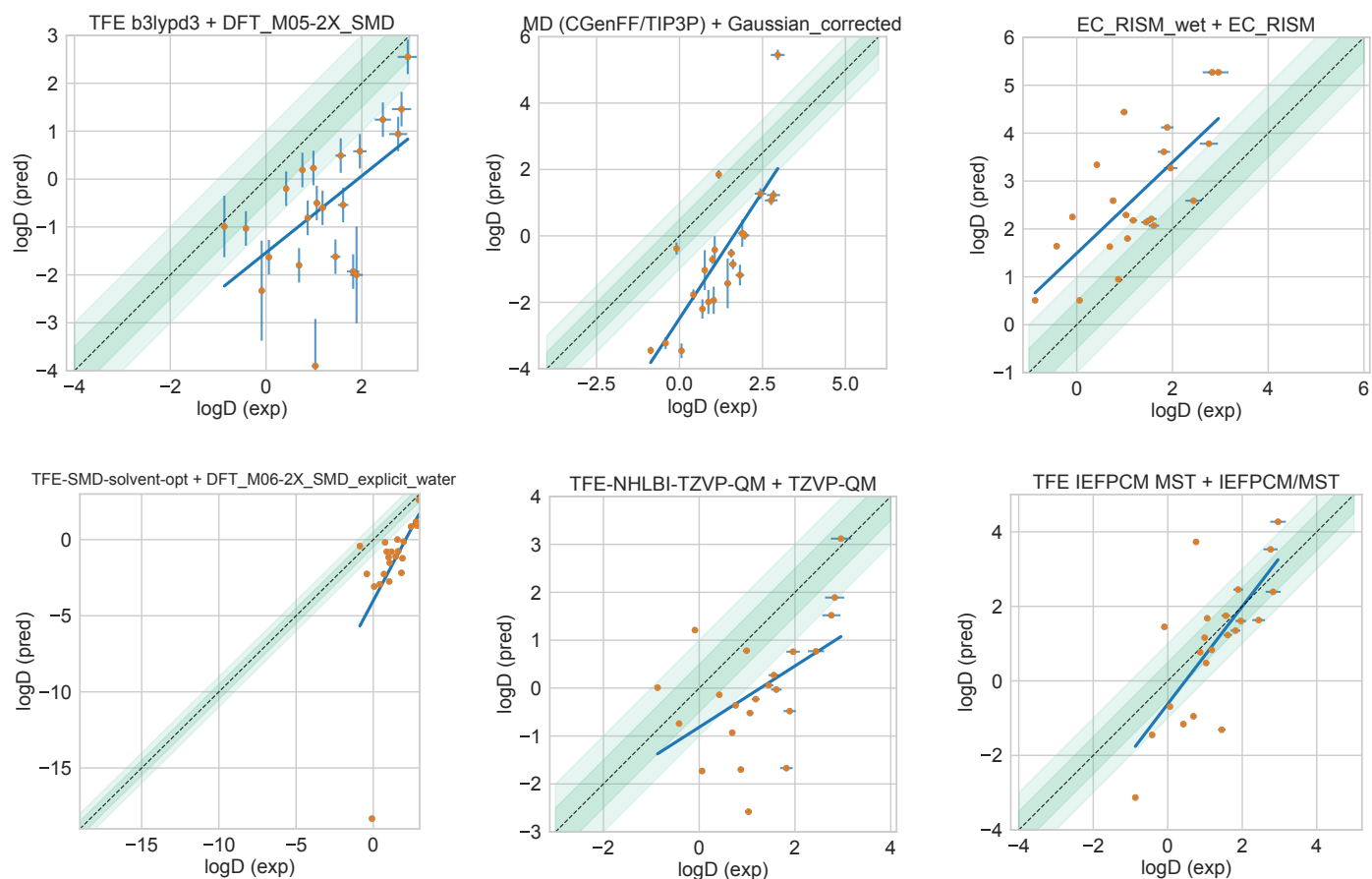


Figure 16. Predicted vs. experimental value correlation plots of all $\log D$ estimation methods in the SAMPL7 challenge. Dark and light green shaded areas indicate 0.5 and 1.0 units of error. Error bars indicate standard error of the mean of predicted and experimental values. Some SEM values are too small to be seen under the data points. Performance statistics of all methods is available in Table S4

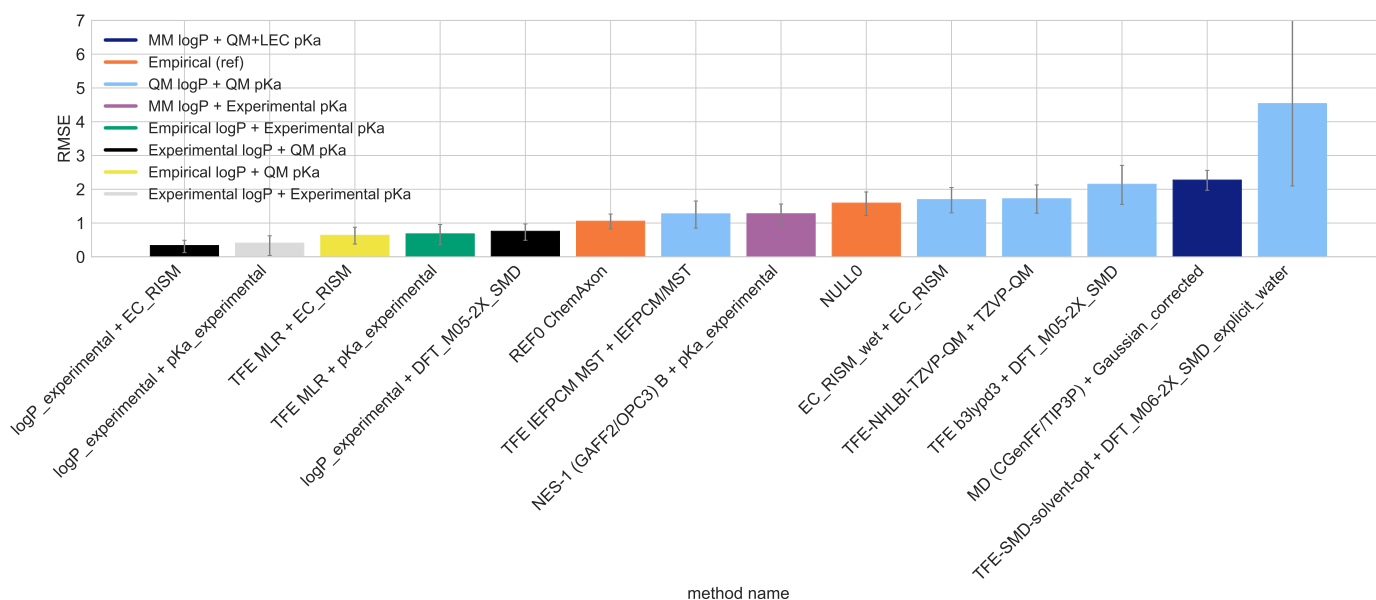


Figure 17. log D values from a combination of the best pK_a and log P are typically superior. Shown is the RMSE in calculated log D values, with error bars denoting 95% confidence intervals from bootstrapping over challenge molecules. This plot is similar to Figure 3.3.1A, except it includes some additional pK_a and log P combinations (for log D estimation). Method *logP_experimental + EC_RISM* combines the experimental log P with the top performing pK_a method (based on RMSE). Method *logP_experimental + pKa_experimental* combines the experimental log P and pK_a value. Method *TFE_MLR + EC_RISM* combines the best performing (based on RMSE) log P and pK_a methods. Method *TFE_MLR + pKa_experimental* combines the best performing (based on RMSE) log P method with the experimental pK_a . Method *logP_experimental + DFT_M05-2X_SMD* combines the experimental log P with an average performing pK_a method. Method *NES-1 (GAFF2/OPC3) B + pKa_experimental* combines a log P method with average performance with the experimental pK_a . All other methods are the same as in Figure 3.3.1A.

4 Conclusions

Here, a community-wide blind prediction challenge was held that focused on partitioning and pK_a for 22 compounds composed of a series of N-acylsulfonamides and related bioisosteres. Participants had the option of submitting predictions for both, or either, challenge.

In the SAMPL7 log P challenge, participants were asked to predict a partition coefficient for each compound between octanol and water and report the result as a transfer free energy. A total of 17 research groups participated, submitting 33 blind submissions total. Many submissions achieved a RMSE around 1.0 or lower for log P predictions, but none were below 0.5 log P units. RMSEs ranged from 0.6 to 4 log P units– 15 methods achieved a RMSE of 1.0 or lower, while a RMSE between 1 and 4 log units was observed for the majority of methods. Many methods achieved an accuracy similar to the null model which had a RMSE of 1.2 and predicted that each compound had a constant log P value of 2.66. A few methods outperformed the null model (4 were empirical and 1 was an QM based method). In general, empirical methods tended to perform better than other methods, which makes sense given the availability of octanol-water log P training data.

Performance in the SAMPL7 log P challenge was poorer than in the SAMPL6 log P challenge. In the SAMPL6 log P challenge, 10 methods achieved a RMSE \leq 0.5 log P units, while here, none did. In general, the SAMPL7 molecules were more flexible, which may have contributed to this accuracy difference. The chemical diversity in the SAMPL6 challenge dataset was limited to 6 molecules with 4-amino quinazoline groups and 2 molecules with a benzimidazole group. The SAMPL7 set was larger and more diverse, thus possibly more challenging.

For ranked submissions, we identified 5 consistently well-performing methods for log P evaluations based on several statistical metrics. These particularly well performing methods included three empirical methods, a QM-based physical method, and a MM-based physical method.

To see if any molecules posed particular challenges, we looked at log P prediction accuracy for each molecule across all methods. Compounds belonging to the isoxazole compound class had higher log P prediction errors. MM-based physical methods tended to make predictions that were less accurate for molecules belonging to the isoxazole compound class compared to QM-based physical and empirical method categories.

692 In the SAMPL7 pK_a challenge, participants predicted free energies for transitions between microstates. Predicted relative
693 free energies were then converted to macroscopic pK_a values in order to compare participants' predictions to experimental pK_a
694 values and calculate performance statistics of predictions. This format allowed us to avoid some of the challenges of matching
695 microscopic transitions to macroscopic pK_a values [43], making analysis more straightforward. As noted above, some matching
696 is still required, but this approach eliminates uncertainty about which transitions are predicted.

697 Macroscopic pK_a evaluations relied on accuracy and correlation metrics. No method achieved a RMSE around 0.5 or lower for
698 macroscopic pK_a predictions for the challenge molecules which means methods did not achieve experimental accuracy, which is
699 likely around 0.5 pK_a units [112]. Methods had RMSE values between 0.7 to 5.4 pK_a units. Compared to the previous SAMPL6 pK_a
700 challenge, accuracy remains roughly the same. Out of all submitted methods in SAMPL7, two methods achieved a RMSE lower
701 than 1 pK_a unit (one of which was a commercially available method that we used as a reference method), while a RMSE between
702 1.8 and 5.4 log units was observed for the majority of methods. In terms of correlation, predictions had R^2 values ranging from
703 0.03 to 0.93 and only two methods achieved an R^2 greater than 0.9.

704 We tested ChemAxon's Chemicalize toolkit [83] as an empirical reference method to make macroscopic pK_a predictions and
705 it performed better than other methods. Excluding the reference method, the two best performing methods across several
706 performance statistics were both QM-based physical methods.

707 For microscopic pK_a , we find that some transitions are much more consistently predicted than others, but in some cases
708 there is broad disagreement even about the sign of the free energy change associated with a particular transition – so methods
709 disagree as to which protonation state or tautomer is preferred at the reference pH. Participants agreed on the sign of predic-
710 tions for roughly 56% of all microstates, while 38% disagreed on sign (predictions were negative or positive). Certain chemical
711 transformations were found to have a high level of disagreement, especially protonation of nitrogens in 1,2,3-triazoles, isoxa-
712 zoles, as well as those in terminal nitrogen groups. Transitions involving keto-enol neutral state tautomerism also often lead to
713 sign disagreement.

714 The current challenge combined log P and pK_a submissions in order to evaluate the current state of log D predictions. In
715 general we find that the accuracy of octanol-water log P predictions in SAMPL7 is higher than that of cyclohexane-water log D
716 predictions in SAMPL5. Half of the methods in the current challenge achieved a RMSE below 2 log D units, while no submis-
717 sions achieved this in the SAMPL5 challenge. Given the abundance of literature octanol-water partitioning and distribution data
718 (compared to cyclohexane-water data in SAMPL5) it makes sense that accuracy would be higher here in SAMPL7 since trained
719 methods (i.e. empirical methods and implicit solvent QM) are impacted by availability of training data.

720 5 Code and Data Availability

721 All SAMPL7 physical property instructions, submissions, experimental data and analysis are available at

722 https://github.com/samplchallenges/SAMPL7/tree/master/physical_property.

723 Figures and supporting material for this paper can be found at

724 <https://github.com/MobleyLab/sampl7-physical-property-challenge-manuscript>. This repository contains graphs and plots from the
725 paper, some of which are available in the main SAMPL7 physical property repository listed directly above, but also includes:

- 726 • A graph that shows the distribution of molecular properties of the 22 compounds from the SAMPL7 physical property blind
727 challenge.
- 728 • Details of MM-based physical methods that made log P predictions.
- 729 • A table that lists additional info for microscopic pK_a predictions. The table lists the: microstate, total number of relative
730 free energy predictions, average relative free energy prediction, average relative free energy prediction STD, Minimum
731 relative free energy prediction, maximum relative free energy prediction, number of (+) sign predictions, number of (-) sign
732 predictions, number of neutral (0) sign predictions, and Shannon entropy (H).
- 733 • A table of the number of states per charge state for the microstates used in the SAMPL7 pK_a challenge.
- 734 • A table of the SAMPL7 molecule ID, compound class, and isomeric SMILES of SAMPL7 physical property challenge molecules.
- 735 • Structures of the molecules in the SAMPL7 physical property challenge grouped by compound class.
- 736 • A figure showing an example of a relative free energy network.
- 737 • A figure showing chemical transformations that repeatedly show up as having large disagreement on the sign of the relative
738 free energy prediction in the pK_a challenge.
- 739 • Structures of microstates where relative microstate free energy predictions disagree for the pK_a challenge.
- 740 • A figure showing the Shannon entropy per microstate transition in the pK_a challenge.

6 Overview of Supplementary Information

Contents of Supplementary Information

- **Table S1** Distribution of molecular properties of the 22 compounds from the SAMPL7 physical property blind challenge.
- **Table S1** Evaluation statistics calculated for all methods in the log P challenge.
- **Table S2** Overall correlation assessment for all methods participating in the SAMPL7 log P challenge.
- **Table S2** Details MM-based physical methods that made log P predictions.
- **Table S3** Evaluation statistics calculated for all methods in the pK_a challenge.
- **Table S5** Additional info for microscopic pK_a predictions.
- **Table S7** Number of states per charge state for the microstates used in the SAMPL7 pK_a challenge.
- **Table S4** Evaluation statistics calculated for all log D estimates.
- **Figure S3** SMILES and compound class of SAMPL7 physical property challenge molecules.
- **Table S6** Compound classes and structures of the molecules in the SAMPL7 physical property challenge.

7 Author Contributions

Conceptualization, TDB, DLM; Methodology, TDB, DLM, MRG, NT, SMK; Software, TDB, JM, YZ, NT; Formal Analysis, TDB; Investigation, TDB, DLM; Resources, DLM; Data Curation, TDB; Writing-Original Draft, TDB, DLM; Writing - Review and Editing, TDB, DLM, JM, SMK; Visualization, TDB, YZ; Supervision, DLM; Project Administration, DLM; Funding Acquisition, DLM, TDB.

8 Acknowledgments

We appreciate Michael Gilson at the University of California of San Diego (UCSD) for making the introduction which made this challenge possible. TDB and DLM gratefully acknowledge support from NIH Grant R01GM124270 supporting the SAMPL Blind challenges. TDB acknowledges and appreciates support from the Association for Computing Machinery's Special Interest Group on High Performance Computing (ACM SIGHPC) and Intel Fellowship. DLM appreciates financial support from the National Institutes of Health (1R01GM124270-01A1) and the National Science Foundation (CHE 1352608). MRG and YZ acknowledge support from the National Science Foundation (MCB-1519640). SMK and NK acknowledge support from the Deutsche Forschungsgemeinschaft (DFG, German Research Foundation) under Germany's Excellence Strategy – EXC-2033 – Projektnummer 390677874, and under the Research Unit FOR 1979. SMK and NK thank the IT and Media Center (ITMC) of the TU Dortmund for computational support.

9 Disclaimers

The content is solely the responsibility of the authors and does not necessarily represent the official views of the National Institutes of Health.

10 Disclosures

David L. Mobley serves on the Scientific Advisory Board of OpenEye Scientific Software and is an Open Science Fellow with Silicon Therapeutics, a subsidiary of Ruyvant.

References

- [1] **Manallack DT**. The pK_a Distribution of Drugs: Application to Drug Discovery. *Perspect Medicin Chem*. 2007 Jan; 1:1177391X0700100. doi: [10.1177/1177391X0700100003](https://doi.org/10.1177/1177391X0700100003).
- [2] **Charifson PS**, Walters WP. Acidic and Basic Drugs in Medicinal Chemistry: A Perspective. *J Med Chem*. 2014 Dec; 57(23):9701–9717. doi: [10.1021/jm501000a](https://doi.org/10.1021/jm501000a).
- [3] **Aguilar B**, Anandakrishnan R, Ruscio JZ, Onufriev AV. Statistics and Physical Origins of pK and Ionization State Changes upon Protein-Ligand Binding. *Biophysical Journal*. 2010 Mar; 98(5):872–880. doi: [10.1016/j.bpj.2009.11.016](https://doi.org/10.1016/j.bpj.2009.11.016).
- [4] **Rupp M**, Korner R, V Tetko I. Predicting the pK_a of Small Molecules. *CCHTS*. 2011 Jun; 14(5):307–327. doi: [10.2174/138620711795508403](https://doi.org/10.2174/138620711795508403).
- [5] **Meanwell NA**. Improving Drug Candidates by Design: A Focus on Physicochemical Properties As a Means of Improving Compound Disposition and Safety. *Chem Res Toxicol*. 2011 Sep; 24(9):1420–1456. doi: [10.1021/tx200211v](https://doi.org/10.1021/tx200211v).

- 783 [6] **Giaginis C**, Tsantili-Kakoulidou A. Alternative Measures of Lipophilicity: From Octanol–Water Partitioning to IAM Retention. *Journal of*
784 *Pharmaceutical Sciences*. 2008 Aug; 97(8):2984–3004. doi: [10.1002/jps.21244](https://doi.org/10.1002/jps.21244).
- 785 [7] **Lang BE**. Solubility of Water in Octan-1-OL from (275 to 369) K. *J Chem Eng Data*. 2012 Aug; 57(8):2221–2226. doi: [10.1021/je3001427](https://doi.org/10.1021/je3001427).
- 786 [8] **Nicholls A**, Mobley DL, Guthrie JP, Chodera JD, Bayly CI, Cooper MD, Pande VS. Predicting Small-Molecule Solvation Free Energies: An
787 Informal Blind Test for Computational Chemistry. *J Med Chem*. 2008 Feb; 51(4):769–779. doi: [10.1021/jm070549+](https://doi.org/10.1021/jm070549+).
- 788 [9] **Guthrie JP**. A Blind Challenge for Computational Solvation Free Energies: Introduction and Overview. *J Phys Chem B*. 2009 Apr;
789 113(14):4501–4507. doi: [10.1021/jp806724u](https://doi.org/10.1021/jp806724u).
- 790 [10] **Mobley DL**, Liu S, Cerutti DS, Swope WC, Rice JE. Alchemical Prediction of Hydration Free Energies for SAMPL. *J Comput Aided Mol Des*.
791 2012 May; 26(5):551–562. doi: [10.1007/s10822-011-9528-8](https://doi.org/10.1007/s10822-011-9528-8).
- 792 [11] **Geballe MT**, Skillman AG, Nicholls A, Guthrie JP, Taylor PJ. The SAMPL2 Blind Prediction Challenge: Introduction and Overview. *J Comput*
793 *Aided Mol Des*. 2010 Apr; 24(4):259–279. doi: [10.1007/s10822-010-9350-8](https://doi.org/10.1007/s10822-010-9350-8).
- 794 [12] **Mobley DL**, Wymer KL, Lim NM, Guthrie JP. Blind Prediction of Solvation Free Energies from the SAMPL4 Challenge. *J Comput Aided Mol*
795 *Des*. 2014 Mar; 28(3):135–150. doi: [10.1007/s10822-014-9718-2](https://doi.org/10.1007/s10822-014-9718-2).
- 796 [13] **Muddana HS**, Fenley AT, Mobley DL, Gilson MK. The SAMPL4 Host–Guest Blind Prediction Challenge: An Overview. *J Comput Aided Mol*
797 *Des*. 2014 Apr; 28(4):305–317. doi: [10.1007/s10822-014-9735-1](https://doi.org/10.1007/s10822-014-9735-1).
- 798 [14] **Yin J**, Henriksen NM, Slochow DR, Shirts MR, Chiu MW, Mobley DL, Gilson MK. Overview of the SAMPL5 Host–Guest Challenge: Are We
799 Doing Better? *J Comput Aided Mol Des*. 2017 Jan; 31(1):1–19. doi: [10.1007/s10822-016-9974-4](https://doi.org/10.1007/s10822-016-9974-4).
- 800 [15] **Rizzi A**, Jensen T, Slochow DR, Aldeghi M, Gapsys V, Ntekoumes D, Bosisio S, Papadourakis M, Henriksen NM, de Groot BL, Cournia Z,
801 Dickson A, Michel J, Gilson MK, Shirts MR, Mobley DL, Chodera JD. The SAMPL6 SAMPLing Challenge: Assessing the Reliability and Efficiency
802 of Binding Free Energy Calculations. *J Comput Aided Mol Des*. 2020 May; 34(5):601–633. doi: [10.1007/s10822-020-00290-5](https://doi.org/10.1007/s10822-020-00290-5).
- 803 [16] **Rizzi A**, Murkli S, McNeill JN, Yao W, Sullivan M, Gilson MK, Chiu MW, Isaacs L, Gibb BC, Mobley DL, Chodera JD. Overview of the SAMPL6
804 Host–Guest Binding Affinity Prediction Challenge. *J Comput Aided Mol Des*. 2018 Oct; 32(10):937–963. doi: [10.1007/s10822-018-0170-6](https://doi.org/10.1007/s10822-018-0170-6).
- 805 [17] **Amezcuca M**, El Khoury L, Mobley DL. SAMPL7 Host–Guest Challenge Overview: Assessing the Reliability of Polarizable and Non-Polarizable
806 Methods for Binding Free Energy Calculations. *J Comput Aided Mol Des*. 2021 Jan; 35(1):1–35. doi: [10.1007/s10822-020-00363-5](https://doi.org/10.1007/s10822-020-00363-5).
- 807 [18] **Muddana HS**, Daniel Varnado C, Bielawski CW, Urbach AR, Isaacs L, Geballe MT, Gilson MK. Blind Prediction of Host–Guest Binding
808 Affinities: A New SAMPL3 Challenge. *J Comput Aided Mol Des*. 2012 May; 26(5):475–487. doi: [10.1007/s10822-012-9554-1](https://doi.org/10.1007/s10822-012-9554-1).
- 809 [19] **Khalak Y**, Tresadern G, de Groot BL, Gapsys V. Non-Equilibrium Approach for Binding Free Energies in Cyclodextrins in SAMPL7: Force
810 Fields and Software. *J Comput Aided Mol Des*. 2021 Jan; 35(1):49–61. doi: [10.1007/s10822-020-00359-1](https://doi.org/10.1007/s10822-020-00359-1).
- 811 [20] **Mobley DL**, Liu S, Lim NM, Wymer KL, Perryman AL, Forli S, Deng N, Su J, Branson K, Olson AJ. Blind Prediction of HIV Integrase Binding
812 from the SAMPL4 Challenge. *J Comput Aided Mol Des*. 2014 Apr; 28(4):327–345. doi: [10.1007/s10822-014-9723-5](https://doi.org/10.1007/s10822-014-9723-5).
- 813 [21] **Benson ML**, Faver JC, Ucisik MN, Dashti DS, Zheng Z, Merz KM. Prediction of Trypsin/Molecular Fragment Binding Affinities by Free Energy
814 Decomposition and Empirical Scores. *J Comput Aided Mol Des*. 2012 May; 26(5):647–659. doi: [10.1007/s10822-012-9567-9](https://doi.org/10.1007/s10822-012-9567-9).
- 815 [22] **Galicchio E**, Deng N, He P, Wickstrom L, Perryman AL, Santiago DN, Forli S, Olson AJ, Levy RM. Virtual Screening of Integrase Inhibitors
816 by Large Scale Binding Free Energy Calculations: The SAMPL4 Challenge. *J Comput Aided Mol Des*. 2014 Apr; 28(4):475–490. doi:
817 [10.1007/s10822-014-9711-9](https://doi.org/10.1007/s10822-014-9711-9).
- 818 [23] **Hogues H**, Sulea T, Purisima EO. Exhaustive Docking and Solvated Interaction Energy Scoring: Lessons Learned from the SAMPL4 Chal-
819 lenge. *J Comput Aided Mol Des*. 2014 Apr; 28(4):417–427. doi: [10.1007/s10822-014-9715-5](https://doi.org/10.1007/s10822-014-9715-5).
- 820 [24] **Kulp JL**, Blumenthal SN, Wang Q, Bryan RL, Guarnieri F. A Fragment-Based Approach to the SAMPL3 Challenge. *J Comput Aided Mol Des*.
821 2012 May; 26(5):583–594. doi: [10.1007/s10822-012-9546-1](https://doi.org/10.1007/s10822-012-9546-1).
- 822 [25] **Kumar A**, Zhang KYJ. Computational Fragment-Based Screening Using RosettaLigand: The SAMPL3 Challenge. *J Comput Aided Mol Des*.
823 2012 May; 26(5):603–616. doi: [10.1007/s10822-011-9523-0](https://doi.org/10.1007/s10822-011-9523-0).
- 824 [26] **Deng N**, Forli S, He P, Perryman A, Wickstrom L, Vijayan RSK, Tiefenbrunn T, Stout D, Gallicchio E, Olson AJ, Levy RM. Distinguishing
825 Binders from False Positives by Free Energy Calculations: Fragment Screening Against the Flap Site of HIV Protease. *J Phys Chem B*. 2015
826 Jan; 119(3):976–988. doi: [10.1021/jp506376z](https://doi.org/10.1021/jp506376z).
- 827 [27] **Işik M**, Levorse D, Rustenburg AS, Ndukwe IE, Wang H, Wang X, Reibarkh M, Martin GE, Makarov AA, Mobley DL, Rhodes T, Chodera JD.
828 pKa Measurements for the SAMPL6 Prediction Challenge for a Set of Kinase Inhibitor-like Fragments. *J Comput Aided Mol Des*. 2018 Oct;
829 32(10):1117–1138. doi: [10.1007/s10822-018-0168-0](https://doi.org/10.1007/s10822-018-0168-0).

- 830 [28] **Selwa E**, Kenney IM, Beckstein O, Iorga BI. SAMPL6: Calculation of Macroscopic pKa Values from Ab Initio Quantum Mechanical Free
831 Energies. *J Comput Aided Mol Des.* 2018 Oct; 32(10):1203–1216. doi: [10.1007/s10822-018-0138-6](https://doi.org/10.1007/s10822-018-0138-6).
- 832 [29] **Bannan CC**, Mobley DL, Skillman AG. SAMPL6 Challenge Results from pK_a Predictions Based on a General Gaussian Process Model.
833 *J Comput Aided Mol Des.* 2018 Oct; 32(10):1165–1177. doi: [10.1007/s10822-018-0169-z](https://doi.org/10.1007/s10822-018-0169-z).
- 834 [30] **Zeng Q**, Jones MR, Brooks BR. Absolute and Relative pKa Predictions via a DFT Approach Applied to the SAMPL6 Blind Challenge. *J Comput*
835 *Aided Mol Des.* 2018 Oct; 32(10):1179–1189. doi: [10.1007/s10822-018-0150-x](https://doi.org/10.1007/s10822-018-0150-x).
- 836 [31] **Tielker N**, Eberlein L, Güssregen S, Kast SM. The SAMPL6 Challenge on Predicting Aqueous pKa Values from EC-RISM Theory. *J Comput*
837 *Aided Mol Des.* 2018 Oct; 32(10):1151–1163. doi: [10.1007/s10822-018-0140-z](https://doi.org/10.1007/s10822-018-0140-z).
- 838 [32] **Pracht P**, Wilcken R, Udvarhelyi A, Rodde S, Grimme S. High Accuracy Quantum-Chemistry-Based Calculation and Blind Prediction
839 of Macroscopic pKa Values in the Context of the SAMPL6 Challenge. *J Comput Aided Mol Des.* 2018 Oct; 32(10):1139–1149. doi:
840 [10.1007/s10822-018-0145-7](https://doi.org/10.1007/s10822-018-0145-7).
- 841 [33] **Prasad S**, Huang J, Zeng Q, Brooks BR. An Explicit-Solvent Hybrid QM and MM Approach for Predicting pKa of Small Molecules in SAMPL6
842 Challenge. *J Comput Aided Mol Des.* 2018 Oct; 32(10):1191–1201. doi: [10.1007/s10822-018-0167-1](https://doi.org/10.1007/s10822-018-0167-1).
- 843 [34] **Bannan CC**, Burley KH, Chiu M, Shirts MR, Gilson MK, Mobley DL. Blind Prediction of Cyclohexane–Water Distribution Coefficients from
844 the SAMPL5 Challenge. *J Comput Aided Mol Des.* 2016 Nov; 30(11):927–944. doi: [10.1007/s10822-016-9954-8](https://doi.org/10.1007/s10822-016-9954-8).
- 845 [35] **Rustenburg AS**, Dancer J, Lin B, Feng JA, Ortwine DF, Mobley DL, Chodera JD. Measuring Experimental Cyclohexane-Water Distribution
846 Coefficients for the SAMPL5 Challenge. *J Comput Aided Mol Des.* 2016 Nov; 30(11):945–958. doi: [10.1007/s10822-016-9971-7](https://doi.org/10.1007/s10822-016-9971-7).
- 847 [36] **Kamath G**, Kurnikov I, Fain B, Leontyev I, Illarionov A, Butin O, Olevanov M, Pereyaslavets L. Prediction of Cyclohexane-Water Distribution
848 Coefficient for SAMPL5 Drug-like Compounds with the QMPFF3 and ARROW Polarizable Force Fields. *J Comput Aided Mol Des.* 2016 Nov;
849 30(11):977–988. doi: [10.1007/s10822-016-9958-4](https://doi.org/10.1007/s10822-016-9958-4).
- 850 [37] **Klamt A**, Eckert F, Reinisch J, Wichmann K. Prediction of Cyclohexane-Water Distribution Coefficients with COSMO-RS on the SAMPL5 Data
851 Set. *J Comput Aided Mol Des.* 2016 Nov; 30(11):959–967. doi: [10.1007/s10822-016-9927-y](https://doi.org/10.1007/s10822-016-9927-y).
- 852 [38] **Işık M**, Bergazin TD, Fox T, Rizzi A, Chodera JD, Mobley DL. Assessing the Accuracy of Octanol–Water Partition Coefficient Predictions in
853 the SAMPL6 Part II Log P Challenge. *J Comput Aided Mol Des.* 2020 Apr; 34(4):335–370. doi: [10.1007/s10822-020-00295-0](https://doi.org/10.1007/s10822-020-00295-0).
- 854 [39] **Fan S**, Iorga BI, Beckstein O. Prediction of Octanol-Water Partition Coefficients for the SAMPL6- $\log P$ Molecules Using Molecu-
855 lar Dynamics Simulations with OPLS-AA, AMBER and CHARMM Force Fields. *J Comput Aided Mol Des.* 2020 May; 34(5):543–560. doi:
856 [10.1007/s10822-019-00267-z](https://doi.org/10.1007/s10822-019-00267-z).
- 857 [40] **Zamora WJ**, Pinheiro S, German K, Ràfols C, Curutchet C, Luque FJ. Prediction of the N-Octanol/Water Partition Coefficients in the SAMPL6
858 Blind Challenge from MST Continuum Solvation Calculations. *J Comput Aided Mol Des.* 2020 Apr; 34(4):443–451. doi: [10.1007/s10822-019-00262-4](https://doi.org/10.1007/s10822-019-00262-4).
- 859 [41] **Jones MR**, Brooks BR. Quantum Chemical Predictions of Water–Octanol Partition Coefficients Applied to the SAMPL6 logP Blind Challenge.
860 *J Comput Aided Mol Des.* 2020 May; 34(5):485–493. doi: [10.1007/s10822-020-00286-1](https://doi.org/10.1007/s10822-020-00286-1).
- 862 [42] **Pickard FC**, König G, Tofoleanu F, Lee J, Simmonett AC, Shao Y, Ponder JW, Brooks BR. Blind Prediction of Distribution in the SAMPL5
863 Challenge with QM Based Protomer and pKa Corrections. *J Comput Aided Mol Des.* 2016 Nov; 30(11):1087–1100. doi: [10.1007/s10822-016-9955-7](https://doi.org/10.1007/s10822-016-9955-7).
- 864 [43] **Işık M**, Rustenburg AS, Rizzi A, Gunner MR, Mobley DL, Chodera JD. Overview of the SAMPL6 pKa Challenge: Evaluating Small Molecule
865 Microscopic and Macroscopic pKa Predictions. *J Comput Aided Mol Des.* 2021 Feb; 35(2):131–166. doi: [10.1007/s10822-020-00362-6](https://doi.org/10.1007/s10822-020-00362-6).
- 866 [44] **Işık M**, Levorse D, Mobley DL, Rhodes T, Chodera JD. Octanol–Water Partition Coefficient Measurements for the SAMPL6 Blind Prediction
867 Challenge. *J Comput Aided Mol Des.* 2020 Apr; 34(4):405–420. doi: [10.1007/s10822-019-00271-3](https://doi.org/10.1007/s10822-019-00271-3).
- 869 [45] ACD/pKa Classic (ACD/Percepta Kernel v1.6). Advanced Chem-istry Development, Inc., Toronto, ON, Canada, 2018.;. <https://www.acdlabs.com/products/percepta/predictors/pKa/>.
- 870 [46] **Shelley JC**, Cholleti A, Frye LL, Greenwood JR, Timlin MR, Uchimaya M. Epik: A Software Program for pKa Prediction and Protonation State
871 Generation for Drug-like Molecules. *J Comput Aided Mol Des.* 2007 Dec; 21(12):681–691. doi: [10.1007/s10822-007-9133-z](https://doi.org/10.1007/s10822-007-9133-z).
- 872 [47] MoKa; Molecular Discovery, Hertfordshire, UK, 2018.;. <https://www.moldiscovery.com/software/moka/>.
- 873 [48] Simulations Plus ADMET Predictor v8.5; Simulations Plus, Lancaster, CA, 2018.;. <https://www.simulations-plus.com/software/admetpredictor/physicochemical-biopharmaceutical/>.
- 874
875

- 876 [49] **Tissandier MD**, Cowen KA, Feng WY, Gundlach E, Cohen MH, Earhart AD, Coe JV, Tuttle TR. The Proton's Absolute Aqueous Enthalpy and
877 Gibbs Free Energy of Solvation from Cluster-Ion Solvation Data. *J Phys Chem A*. 1998 Oct; 102(40):7787–7794. doi: [10.1021/jp982638r](https://doi.org/10.1021/jp982638r).
- 878 [50] **Klamt A**, Eckert F, Diedenhofen M, Beck ME. First Principles Calculations of Aqueous pK_a Values for Organic and Inorganic Acids Using
879 COSMO-RS Reveal an Inconsistency in the Slope of the pK_a Scale. *J Phys Chem A*. 2003 Nov; 107(44):9380–9386. doi: [10.1021/jp034688o](https://doi.org/10.1021/jp034688o).
- 880 [51] **Alongi KS**, Shields GC. Theoretical Calculations of Acid Dissociation Constants: A Review Article. In: *Annual Reports in Computational*
881 *Chemistry*, vol. 6 Elsevier; 2010.p. 113–138. doi: [10.1016/S1574-1400\(10\)06008-1](https://doi.org/10.1016/S1574-1400(10)06008-1).
- 882 [52] **Liao C**, Nicklaus MC. Comparison of Nine Programs Predicting pK_a Values of Pharmaceutical Substances. *J Chem Inf Model*. 2009 Dec;
883 49(12):2801–2812. doi: [10.1021/ci900289x](https://doi.org/10.1021/ci900289x).
- 884 [53] **Bochevarov AD**, Watson MA, Greenwood JR, Philipp DM. Multiconformation, Density Functional Theory-Based pK_a Prediction in Appli-
885 cation to Large, Flexible Organic Molecules with Diverse Functional Groups. *J Chem Theory Comput*. 2016 Dec; 12(12):6001–6019. doi:
886 [10.1021/acs.jctc.6b00805](https://doi.org/10.1021/acs.jctc.6b00805).
- 887 [54] **Tielker N**, Eberlein L, Chodun C, Güssregen S, Kast SM. pK_a Calculations for Tautomerizable and Conformationally Flexible Molecules:
888 Partition Function vs. State Transition Approach. *J Mol Model*. 2019 May; 25(5):139. doi: [10.1007/s00894-019-4033-4](https://doi.org/10.1007/s00894-019-4033-4).
- 889 [55] **Gunner MR**, Murakami T, Rustenburg AS, Işık M, Chodera JD. Standard State Free Energies, Not pK_a s, Are Ideal for Describing Small
890 Molecule Protonation and Tautomeric States. *J Comput Aided Mol Des*. 2020 May; 34(5):561–573. doi: [10.1007/s10822-020-00280-7](https://doi.org/10.1007/s10822-020-00280-7).
- 891 [56] **Marenich AV**, Cramer CJ, Truhlar DG. Universal Solvation Model Based on Solute Electron Density and on a Continuum Model of the
892 Solvent Defined by the Bulk Dielectric Constant and Atomic Surface Tensions. *J Phys Chem B*. 2009 May; 113(18):6378–6396. doi:
893 [10.1021/jp810292n](https://doi.org/10.1021/jp810292n).
- 894 [57] **Marenich AV**, Cramer CJ, Truhlar DG. Generalized Born Solvation Model SM12. *J Chem Theory Comput*. 2013 Jan; 9(1):609–620. doi:
895 [10.1021/ct300900e](https://doi.org/10.1021/ct300900e).
- 896 [58] **Loschen C**, Reinisch J, Klamt A. COSMO-RS Based Predictions for the SAMPL6 logP Challenge. *Journal of Computer-Aided Molecular Design*.
897 2019 Nov; doi: [10.1007/s10822-019-00259-z](https://doi.org/10.1007/s10822-019-00259-z).
- 898 [59] **Klamt A**, Eckert F, Diedenhofen M. Prediction of the Free Energy of Hydration of a Challenging Set of Pesticide-Like Compounds. *J Phys*
899 *Chem B*. 2009 Apr; 113(14):4508–4510. doi: [10.1021/jp805853y](https://doi.org/10.1021/jp805853y).
- 900 [60] **Klamt A**. Conductor-like Screening Model for Real Solvents: A New Approach to the Quantitative Calculation of Solvation Phenomena. *J*
901 *Phys Chem*. 1995 Feb; 99(7):2224–2235. doi: [10.1021/j100007a062](https://doi.org/10.1021/j100007a062).
- 902 [61] **Klamt A**, Jonas V, Bürger T, Lohrenz JCW. Refinement and Parametrization of COSMO-RS. *J Phys Chem A*. 1998 Jun; 102(26):5074–5085.
903 doi: [10.1021/jp980017s](https://doi.org/10.1021/jp980017s).
- 904 [62] **Li H**, Chowdhary J, Huang L, He X, Mackerell AD, Roux B. Drude Polarizable Force Field for Molecular Dynamics Simulations of Saturated
905 and Unsaturated Zwitterionic Lipids. *J Chem Theory Comput*. 2017 Sep; 13(9):4535–4552. doi: [10.1021/acs.jctc.7b00262](https://doi.org/10.1021/acs.jctc.7b00262).
- 906 [63] **Kamath G**, Kurnikov I, Fain B, Leontyev I, Illarionov A, Butin O, Olevanov M, Pereyaslavets L. Prediction of Cyclohexane-Water Distribution
907 Coefficient for SAMPL5 Drug-like Compounds with the QMPFF3 and ARROW Polarizable Force Fields. *J Comput Aided Mol Des*. 2016 Nov;
908 30(11):977–988. doi: [10.1007/s10822-016-9958-4](https://doi.org/10.1007/s10822-016-9958-4).
- 909 [64] **Wang J**, Wolf RM, Caldwell JW, Kollman PA, Case DA. Development and Testing of a General Amber Force Field. *J Comput Chem*. 2004 Jul;
910 25(9):1157–1174. doi: [10.1002/jcc.20035](https://doi.org/10.1002/jcc.20035).
- 911 [65] **Vassetz D**, Pagliai M, Procacci P. Assessment of GAFF2 and OPLS-AA General Force Fields in Combination with the Water Models TIP3P,
912 SPCE, and OPC3 for the Solvation Free Energy of Druglike Organic Molecules. *Journal of Chemical Theory and Computation*. 2019 Mar;
913 15(3):1983–1995. doi: [10.1021/acs.jctc.8b01039](https://doi.org/10.1021/acs.jctc.8b01039).
- 914 [66] **Vanommeslaeghe K**, Hatcher E, Acharya C, Kundu S, Zhong S, Shim J, Darian E, Guvench O, Lopes P, Vorobyov I, Mackerell AD. CHARMM
915 General Force Field: A Force Field for Drug-like Molecules Compatible with the CHARMM All-Atom Additive Biological Force Fields. *J Comput*
916 *Chem*. 2009; p. NA–NA. doi: [10.1002/jcc.21367](https://doi.org/10.1002/jcc.21367).
- 917 [67] **Dodda LS**, Cabeza de Vaca I, Tirado-Rives J, Jorgensen WL. LigParGen Web Server: An Automatic OPLS-AA Parameter Generator for Organic
918 Ligands. *Nucleic Acids Research*. 2017 Jul; 45(W1):W331–W336. doi: [10.1093/nar/gkx312](https://doi.org/10.1093/nar/gkx312).
- 919 [68] **Jorgensen WL**, Chandrasekhar J, Madura JD, Impey RW, Klein ML. Comparison of Simple Potential Functions for Simulating Liquid Water.
920 *The Journal of Chemical Physics*. 1983 Jul; 79(2):926–935. doi: [10.1063/1.445869](https://doi.org/10.1063/1.445869).
- 921 [69] **Izadi S**, Onufriev AV. Accuracy Limit of Rigid 3-Point Water Models. *The Journal of Chemical Physics*. 2016 Aug; 145(7):074501. doi:
922 [10.1063/1.4960175](https://doi.org/10.1063/1.4960175).

- 923 [70] **Işık M**, Bergazin TD, Fox T, Rizzi A, Chodera JD, Mobley DL. Assessing the Accuracy of Octanol–Water Partition Coefficient Predictions in
924 the SAMPL6 Part II Log P Challenge. *J Comput Aided Mol Des.* 2020 Apr; 34(4):335–370. doi: [10.1007/s10822-020-00295-0](https://doi.org/10.1007/s10822-020-00295-0).
- 925 [71] **Procacci P**, Cardelli C. Fast Switching Alchemical Transformations in Molecular Dynamics Simulations. *J Chem Theory Comput.* 2014 Jul;
926 10(7):2813–2823. doi: [10.1021/ct500142c](https://doi.org/10.1021/ct500142c).
- 927 [72] **Jarzynski C**. Nonequilibrium Equality for Free Energy Differences. *Phys Rev Lett.* 1997 Apr; 78(14):2690–2693. doi: [10.1103/Phys-
928 RevLett.78.2690](https://doi.org/10.1103/PhysRevLett.78.2690).
- 929 [73] **Zwanzig RW**. High-Temperature Equation of State by a Perturbation Method. I. Nonpolar Gases. *The Journal of Chemical Physics.* 1954
930 Aug; 22(8):1420–1426. doi: [10.1063/1.1740409](https://doi.org/10.1063/1.1740409).
- 931 [74] **Kirkwood JG**. Statistical Mechanics of Fluid Mixtures. *The Journal of Chemical Physics.* 1935 May; 3(5):300–313. doi: [10.1063/1.1749657](https://doi.org/10.1063/1.1749657).
- 932 [75] **Bennett CH**. Efficient Estimation of Free Energy Differences from Monte Carlo Data. *Journal of Computational Physics.* 1976 Oct; 22(2):245–
933 268. doi: [10.1016/0021-9991\(76\)90078-4](https://doi.org/10.1016/0021-9991(76)90078-4).
- 934 [76] **Shirts MR**, Chodera JD. Statistically Optimal Analysis of Samples from Multiple Equilibrium States. *J Chem Phys.* 2008 Sep; 129(12):124105.
935 doi: [10.1063/1.2978177](https://doi.org/10.1063/1.2978177).
- 936 [77] **Prasad S**, Brooks BR. A Deep Learning Approach for the Blind logP Prediction in SAMPL6 Challenge. *J Comput Aided Mol Des.* 2020 May;
937 34(5):535–542. doi: [10.1007/s10822-020-00292-3](https://doi.org/10.1007/s10822-020-00292-3).
- 938 [78] **Schroeter TS**, Schwaighofer A, Mika S, Ter Laak A, Suelzle D, Ganzer U, Heinrich N, Müller KR. Predicting Lipophilicity of Drug-Discovery
939 Molecules Using Gaussian Process Models. *ChemMedChem.* 2007 Sep; 2(9):1265–1267. doi: [10.1002/cmdc.200700041](https://doi.org/10.1002/cmdc.200700041).
- 940 [79] **Işık M**, Bergazin TD, Fox T, Rizzi A, Chodera JD, Mobley DL. Assessing the Accuracy of Octanol–Water Partition Coefficient Predictions in
941 the SAMPL6 Part II Log P Challenge. *J Comput Aided Mol Des.* 2020 Apr; 34(4):335–370. doi: [10.1007/s10822-020-00295-0](https://doi.org/10.1007/s10822-020-00295-0).
- 942 [80] **Francisco KR**, Varricchio C, Paniak TJ, Kozłowski MC, Brancale A, Ballatore C. Structure Property Relationships of N-Acylsulfonamides and
943 Related Bioisosteres. *European Journal of Medicinal Chemistry.* 2021 Mar; p. 113399. doi: [10.1016/j.ejmech.2021.113399](https://doi.org/10.1016/j.ejmech.2021.113399).
- 944 [81] RDKit: Open-source cheminformatics;. <http://www.rdkit.org>.
- 945 [82] Quacpac Toolkit 2020.2.0 OpenEye Scientific Software, Santa Fe, NM;. <http://www.eyesopen.com>.
- 946 [83] Chemicalize Toolkit: Property and structure calculator, accessed 2020. Developed by ChemAxon;. <https://chemicalize.com/>.
- 947 [84] **Greenwood JR**, Calkins D, Sullivan AP, Shelley JC. Towards the Comprehensive, Rapid, and Accurate Prediction of the Favorable Tautomeric
948 States of Drug-like Molecules in Aqueous Solution. *J Comput Aided Mol Des.* 2010 Jun; 24(6-7):591–604. doi: [10.1007/s10822-010-9349-1](https://doi.org/10.1007/s10822-010-9349-1).
- 949 [85] **Tielker N**, Tomazic D, Heil J, Kloss T, Ehrhart S, Güssregen S, Schmidt KF, Kast SM. The SAMPL5 Challenge for Embedded-Cluster Integral
950 Equation Theory: Solvation Free Energies, Aqueous pK a, and Cyclohexane–Water Log D. *J Comput Aided Mol Des.* 2016 Nov; 30(11):1035–
951 1044. doi: [10.1007/s10822-016-9939-7](https://doi.org/10.1007/s10822-016-9939-7).
- 952 [86] **Tielker N**, Eberlein L, Hessler G, Schmidt KF, Güssregen S, Kast SM. Quantum–Mechanical Property Prediction of Solvated Drug Molecules:
953 What Have We Learned from a Decade of SAMPL Blind Prediction Challenges? *J Comput Aided Mol Des.* 2021 Apr; 35(4):453–472. doi:
954 [10.1007/s10822-020-00347-5](https://doi.org/10.1007/s10822-020-00347-5).
- 955 [87] **Bannan CC**, Burley KH, Chiu M, Shirts MR, Gilson MK, Mobley DL. Blind Prediction of Cyclohexane–Water Distribution Coefficients from
956 the SAMPL5 Challenge. *J Comput Aided Mol Des.* 2016 Nov; 30(11):927–944. doi: [10.1007/s10822-016-9954-8](https://doi.org/10.1007/s10822-016-9954-8).
- 957 [88] **Bannan CC**, Burley KH, Chiu M, Shirts MR, Gilson MK, Mobley DL. Blind Prediction of Cyclohexane–Water Distribution Coefficients from
958 the SAMPL5 Challenge. *J Comput Aided Mol Des.* 2016 Nov; 30(11):927–944. doi: [10.1007/s10822-016-9954-8](https://doi.org/10.1007/s10822-016-9954-8).
- 959 [89] **Donyapour N**, Dickson A. Predicting partition coefficients for the SAMPL7 physical property challenge using the ClassicalGSG method.
960 *Journal of Computer-Aided Molecular Design.* 2021; .
- 961 [90] **Perez KL**, Pinheiro S, Zamora W. Multiple Linear Regression Models for Predicting the n-Octanol/Water Partition Coefficients in the SAMPL7
962 Blind Challenge. *Journal of Computer-Aided Molecular Design.* 2021; .
- 963 [91] **Lenselink EB**, Stouten PFW. Multitask machine learning models for predicting lipophilicity (logP). *Journal of Computer-Aided Molecular
964 Design.* 2021; .
- 965 [92] **Warnau J**, Wichmann K, Reinisch J. COSMO-RS predictions of LogP in the SAMPL7 blind challenge. *Journal of Computer-Aided Molecular
966 Design.* 2021; .

- 967 [93] **Viayna A**, Pinheiro S, Curutchet C, Luque FJ, Zamora WJ. Prediction of n-octanol/water partition coefficients and acidity constants (pKa) in
968 the SAMPL7 blind challenge with the IEFFPCM-MST model. *Journal of Computer-Aided Molecular Design*. 2021; .
- 969 [94] **Fan S**, Nedev H, Vijayan R, Iorga BI, Beckstein O. Precise force-field-based calculations of octanol-water partition coefficients for the
970 SAMPL7 molecules. *Journal of Computer-Aided Molecular Design*. 2021; .
- 971 [95] **Tielker N**, Güssregen S, Kast SM. SAMPL7 physical property prediction from EC-RISM theory. *Journal of Computer-Aided Molecular Design*.
972 2021; .
- 973 [96] **Falcioni F**, Kalayan J, Henchman R. Energy-Entropy Prediction of Octanol-Water LogP of SAMPL7 N-Acyl Sulfonamide Bioisosters. *Journal*
974 *of Computer-Aided Molecular Design*. 2021; .
- 975 [97] **Findik BK**, Haslak ZP, Arslan E, Aviyente V. SAMPL7 Blind Challenge: Quantum-Mechanical Prediction of Partition Coefficients and Acid
976 Dissociation Constants for Small Drug-like Molecules. *Journal of Computer-Aided Molecular Design*. 2021; .
- 977 [98] **Kim S**, Chen J, Cheng T, Gindulyte A, He J, He S, Li Q, Shoemaker BA, Thiessen PA, Yu B, Zaslavsky L, Zhang J, Bolton EE. PubChem in 2021:
978 New Data Content and Improved Web Interfaces. *Nucleic Acids Research*. 2021 Jan; 49(D1):D1388–D1395. doi: 10.1093/nar/gkaa971.
- 979 [99] DrugBank: Online database of drug and drug target information;. <https://www.drugbank.com/>.
- 980 [100] **O'Boyle NM**, Banck M, James CA, Morley C, Vandermeersch T, Hutchison GR. Open Babel: An Open Chemical Toolbox. *J Cheminformatics*.
981 2011 Oct; 3:33. doi: 10.1186/1758-2946-3-33.
- 982 [101] Chemprop: Directed message passing neural network;. <https://chemprop.readthedocs.io/en/latest/>.
- 983 [102] **Yang K**, Swanson K, Jin W, Coley C, Eiden P, Gao H, Guzman-Perez A, Hopper T, Kelley B, Mathea M, Palmer A, Settels V, Jaakkola T, Jensen
984 K, Barzilay R. Analyzing Learned Molecular Representations for Property Prediction. *J Chem Inf Model*. 2019 Aug; 59(8):3370–3388. doi:
985 10.1021/acs.jcim.9b00237.
- 986 [103] COSMOquick: COSMO-RS based toolbox;. [https://www.3ds.com/products-services/biovia/products/molecular-modeling-simulation/
987 solvation-chemistry/cosmoquick/](https://www.3ds.com/products-services/biovia/products/molecular-modeling-simulation/solvation-chemistry/cosmoquick/).
- 988 [104] COSMOconf: A flexible conformer generator for COSMO-RS;. [https://www.3ds.com/products-services/biovia/products/
989 molecular-modeling-simulation/solvation-chemistry/cosmoconf/](https://www.3ds.com/products-services/biovia/products/molecular-modeling-simulation/solvation-chemistry/cosmoconf/).
- 990 [105] **Balasubramani SG**, Chen GP, Coriani S, Diedenhofen M, Frank MS, Franzke YJ, Furche F, Grotjahn R, Harding ME, Hättig C, Hellweg A,
991 Helmich-Paris B, Holzer C, Huniar U, Kaupp M, Marefat Khah A, Karbalaeei Khani S, Müller T, Mack F, Nguyen BD, et al. TURBOMOLE:
992 Modular Program Suite for *Ab Initio* Quantum-Chemical and Condensed-Matter Simulations. *J Chem Phys*. 2020 May; 152(18):184107. doi:
993 10.1063/5.0004635.
- 994 [106] TURBOMOLE V7.5. University of Karlsruhe and Forschungszentrum Karlsruhe GmbH, 1989-2007, TURBOMOLE GmbH, since 2007;. [https:
995 //www.turbomole.org](https://www.turbomole.org/).
- 996 [107] BIOVIA COSMOtherm: Tool for predictive property calculation of liquids. Version 2020. Dassault Systemes;. [https://www.3ds.com/
997 products-services/biovia/products/molecular-modeling-simulation/solvation-chemistry/cosmotherm/](https://www.3ds.com/products-services/biovia/products/molecular-modeling-simulation/solvation-chemistry/cosmotherm/).
- 998 [108] **Miteva MA**, Guyon F, Tuffery P. Frog2: Efficient 3D Conformation Ensemble Generator for Small Compounds. *Nucleic Acids Research*.
999 2010 Jul; 38(Web Server):W622–W627. doi: 10.1093/nar/gkq325.
- 1000 [109] Frog v2.14: FRee On line druG conformation generation;. <https://bioserv.rpbs.univ-paris-diderot.fr/services/Frog2/>.
- 1001 [110] **Brown TN**, Mora-Diez N. Computational Determination of Aqueous pK_a Values of Protonated Benzimidazoles (Part 2). *J Phys Chem B*.
1002 2006 Oct; 110(41):20546–20554. doi: 10.1021/jp0639501.
- 1003 [111] **Zamora WJ**, Curutchet C, Campanera JM, Luque FJ. Prediction of pH-Dependent Hydrophobic Profiles of Small Molecules from Mier-
1004 tus–Scrocco–Tomasi Continuum Solvation Calculations. *J Phys Chem B*. 2017 Oct; 121(42):9868–9880. doi: 10.1021/acs.jpcc.7b08311.
- 1005 [112] **Fraczkiewicz R**. In Silico Prediction of Ionization. In: *Comprehensive Medicinal Chemistry II* Elsevier; 2007.p. 603–626. doi: 10.1016/B0-08-
1006 045044-X/00143-7.

1007 **11 Supplementary Information**

1008 **11.1 Supplementary figures and tables**

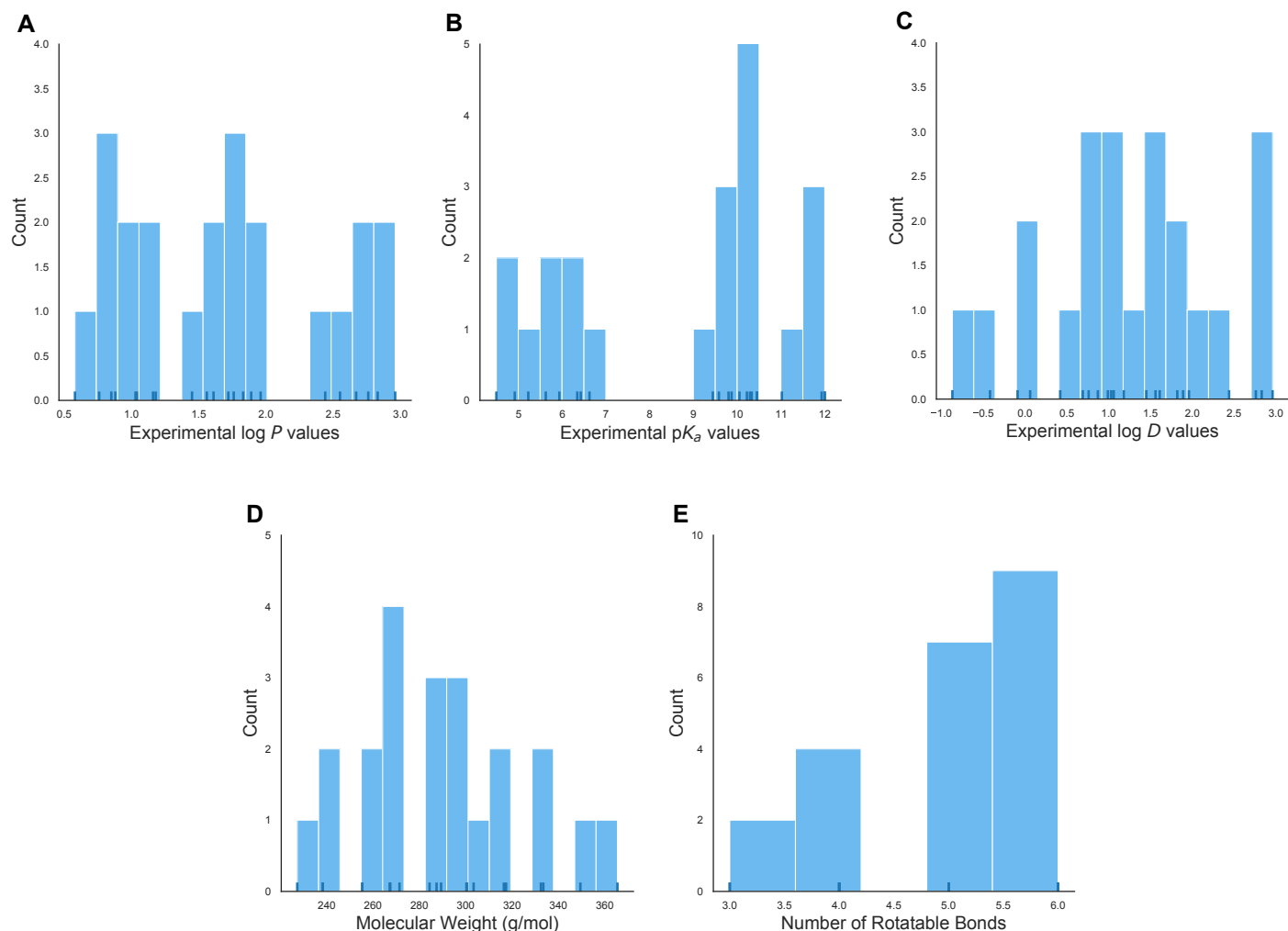


Figure S1. Distribution of molecular properties of the 22 compounds from the SAMPL7 physical property blind challenge. (A) Histogram of log P measurements collected with Sirius T3 instrument. The ticks along the x-axis indicate the individual values. Compounds have experimental log P values in the range of 0.58-2.96. (B) Histogram of pK_a measurements collected with Sirius T3 instrument. Eight compounds have measured pK_a 's in the range of 4.49-6.62 and eleven in the range 9.58- 11.93. Two compounds are included here as having pK_a 's of 12, but actually had experimental values greater than 12, and were therefore outside of the experimental detection range. (C) Histogram of log D measurements between n-octanol and aqueous buffer at pH 7.4 were determined via potentiometric titrations using a Sirius T3 instrument, except for compounds SM27, SM28, SM30-SM34, SM36-SM39 which had log $D_{7.4}$ values determined via shake-flask assay. log D measurements ranged from -0.87-2.96. (D) Histogram of molecular weights calculated for the compounds in the SAMPL7 dataset. The molecular weight ranged from 227-365 Da. (E) Histogram of the number of rotatable bonds in each molecule. The number of rotatable bonds in challenge molecules ranged from 3-6.

Table S1. Evaluation statistics calculated for all methods in the log P challenge. Submitted predictions are represented by their method name. There are six error metrics reported: the root-mean-squared error (RMSE), mean absolute error (MAE), mean (signed) error (ME), coefficient of determination (R^2), linear regression slope (m), and Kendall's Rank Correlation Coefficient (τ), and error slope (ES). The mean and 95% confidence intervals of each statistic is presented. This table is ranked by increasing RMSE.

Method Name	Category	Submission Type	RMSE	MAE	ME	R^2	m	Kendall's Tau	ES
ClassicalGSG DB2	Empirical	Blind	0.55 [0.38, 0.69]	0.44 [0.31, 0.58]	0.05 [-0.20, 0.26]	0.51 [0.18, 0.82]	0.71 [0.36, 1.06]	0.51 [0.18, 0.78]	0.81 [0.62, 1.03]
TFE MLR	Empirical	Blind	0.58 [0.34, 0.83]	0.41 [0.26, 0.60]	-0.04 [-0.30, 0.19]	0.43 [0.06, 0.80]	0.60 [0.21, 0.95]	0.56 [0.23, 0.82]	1.38 [1.27, 1.45]
ClassicalGSG DB4	Empirical	Blind	0.65 [0.50, 0.78]	0.55 [0.41, 0.69]	0.25 [0.01, 0.50]	0.51 [0.19, 0.76]	0.82 [0.39, 1.22]	0.45 [0.15, 0.71]	0.57 [0.46, 0.85]
Chemprop	Empirical	Blind	0.66 [0.39, 0.88]	0.48 [0.30, 0.68]	-0.17 [-0.44, 0.08]	0.41 [0.11, 0.76]	0.69 [0.31, 1.08]	0.54 [0.25, 0.82]	1.03 [0.79, 1.21]
TFE-SM8-vacuum-opt	Physical (QM)	Blind	0.67 [0.45, 0.86]	0.51 [0.33, 0.69]	0.15 [-0.13, 0.42]	0.45 [0.11, 0.75]	0.80 [0.33, 1.23]	0.50 [0.18, 0.76]	0.99 [0.75, 1.20]
GROVER	Empirical	Blind	0.69 [0.41, 0.96]	0.49 [0.31, 0.71]	-0.21 [-0.50, 0.05]	0.33 [0.04, 0.70]	0.56 [0.18, 0.92]	0.37 [0.05, 0.66]	0.87 [0.62, 1.09]
ClassicalGSG DB1	Empirical	Blind	0.76 [0.56, 0.96]	0.62 [0.45, 0.82]	0.10 [-0.23, 0.40]	0.28 [0.06, 0.60]	0.61 [0.26, 0.99]	0.36 [0.04, 0.63]	0.63 [0.43, 0.85]
ffsampled_deeplearning_cl1	Empirical	Blind	0.77 [0.44, 1.04]	0.51 [0.29, 0.77]	-0.25 [-0.58, 0.04]	0.31 [0.05, 0.70]	0.63 [0.24, 1.05]	0.42 [0.06, 0.74]	0.99 [0.72, 1.19]
ClassicalGSG DB3	Empirical	Blind	0.77 [0.57, 0.96]	0.62 [0.43, 0.82]	-0.15 [-0.46, 0.16]	0.51 [0.18, 0.78]	1.08 [0.55, 1.59]	0.48 [0.15, 0.75]	0.60 [0.42, 0.89]
COSMO-RS	Physical (QM)	Blind	0.78 [0.49, 1.01]	0.57 [0.36, 0.80]	-0.30 [-0.61, -0.01]	0.49 [0.17, 0.79]	0.97 [0.49, 1.45]	0.53 [0.25, 0.78]	0.97 [0.74, 1.18]
TFE_Attractive_FP	Empirical	Blind	0.79 [0.47, 1.07]	0.57 [0.36, 0.82]	-0.18 [-0.53, 0.12]	0.19 [0.00, 0.61]	0.44 [0.04, 0.87]	0.34 [-0.02, 0.69]	0.93 [0.69, 1.13]
ffsampled_deeplearning_cl2	Empirical	Blind	0.82 [0.48, 1.11]	0.56 [0.32, 0.83]	-0.37 [-0.69, -0.08]	0.36 [0.07, 0.72]	0.73 [0.31, 1.16]	0.40 [0.07, 0.69]	0.94 [0.67, 1.15]
TFE-SM12-vacuum-opt	Physical (QM)	Blind	0.82 [0.61, 1.02]	0.66 [0.47, 0.87]	0.28 [-0.06, 0.60]	0.41 [0.08, 0.72]	0.90 [0.36, 1.42]	0.39 [0.05, 0.67]	0.88 [0.65, 1.09]
TFE-SM8-solvent-opt	Physical (QM)	Blind	0.97 [0.71, 1.20]	0.78 [0.55, 1.02]	0.65 [0.35, 0.94]	0.42 [0.10, 0.70]	0.83 [0.35, 1.31]	0.44 [0.13, 0.69]	0.71 [0.47, 0.94]
REF1 ChemAxon	Empirical	Reference	1.00 [0.79, 1.20]	0.85 [0.63, 1.08]	0.46 [0.08, 0.83]	0.39 [0.10, 0.70]	0.98 [0.45, 1.53]	0.40 [0.09, 0.68]	0.13 [-0.00, 0.29]
TFE IEFFPCM MST	Physical (QM)	Blind	1.03 [0.65, 1.41]	0.80 [0.56, 1.10]	-0.07 [-0.53, 0.33]	0.27 [0.01, 0.68]	0.85 [0.12, 1.50]	0.42 [0.10, 0.70]	1.07 [0.88, 1.23]
TFE MD neat oct (GAFF/TIP4P)	Physical (MM)	Blind	1.11 [0.74, 1.43]	0.83 [0.52, 1.15]	-0.74 [-1.10, -0.40]	0.56 [0.24, 0.82]	1.25 [0.64, 1.83]	0.58 [0.27, 0.82]	1.30 [1.19, 1.40]
NULL0 mean clogP FDA	Empirical	Reference	1.20 [0.94, 1.42]	1.01 [0.73, 1.28]	-0.96 [-1.26, -0.64]	0.00 [0.00, 0.00]	0.00 [-0.00, 0.00]	nan [nan, nan]	0.18 [0.04, 0.32]
NES-1 (GAFF2/OPC3) G	Physical (MM)	Blind	1.21 [0.92, 1.51]	1.03 [0.78, 1.31]	-0.13 [-0.63, 0.37]	0.22 [0.01, 0.59]	0.88 [0.15, 1.59]	0.34 [0.02, 0.63]	1.23 [1.11, 1.33]
NES-1 (GAFF2/OPC3) J	Physical (MM)	Blind	1.28 [0.97, 1.58]	1.08 [0.81, 1.38]	0.01 [-0.54, 0.53]	0.21 [0.01, 0.63]	0.92 [0.09, 1.76]	0.33 [0.00, 0.64]	1.21 [1.08, 1.33]
NES-1 (GAFF2/OPC3) B	Physical (MM)	Blind	1.42 [1.02, 1.81]	1.13 [0.79, 1.51]	-0.51 [-1.08, 0.05]	0.27 [0.02, 0.65]	1.11 [0.30, 1.91]	0.36 [0.05, 0.65]	1.17 [1.01, 1.31]
MD (GAFF/TIP3P)	Physical (MM)	Blind	1.43 [1.15, 1.71]	1.30 [1.06, 1.56]	-1.30 [-1.56, -1.06]	0.48 [0.22, 0.79]	0.77 [0.45, 1.12]	0.55 [0.28, 0.80]	0.94 [0.80, 1.09]
TFE wet oct (GAFF/TIP4P)	Physical (MM)	Blind	1.47 [1.16, 1.77]	1.30 [1.03, 1.60]	-1.30 [-1.60, -1.03]	0.42 [0.10, 0.75]	0.80 [0.30, 1.30]	0.47 [0.14, 0.75]	1.15 [1.03, 1.27]
TFE-NHLBI-TZVP-QM	Physical (QM)	Blind	1.55 [1.19, 1.88]	1.34 [1.02, 1.67]	1.32 [1.00, 1.67]	0.52 [0.19, 0.78]	1.16 [0.59, 1.65]	0.51 [0.19, 0.78]	0.05 [-0.00, 0.17]
0.05 MD (CGenFF/TIP3P)	Physical (MM)	Blind	1.63 [1.25, 1.98]	1.41 [1.08, 1.76]	-1.38 [-1.74, -1.02]	0.54 [0.26, 0.82]	1.26 [0.81, 1.76]	0.52 [0.26, 0.76]	0.90 [0.70, 1.07]
EC_RISM_wet	Physical (QM)	Blind	1.84 [1.31, 2.36]	1.49 [1.07, 1.96]	-1.49 [-1.96, -1.06]	0.29 [0.05, 0.68]	0.96 [0.37, 1.57]	0.38 [0.08, 0.67]	0.67 [0.45, 0.90]
TFE-SMD-vacuum-opt	Physical (QM)	Blind	1.96 [1.60, 2.30]	1.76 [1.42, 2.13]	1.76 [1.42, 2.13]	0.44 [0.12, 0.68]	1.04 [0.46, 1.59]	0.41 [0.03, 0.70]	0.68 [0.50, 0.87]
MD-EE-MCC (GAFF-TIP4P-Ew)	Physical (MM)	Blind	2.06 [1.48, 2.59]	1.61 [1.09, 2.17]	-0.93 [-1.70, -0.17]	0.03 [0.00, 0.28]	0.47 [-0.53, 1.49]	0.11 [-0.16, 0.38]	0.76 [0.51, 1.03]
MD (OPLS-AA/TIP4P)	Physical (MM)	Blind	2.19 [1.69, 2.65]	1.82 [1.31, 2.34]	-1.35 [-2.03, -0.60]	0.28 [0.06, 0.58]	1.47 [0.58, 2.55]	0.36 [0.07, 0.62]	0.73 [0.48, 0.97]
TFE b3lypd3	Physical (QM)	Blind	2.19 [1.76, 2.57]	1.98 [1.59, 2.37]	1.98 [1.59, 2.37]	0.40 [0.10, 0.67]	1.06 [0.47, 1.64]	0.45 [0.11, 0.72]	0.22 [0.09, 0.41]
MD LigParGen (OPLS-AA/TIP4P)	Physical (MM)	Blind	2.28 [1.80, 2.71]	1.95 [1.46, 2.44]	0.35 [-0.60, 1.29]	0.07 [0.00, 0.37]	0.83 [-0.51, 2.26]	0.19 [-0.14, 0.50]	0.65 [0.42, 0.88]
TFE-SMD-solvent-opt	Physical (QM)	Blind	2.39 [1.97, 2.78]	2.19 [1.79, 2.60]	2.19 [1.79, 2.60]	0.40 [0.09, 0.67]	1.09 [0.45, 1.67]	0.42 [0.09, 0.68]	0.51 [0.34, 0.68]
Ensemble EPI physprop	Empirical	Blind	2.73 [2.27, 3.16]	2.54 [2.13, 2.98]	2.54 [2.13, 2.98]	0.33 [0.04, 0.64]	-0.30 [-0.49, -0.10]	-0.35 [-0.60, -0.03]	-0.00 [-0.00, -0.00]
Ensemble Martel	Empirical	Blind	3.29 [2.89, 3.68]	3.16 [2.78, 3.55]	3.16 [2.78, 3.55]	0.39 [0.05, 0.73]	-0.25 [-0.40, -0.09]	-0.46 [-0.72, -0.14]	-0.00 [-0.00, -0.00]
QSPR_Mordred2D_TPOT_AutoML	Empirical	Blind	3.64 [3.01, 4.24]	3.36 [2.80, 3.96]	3.36 [2.80, 3.96]	0.39 [0.10, 0.71]	-0.72 [-1.12, -0.33]	-0.37 [-0.65, -0.04]	-0.00 [-0.00, -0.00]
TFE-NHLBI-NN-IN	Empirical	Blind	3.97 [3.57, 4.34]	3.85 [3.45, 4.25]	3.85 [3.45, 4.25]	0.00 [0.00, 0.15]	0.02 [-0.30, 0.34]	0.02 [-0.23, 0.27]	0.01 [-0.00, 0.02]

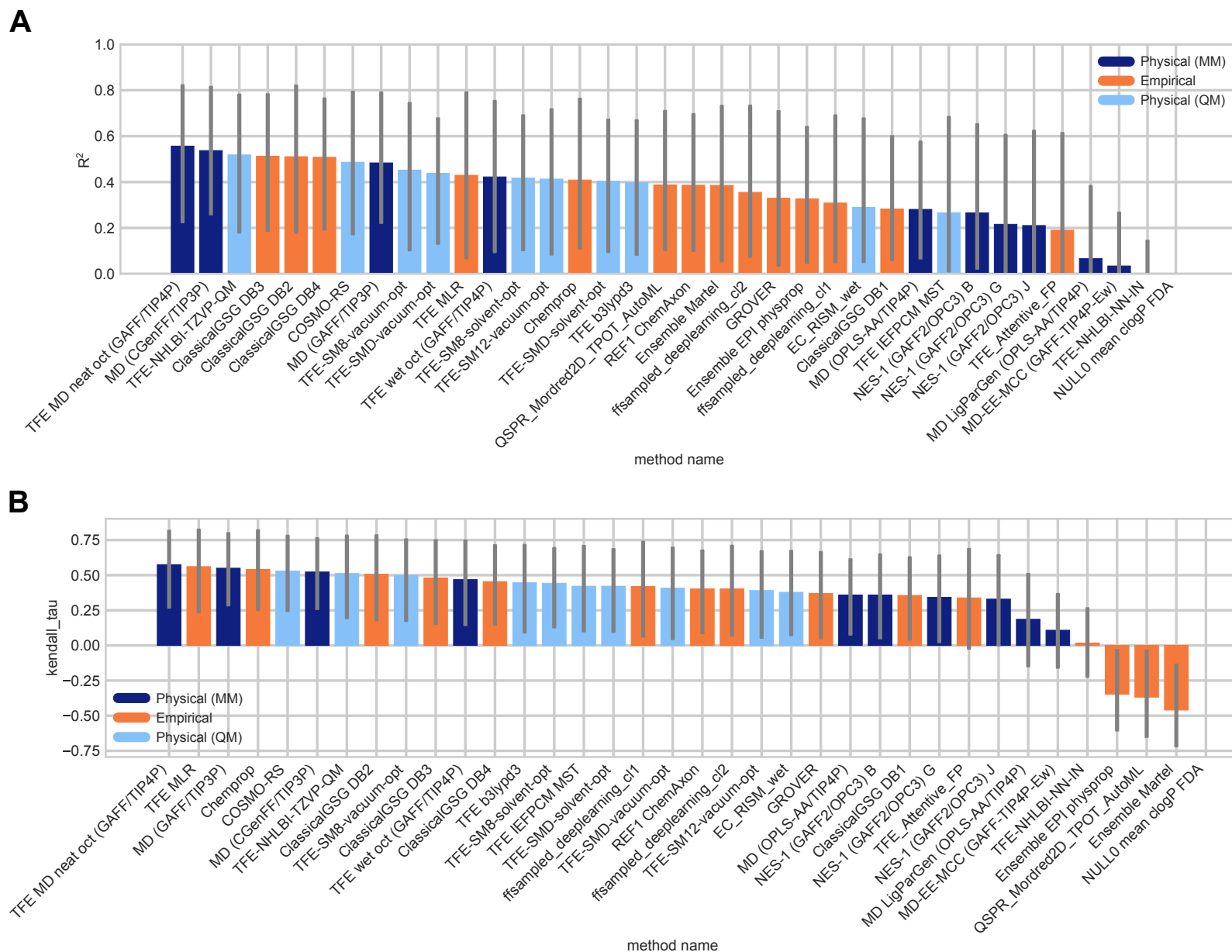


Figure S2. Overall correlation assessment for all methods participating in the SAMPL7 log P challenge show that the uncertainty of each correlation statistic is quite high, not allowing a true ranking based on correlation. Pearson's R^2 and Kendall's Rank Correlation Coefficient Tau (τ) are shown, with error bars denoting 95% confidence intervals obtained by bootstrapping over challenge molecules. Submitted methods are listed in Table 1. The submission *REF1 ChemAxon* was a reference method included after the blind challenge submission deadline, and *NULL0 mean clogP FDA* is the null prediction method; all others refer to blind predictions. Most methods have a statistically indistinguishable performance on ranking because of the small dynamic range of the dataset. Evaluation statistics calculated for all methods are available in Table S1 of the Supplementary Information.

Table S2. Details of MM-based physical methods in the log *P* prediction challenge. Force fields, water models, and octanol phase choice are reported. A dry octanol phase indicates the octanol phase was composed of only octanol. A wet octanol phase indicates the octanol phase was treated as a mixture of octanol and water. RMSE, MAE, R^2 , and Kendall's Tau values are reported as mean and 95% confidence intervals.

Method Name	Force Field	Water Model	Octanol Phase	RMSE	MAE	R^2	Kendall's Tau
<i>TFE MD neat oct (GAFF/TIP4P)</i>	GAFF	TIP4P	dry	1.11 [0.74, 1.43]	0.83 [0.52, 1.15]	0.56 [0.24, 0.82]	0.58 [0.27, 0.82]
<i>NES-1 (GAFF2/OPC3) G</i>	GAFF2	OPC3	dry	1.21 [0.92, 1.51]	1.03 [0.78, 1.31]	0.22 [0.01, 0.59]	0.34 [0.02, 0.63]
<i>NES-1 (GAFF2/OPC3) J</i>	GAFF2	OPC3	dry	1.28 [0.97, 1.58]	1.08 [0.81, 1.38]	0.21 [0.01, 0.63]	0.33 [0.00, 0.64]
<i>NES-1 (GAFF2/OPC3) B</i>	GAFF2	OPC3	dry	1.42 [1.02, 1.81]	1.13 [0.79, 1.51]	0.27 [0.02, 0.65]	0.36 [0.05, 0.65]
<i>MD (GAFF/TIP3P)</i>	GAFF	TIP3P	dry	1.43 [1.15, 1.71]	1.30 [1.06, 1.56]	0.48 [0.22, 0.79]	0.55 [0.28, 0.80]
<i>TFE wet oct (GAFF/TIP4P)</i>	GAFF	TIP4P	wet	1.47 [1.16, 1.77]	1.30 [1.03, 1.60]	0.42 [0.10, 0.75]	0.47 [0.14, 0.75]
<i>MD (CGenFF/TIP3P)</i>	CGenFF	TIP3P	dry	1.63 [1.25, 1.98]	1.41 [1.08, 1.76]	0.54 [0.26, 0.82]	0.52 [0.26, 0.76]
<i>MD-EE-MCC (GAFF-TIP4P-Ew)</i>	GAFF	TIP4P-eW	dry	2.06 [1.48, 2.59]	1.61 [1.09, 2.17]	0.03 [0.00, 0.28]	0.11 [-0.16, 0.38]
<i>MD (OPLS-AA/TIP4P)</i>	OPLS-AA	TIP4P	dry	2.19 [1.69, 2.65]	1.82 [1.31, 2.34]	0.28 [0.06, 0.58]	0.36 [0.07, 0.62]
<i>MD LigParGen (OPLS-AA/TIP4P)</i>	OPLS-AA	TIP4P	dry	2.28 [1.80, 2.71]	1.95 [1.46, 2.44]	0.07 [0.00, 0.37]	0.19 [-0.14, 0.50]

Table S3. Evaluation statistics calculated for all methods in the pK_a challenge. Submitted predictions are represented by their method name. There are six error metrics reported: the root-mean-squared error (RMSE), mean absolute error (MAE), mean (signed) error (ME), coefficient of determination (R^2), linear regression slope (m), Kendall's Rank Correlation Coefficient (τ), and error slope (ES). The mean and 95% confidence intervals of each statistic is presented. This table is ranked by increasing RMSE.

Method Name	Category	Submission Type	RMSE	MAE	ME	R^2	m	Kendall's Tau	ES
<i>REF00_Chemaxon_Chemicalize</i>	QSPR/ML	Reference	0.71 [0.50, 0.90]	0.56 [0.38, 0.76]	0.09 [-0.23, 0.38]	0.91 [0.86, 0.96]	0.88 [0.72, 1.02]	0.73 [0.51, 0.90]	0.83 [0.58, 1.04]
<i>EC_RISM</i>	QM	Blind	0.72 [0.45, 0.95]	0.53 [0.33, 0.75]	0.20 [-0.10, 0.50]	0.93 [0.87, 0.98]	0.80 [0.72, 0.91]	0.81 [0.63, 0.96]	1.32 [1.19, 1.42]
<i>IEFPCM/MST</i>	QM	Blind	1.82 [1.00, 2.69]	1.30 [0.84, 1.92]	0.25 [-0.46, 1.09]	0.56 [0.22, 0.87]	0.86 [0.53, 1.18]	0.52 [0.22, 0.76]	1.00 [0.80, 1.17]
<i>DFT_M05-2X_SMD</i>	QM	Blind	2.90 [2.04, 3.69]	2.28 [1.53, 3.10]	-0.78 [-2.02, 0.41]	0.03 [0.00, 0.37]	0.15 [-0.32, 0.53]	0.17 [-0.22, 0.54]	0.55 [0.31, 0.81]
<i>TZVP-QM</i>	QM	Blind	2.90 [2.52, 3.25]	2.75 [2.34, 3.14]	1.20 [0.02, 2.33]	0.23 [0.03, 0.60]	-0.11 [-0.20, -0.04]	-0.14 [-0.49, 0.23]	-0.00 [-0.00, -0.00]
<i>Standard Gaussian Process</i>	QSPR/ML	Blind	3.49 [2.76, 4.12]	2.91 [2.06, 3.75]	2.47 [1.38, 3.55]	0.30 [0.10, 0.69]	-0.05 [-0.09, -0.02]	-0.42 [-0.70, -0.08]	1.11 [0.96, 1.24]
<i>DFT_M06-2X_SMD_implicit</i>	QM	Blind	4.16 [2.00, 6.38]	2.80 [1.76, 4.33]	-0.07 [-1.61, 1.95]	0.52 [0.39, 0.78]	1.70 [0.80, 2.77]	0.70 [0.48, 0.88]	0.50 [0.30, 0.70]
<i>DFT_M06-2X_SMD_implicit_SAS</i>	QM	Blind	4.16 [2.03, 6.44]	2.81 [1.80, 4.36]	-0.20 [-1.71, 1.85]	0.50 [0.36, 0.77]	1.64 [0.72, 2.72]	0.56 [0.28, 0.81]	0.14 [0.02, 0.31]
<i>DFT_M06-2X_SMD_explicit_water</i>	QM	Blind	5.12 [1.19, 7.92]	2.56 [0.96, 4.76]	-0.35 [-2.62, 1.93]	0.20 [0.00, 0.81]	1.10 [-0.39, 2.50]	0.46 [0.06, 0.78]	0.52 [0.29, 0.77]
<i>Gaussian_corrected</i>	QM+LEC	Blind	5.36 [4.70, 5.95]	5.12 [4.42, 5.79]	5.12 [4.42, 5.79]	0.76 [0.63, 0.88]	0.35 [0.27, 0.45]	0.60 [0.42, 0.76]	0.00 [-0.00, 0.00]

Table S4. Evaluation statistics calculated for all log *D* estimates. Predictions are represented a name based on method names participants submitted to the and log *P* challenges. There are six error metrics reported: the root-mean-squared error (RMSE), mean absolute error (MAE), mean (signed) error (ME), coefficient of determination (R^2), linear regression slope (m), Kendall's Rank Correlation Coefficient (τ), and error slope (ES). The mean and 95% confidence intervals of each statistic is presented. This table is ranked by increasing RMSE.

Method Name	Category	Submission Type	RMSE	MAE	ME	R^2	m	Kendall's Tau	ES
<i>REF0 ChemAxon</i>	Empirical	Reference	1.06 [0.82, 1.27]	0.91 [0.68, 1.14]	0.28 [-0.14, 0.70]	0.27 [0.01, 0.58]	0.54 [0.10, 0.90]	0.31 [-0.02, 0.61]	0.12 [-0.00, 0.28]
<i>TFE IEFPCM MST + IEFPCM/MST</i>	Physical (QM)	Standard	1.27 [0.85, 1.64]	0.98 [0.67, 1.33]	0.24 [-0.28, 0.75]	0.55 [0.17, 0.87]	1.31 [0.71, 1.70]	0.57 [0.27, 0.82]	1.16 [0.89, 1.25]
<i>NULL0</i>	Empirical	Reference	1.59 [1.22, 1.93]	1.35 [1.00, 1.71]	1.23 [0.81, 1.65]	0.00 [0.00, 0.00]	0.00 [0.00, 0.00]	nan [nan, nan]	0.65 [0.44, 0.87]
<i>EC_RISM</i>	Physical (QM)	Standard	1.69 [1.30, 2.05]	1.43 [1.07, 1.82]	-1.43 [-1.81, -1.07]	0.53 [0.20, 0.77]	0.95 [0.54, 1.29]	0.51 [0.21, 0.74]	0.84 [0.64, 1.02]
<i>TFE-NHLBI-TZVP-QM + TZVP-QM</i>	Physical (QM)	Standard	1.72 [1.30, 2.12]	1.47 [1.12, 1.86]	1.26 [0.78, 1.75]	0.25 [0.01, 0.64]	0.64 [0.08, 1.25]	0.38 [0.02, 0.70]	0.05 [-0.00, 0.18]
<i>TFE b3lypd3 + DFT_M05-2X_SMD</i>	Physical (QM)	Standard	2.15 [1.56, 2.71]	1.78 [1.31, 2.31]	1.78 [1.31, 2.31]	0.32 [0.04, 0.66]	0.80 [0.27, 1.30]	0.41 [0.05, 0.72]	0.42 [0.27, 0.70]
<i>MD (CGenFF/TIP3P) + Gaussian_corrected</i>	Physical (MM) + QM+LEC	Standard	2.27 [1.97, 2.55]	2.13 [1.80, 2.45]	1.84 [1.21, 2.35]	0.62 [0.35, 0.84]	1.53 [0.93, 2.18]	0.62 [0.36, 0.82]	0.88 [0.75, 1.00]
<i>TFE-SMD-solvent-opt + DFT_M06-2X_SMD_explicit_water</i>	Physical (QM)	Standard	4.54 [2.09, 7.15]	2.92 [1.88, 4.57]	2.88 [1.80, 4.55]	0.25 [0.11, 0.76]	1.92 [0.53, 4.45]	0.55 [0.22, 0.80]	0.55 [0.38, 0.73]

Table S5. Additional info for microscopic pK_a predictions.

Microstate	Total number of relative free energy predictions	Average relative free energy prediction	Average relative free energy prediction STD	Minimum relative free energy prediction	Maximum relative free energy prediction	Number of (+) sign predictions	Number of (-) sign predictions	Number of neutral (0) sign predictions	Shannon entropy (H)
SM25_micro001	9	-0.6	13.2	-15.6	16.3	4	5	0	0.7
SM25_micro002	8	8.8	10.6	-7.5	20.4	6	2	0	0.6
SM25_micro003	8	9.6	2.7	4.5	12.6	8	0	0	0.0
SM25_micro004	2	-8.9	4.5	-12.1	-5.8	0	2	0	0.0
SM25_micro005	2	-0.8	2.1	-2.3	0.7	1	1	0	0.7
SM26_micro001	9	7.3	2.4	3.0	10.7	9	0	0	0.0
SM26_micro002	8	-6.7	20.5	-31.7	22.1	3	5	0	0.7
SM26_micro003	8	20.9	12.0	0.9	32.4	8	0	0	0.0
SM26_micro004	2	4.3	0.7	3.8	4.8	2	0	0	0.0
SM26_micro005	2	8.1	2.6	6.3	10.0	2	0	0	0.0
SM27_micro001	9	13.4	4.9	6.1	19.0	9	0	0	0.0
SM28_micro001	9	-5.7	25.0	-39.0	23.5	4	5	0	0.7
SM28_micro002	8	17.1	8.0	8.2	26.5	8	0	0	0.0
SM28_micro003	8	0.9	8.3	-10.0	12.6	4	4	0	0.7
SM28_micro004	2	25.1	9.1	18.7	31.5	2	0	0	0.0
SM29_micro001	9	12.6	4.3	6.3	18.7	9	0	0	0.0
SM30_micro001	9	12.3	4.2	5.9	17.7	9	0	0	0.0
SM31_micro001	9	13.2	4.4	6.0	18.1	9	0	0	0.0
SM31_micro002	3	-0.6	6.6	-8.1	4.5	2	1	0	0.6
SM32_micro001	9	12.8	4.6	5.9	18.9	9	0	0	0.0
SM33_micro001	9	11.9	3.9	5.2	17.1	9	0	0	0.0
SM34_micro001	9	13.0	4.6	5.7	19.7	9	0	0	0.0
SM34_micro002	3	-0.9	6.4	-8.1	4.4	2	1	0	0.6
SM35_micro001	9	11.7	4.5	3.2	16.2	9	0	0	0.0
SM35_micro002	8	0.2	1.4	-1.9	2.5	5	2	1	0.9
SM35_micro003	8	12.2	5.6	3.2	18.1	8	0	0	0.0
SM36_micro001	9	10.8	3.1	5.2	14.9	9	0	0	0.0
SM36_micro002	8	1.2	1.8	0.0	4.4	4	1	3	1.0
SM36_micro003	8	10.7	3.3	5.2	14.7	8	0	0	0.0
SM37_micro001	9	0.1	9.4	-11.7	13.7	5	4	0	0.7
SM37_micro002	8	9.8	2.9	3.7	12.7	8	0	0	0.0
SM37_micro003	8	0.7	1.8	-1.5	4.2	4	3	1	1.0
SM37_micro004	8	8.9	3.0	3.8	12.4	8	0	0	0.0
SM37_micro005	7	-2.7	7.6	-10.6	11.0	3	4	0	0.7
SM38_micro001	9	11.6	4.6	5.2	17.5	9	0	0	0.0
SM39_micro001	9	10.1	3.1	5.1	14.6	9	0	0	0.0
SM40_micro001	9	10.8	3.3	5.0	15.7	9	0	0	0.0
SM40_micro002	8	-1.8	10.3	-15.5	11.8	4	4	0	0.7
SM41_micro001	9	8.4	3.5	2.2	14.8	9	0	0	0.0
SM41_micro002	8	-0.5	9.9	-12.9	13.9	4	4	0	0.7
SM42_micro001	9	5.5	4.6	0.2	12.3	9	0	0	0.0
SM42_micro002	8	-0.2	8.6	-10.8	14.3	4	4	0	0.7
SM42_micro003	3	-2.0	3.0	-5.1	1.0	1	2	0	0.6
SM43_micro001	9	5.9	4.4	0.5	13.4	9	0	0	0.0
SM43_micro002	8	0.1	9.4	-11.0	11.0	4	4	0	0.7
SM43_micro003	8	-11.6	38.1	-60.9	38.2	4	4	0	0.7
SM43_micro004	2	-3.6	2.2	-5.2	-2.1	0	2	0	0.0
SM43_micro005	2	0.1	0.4	-0.2	0.4	1	1	0	0.7
SM44_micro001	9	9.5	2.9	4.3	12.9	9	0	0	0.0
SM44_micro002	8	-1.1	7.4	-10.3	9.9	4	4	0	0.7
SM45_micro001	9	9.6	3.1	4.4	14.7	9	0	0	0.0
SM45_micro002	8	-1.0	7.8	-11.0	9.6	4	4	0	0.7
SM46_micro001	9	9.9	4.1	4.0	18.4	9	0	0	0.0
SM46_micro002	8	-0.7	7.5	-9.6	10.5	4	4	0	0.7
SM46_micro003	8	-12.2	37.1	-63.5	39.0	4	4	0	0.7
SM46_micro004	3	6.3	4.5	2.4	11.3	3	0	0	0.0

Table S6. SMILES and compound class of SAMPL7 physical property challenge molecules. A view of the compounds and their classes can be found in Figure S3.

SAMPL7 Molecule ID	Compound Class	Isomeric SMILES
SM25	acylsulfonamide	<chem>O=C(NS(C1=CC=CC=C1)(=O)=O)CCC2=CC=CC=C2</chem>
SM26	acylsulfonamide	<chem>O=S(CCC1=CC=CC=C1)(NC(C)=O)=O</chem>
SM27	oxetane	<chem>O=S(CCC1=CC=CC=C1)(NC2(C)COC2)=O</chem>
SM28	thietane-1,1-dioxide	<chem>O=S(CC1(NC(C)=O)CCC2=CC=CC=C2)(C1)=O</chem>
SM29	oxetane	<chem>CS(NC1(COC1)CCC2=CC=CC=C2)(=O)=O</chem>
SM30	oxetane	<chem>O=S(NC1(COC1)CCC2=CC=CC=C2)(C3=CC=CC=C3)=O</chem>
SM31	oxetane	<chem>O=S(NC1(COC1)CCC2=CC=CC=C2)(N(C)C)=O</chem>
SM32	thietane	<chem>CS(NC1(CSC1)CCC2=CC=CC=C2)(=O)=O</chem>
SM33	thietane	<chem>O=S(NC1(CSC1)CCC2=CC=CC=C2)(C3=CC=CC=C3)=O</chem>
SM34	thietane	<chem>O=S(NC1(CSC1)CCC2=CC=CC=C2)(N(C)C)=O</chem>
SM35	thietane-1-oxide	<chem>CS(N[C@@]1(C[S+])([O-])C1)CCC2=CC=CC=C2)(=O)=O</chem>
SM36	thietane-1-oxide	<chem>O=S(N[C@@]1(C[S+])([O-])C1)CCC2=CC=CC=C2)(C3=CC=CC=C3)=O</chem>
SM37	thietane-1-oxide	<chem>O=S(N[C@@]1(C[S+])([O-])C1)CCC2=CC=CC=C2)(N(C)C)=O</chem>
SM38	thietane-1,1-dioxide	<chem>CS(NC1(CS(C1)(=O)=O)CCC2=CC=CC=C2)(=O)=O</chem>
SM39	thietane-1,1-dioxide	<chem>O=S(NC1(CS(C1)(=O)=O)CCC2=CC=CC=C2)(C3=CC=CC=C3)=O</chem>
SM40	thietane-1,1-dioxide	<chem>O=S(NC1(CS(C1)(=O)=O)CCC2=CC=CC=C2)(N(C)C)=O</chem>
SM41	isoxazole	<chem>O=S(NC1=NOC(C2=CC=CC=C2)=C1)(C)=O</chem>
SM42	isoxazole	<chem>O=S(NC1=NOC(C2=CC=CC=C2)=C1)(C3=CC=CC=C3)=O</chem>
SM43	isoxazole	<chem>O=S(NC1=NOC(C2=CC=CC=C2)=C1)(N(C)C)=O</chem>
SM44	1,2,3-triazole	<chem>O=S(NC(N=N1)=CN1C2=CC=CC=C2)(C)=O</chem>
SM45	1,2,3-triazole	<chem>O=S(NC(N=N1)=CN1C2=CC=CC=C2)(C3=CC=CC=C3)=O</chem>
SM46	1,2,3-triazole	<chem>O=S(NC(N=N1)=CN1C2=CC=CC=C2)(N(C)C)=O</chem>

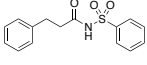
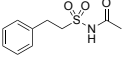
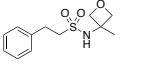
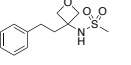
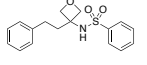
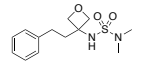
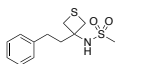
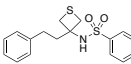
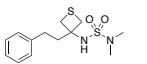
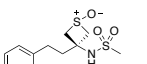
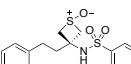
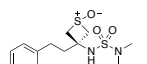
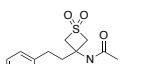
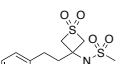
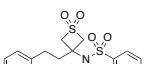
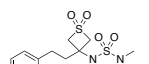
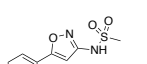
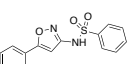
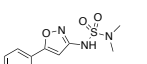
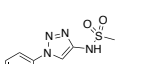
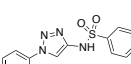
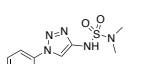
Compound Classes	Structures
acylsulfonamide	  SM25 SM26
oxetane	    SM27 SM29 SM30 SM31
thietane	   SM32 SM33 SM34
thietane-1-oxide	   SM35 SM36 SM37
thietane-1,1-dioxide	    SM28 SM38 SM39 SM40
isoxazole	   SM41 SM42 SM43
1,2,3-triazole	   SM44 SM45 SM46

Figure S3. Compound classes and structures of the molecules in the SAMPL7 physical property challenge. SMILES of the compounds are in Table S3.

Table S7. Number of states per charge state for the microstates used in the SAMPL7 pK_a challenge. The total number of microstates (protomers and tautomers) is listed. Some of the molecules have up to 6 microstates, while others have only 2.

	Charge State				Total #
	+2	+1	0	-1	
SM25	0	1	3	2	6
SM26	0	1	3	2	6
SM27	0	0	1	1	2
SM28	0	1	2	2	5
SM29	0	0	1	1	2
SM30	0	0	1	1	2
SM31	0	1	1	1	3
SM32	0	0	1	1	2
SM33	0	0	1	1	2
SM34	0	1	1	1	3
SM35	0	0	2	3	5
SM36	0	0	2	3	5
SM37	0	2	2	2	6
SM38	0	0	1	1	2
SM39	0	0	1	1	2
SM40	0	1	1	1	3
SM41	0	1	1	1	3
SM42	0	1	2	1	4
SM43	1	2	2	1	6
SM44	0	1	1	1	3
SM45	0	1	1	1	3
SM46	1	2	1	1	5